TECHNICAL REPORT STANDARD PAGE

1. Title and Subtitle
Rehabilitation of Deteriorated Timber Piles using Fiber Reinforced Polymer (FRP) Composites

2. Author(s)
Hota Gangarao (PI), Drew Damich, Mark Skidmore, and John Harper

3. Performing Organization Name and Address
WVU Constructed Facilities Center
PO BOX 6103
Morgantown, WV 26505

4. Sponsoring Agency Name and Address
Louisiana Department of Transportation and Development
P.O. Box 94245
Baton Rouge, LA 70804-9245

5. Report No. 653
FHWA/LA.21/653

6. Report Date
March 2022

7. Performing Organization Code
LTRC Project Number: 15-3ST
SIO Number: DOTDLT1000043

8. Type of Report and Period Covered
Final Report
November 2015-April 2021

9. No. of Pages
200

10. Supplementary Notes
Conducted in Cooperation with the U.S. Department of Transportation, Federal Highway Administration

11. Distribution Statement
Unrestricted. This document is available through the National Technical Information Service, Springfield, VA 21161.

12. Key Words
FRP, timber, piles, wrapping, rehabilitation

13. Abstract
Fiber reinforced polymer (FRP) composite wraps have been used for timber pile repair. However, design guidelines including strengthening equations are lacking for FRP-wrapped timber piles. This study evaluated the bond, bending, shear, and compressive strengths of five FRP-wrapped timber pile systems. Five glass FRP-wrap systems were evaluated: three with different epoxy formulations and one each with polyurethane and phenolic resins. FRP wraps over timber piles with 12-in. bond lengths provided a higher capacity than the ones with 6-in. bond lengths. However, bond strength per inch of bond length is reduced suggesting a non-linear relationship. Epoxy based systems that utilized slow cure and low-viscosity resins developed high bond strengths due to their better penetration into timber substrate. Samples subjected to wet/dry conditions exhibited higher bond strengths due to post curing of the epoxy systems. The pull-off tests resulted in values similar to the bond tests, proving it a useful field evaluation technique. The epoxy and phenolic systems failed under compression with matrix failure (delamination) between layers resulting in highly localized buckling of the fibers.

Failure of the simulated rehabilitation samples with full-cross sectional cuts of timber piles was similar to the test results under pull-off, bond, bending, shear, and axial compression. The evaluation of the crack fillers showed a number of readily available materials exist to repair section loss in a timber pile. The results were applied to design and load rating equations that were developed as a part of this program. These equations account for both the bond and axial strengths based on the test data. In-situ repair guidelines were developed based on the experience in manufacturing the samples for this work and on previous experience. Inspection guidelines were prepared to permit the inspection of FRP-wrapped piles both visual and with advanced nondestructive evaluation techniques. This study also evaluated shear, flexure, and axial compression strengths for the traditional repair methods of timber piles and for the method of FRP-wrap splicing. The two are compared in strength as well as cost of repair. The FRP-wrap method proved to be a superior alternative to traditional methods of repair.

Project Review Committee

Each research project will have an advisory committee appointed by the LTRC Director. The Project Review Committee is responsible for assisting the LTRC Administrator or Manager in the development of acceptable research problem statements, requests for proposals, review of research proposals, oversight of approved research projects, and implementation of findings.

LTRC appreciates the dedication of the following Project Review Committee Members in guiding this research study to fruition.

LTRC Manager

Walid Alaywan, Ph.D., P.E.
Sr. Structures Research Manager

Members

V.J. Gopu, Ph.D., P.E.
Dana Feng, Ph.D., P.E.
Nick Fagerburg, P.E.
Jasmine Galjour, P.E.
Kristopher Wascom, P.E.
Mike Boudreaux, P.E.
Art Aguirre, P.E.

Directorate Implementation Sponsor

Christopher P. Knotts, P.E.
DOTD Chief Engineer

Rehabilitation of Deteriorated Timber Piles using Fiber Reinforced Polymer (FRP) Composites

By
Hota GangaRao, Principal Investigator
Mark Skidmore, Co-principal Investigator
John Harper, Graduate Research Assistant
Drew Damich, Graduate Research Assistant

WVU Constructed Facilities Center
PO BOX 6103
Morgantown, WV 26505

LTRC Project No. 15-3ST
SIO No. DOTDLT1000043

conducted for

Louisiana Department of Transportation and Development
Louisiana Transportation Research Center

March 2022

Abstract

Fiber reinforced polymer (FRP) composite wraps have been used for timber pile repair, but there is a lack of design guidelines including strengthening equations, assuming a pile wrapped with FRP carries the entire load. This study evaluated both the bond and compressive strength of five FRP-wrap systems on whole timber piles. In addition, five glass FRP-wrap systems were evaluated wherein three contained epoxy and one each contained with polyurethane and phenolic resins. Twelve-in. bond lengths provided a higher capacity than 6-in. bond lengths although bond strengths per inch of bond length were reduced suggesting a non-linear relationship between strength vs. length. Epoxy-based systems that utilized slow cure, low-viscosity resins developed high bond strengths due to their better penetration into timber substrate. Samples subjected to wet/dry conditions exhibited higher bond strengths due to moisture uptake in the timber and subsequent swelling. The pull-off tests resulted in similar values to the bond tests, proving it a useful field evaluation technique. Compression evaluations showed additional wrap layers increased the compression capacity of the shells in a nonlinear manner. The epoxy and phenolic systems failed in typical compressive behavior with matrix failure (delamination) between layers resulting in highly localized buckling of the fibers, while the polyurethane system failed in buckling with no fiber failure. Failure of the simulated rehabilitation samples was similar to the compression testing results. Testing under combined axial and bending loads was inconclusive. The evaluation of the crack fillers showed a number of readily available materials exist to repair section loss in a timber pile. The results were applied to design and load rating equations that account for both the bond and axial strengths based on the tested materials. In-situ repair guidelines were developed based on the experience in manufacturing the samples for this work and based on previous experience. Inspection guidelines were prepared to permit the inspection of FRP-wrapped piles both visual and with advanced techniques.

Traditional methods of timber pile repair are tested subsequently, in shear, axial, and flexural stresses. Three traditional repair methods are used: flat steel plate splicing, steel C-channel splicing, and wooden plate splicing. Multiple specimens of each repair type are tested in each of the different testing methods. The test data is analyzed and then compared to the newly proposed method of timber pile splicing that involves using a fiber-reinforced polymer wrap, tested in the same manner as the legacy splicing. From the data analysis of each of the methods, comparisons are made in terms of strength capacity. Of the traditional repair methods, the steel C-channel splicing proves to be the strongest in terms of maximum stress to failure, primarily because of high stiffness when compared with other methods. This is compared to the new FRP splicing method that yields slightly lower overall stress values.

However, both generate adequate strengths for field use. The FRP method can be improved in strength by adding additional wrapping or changing fiber type and orientation if higher strengths are desired. This new method will also provide a longer lasting solution as compared to traditional methods. Fiber reinforced polymer composites, unlike steel or wood, do not erode or corrode when in contact with water. Overall, the proposed FRP splicing method can be improved easily for higher strength by adding extra layers of wrap if needed and will provide a cost-effective, strength sufficient, and long-lasting solution for timber pile repair.

Acknowledgments

The author wishes to thank the Louisiana Department of Transportation and Development (DOTD) for providing the resources necessary for this project and the Louisiana Transportation Research Center (LTRC) for the funding of this study.

The authors are grateful to the project review committee (PRC) for its guidance throughout the study and especially indebted to Walid Alaywan, Ph.D., the project manager, for his active participation in completing this research study.

Implementation Statement

This work will be implemented through the design methodology and guide documents presented herein. Training on these materials will be provided via two workshops presented by WVU-CFC at DOTD facilities.

Table of Contents

List of Tables

List of Figures

Introduction

Timber bridge piles are susceptible to decay near the waterline, and replacement of these piles typically requires cutting out the damaged section and replacing with new wood. Even for this code-approved approach, certain stringent restrictions are in order. This process is difficult to complete and is not a long-term solution as the exposed heartwood tends to rot. Using Fiber reinforced polymer (FRP) wraps to reinforce the decayed area with filler materials to arrest future decay can be a cost-effective and long-lasting method for repair of timber piles. However, the installation methods and design guidelines for piles to be brought back to carry original design loads through FRP repair are severely lacking.

Through this report, the West Virginia University – Constructed Facilities Center (WVU-CFC) provides a cost-effective and durable solution to timber pile repair to the Louisiana Department of Transportation and Development (DOTD) via Louisiana Transportation Research Center (LTRC) Project 15-3ST, SIO No. DOTLT1000043. A thorough testing and evaluation program to determine the bond and axial strength of the wrap applied to timber piles was completed. The results from these laboratory experiments were used to develop a design methodology for future retrofit of timber piles. Lessons learned from the experimental program and WVU-CFC's experience elsewhere were used to develop guide specifications for the installation of FRP wraps on timber piles. A rating methodology has been developed based on the design methodology and the TIMBER rating program used by DOTD. An inspection guide provides DOTD Bridge inspectors with the knowledge necessary to assess the condition of a pile repaired with FRP wraps.

Literature Review

The first task was a comprehensive literature review to evaluate the typical methods for timber pile repair, including concrete encasement, posting/splicing new piles sections, supplemental and new pile placement, additive materials, FRP shells, and FRP wrapping. Evaluating these systems based on cost, repair time, intrusion, and durability reveals that FRP wraps are in many situations more desirable than other repair systems. The following literature review was conducted to determine the best design practices for further implementation of FRP wraps. Sources specified by LTRC, reports, pile maintenance manuals, and the past work conducted by WVU-CFC were carefully assessed. The review primarily focuses on FRP wrap design criteria including fabrics (fiber/orientation), resin systems, number of wraps, wrap configuration, filler materials, bonding, field evaluation, and installation.

Timber Pile Degradation and Repair

According to *AASHTO Maintenance Manual for Roadways and Bridges*, piles typically require little maintenance unless exposed to environmental effects [1]. Exposed timber piles are subjected to numerous decay mechanisms, leading to section loss and significant damage. Given the exposure conditions of the piles and their overall size, the issue is not about pile deterioration, but its service life. Various preservative and treatment methods are commonly applied to timber members to slow the degradation. Various pile repair methods have been implemented to restore the strength loss. In this section, timber deterioration mechanisms will be presented along with the preservation treatments followed by explaining the repair systems and discuss evaluation methods and their effectiveness.

Timber Pile Deterioration

As a natural material, timber is vulnerable to deterioration from a variety of sources if not maintained and treated properly. Sources of decay include moisture, fungi, insects, abrasion, heat, holes, corrosion from metal connectors, and chemicals. Of these, the most common factors affecting piles are moisture, fungi, insects, and abrasion.

Treated timber that is protected from the environment and with a low moisture content (<20-25%) is very durable, and timber continuously submerged in fresh water will show limited decay [2]. However continuous exposure to fluctuating moisture contents causes the wood to swell and shrink irregularly, producing internal damage and external surface checking [3]. Each cycle increases the damage to the wood and exposes more of the cell to the water [4], [5]. In addition to the damages caused by the swelling, moisture cycling can also leach out preservatives and extracts that protect the wood from fungi. Because of this, timbers in the splash zone are especially vulnerable to decay and degradation [5].

Fungi consume wood as food. They are made up interconnected hyphae that spread through pits or penetrate the cell walls of the wood. When elongated, hyphae release enzymes that break down the wood to be absorbed by the fungi as food. When sufficiently fed, fungi will produce fruiting bodies and release spores to infect other wood. Fungi compromise the cell walls of the wood and create section loss and weakening in infected areas. Three main forms of fungal deterioration have been identified: brown rot, white rot, and soft rot [5].

All fungi cause decay and section loss. For larger diameter piles, a form of fungal decay called heart rot can be extremely damaging. During treatment, only the first few inches of the piles are penetrated by the preservative, leaving the interior heartwood unprotected. As the timbers dry out, the piles shrink, which in some instances can cause splits and cracks on the surface. Through these splits, fungal spores can enter the inner heartwood and decay the unprotected core. Though the outer material may remain intact, the interior becomes completely hollowed out over time [6].

Insects such as termites, beetles, and marine borers can also be encountered in different environments. Because they consume the wood as a food source, they cause pile section loss and softening. Furthermore, their burrowing creates openings in the wood through which fungi can enter [7].

In streambeds, the erosion of the base of piles is a commonly encountered problem in many applications. Such deterioration occurs from the impact of materials floating in the water and weathering from the flow of the stream [7].

Preservatives

Although numerous oil-based preservatives are available, perhaps the most common is creosote. Creosote-based preservatives are widely used due to their long history of success. In every environment except when exposed to marine borers, creosote performs well. It also protects the wood from weathering and limits checking and splitting from moisture content changes. Unfortunately, creosote makes surface preparation and cleaning difficult. In addition, as an oil-based substance, it is harmful to marine environments and restricted in those applications. Pentachlorophenol and copper naphthenate are also commonly used oil-based preservatives [8].

Water-based preservatives are more expensive but leave a clear surface finish that can be stained or painted. Of these preservatives, Chromated Copper Arsenate (CCA) commonly is utilized in marine and brackish environments to protect against marine borers and mitigate the environmental impact of oil-based preservatives. However, it contains heavy metals and can be hazardous to human health causing its restriction in residential areas. Additional water-based preservatives include copper naphthenate, acid copper chromate, and ammoniacal copper zinc arsenate [8].

Repair Techniques

The following methods were determined to be commonly used by various state departments of transportation (DOTs) for structural repair: concrete jacketing, posting/splicing, supplemental pile placement, FRP shells, and FRP wraps.

Concrete confinement can be utilized for severely deteriorated piles with a section loss of 10-50% and protects the pile from further abrasion and weathering [9]. Furthermore, it provides an increase in compressive strength beyond the original design strength. The surface of the pile in the area to be repaired is cleaned. A steel reinforcement cage is placed around the pile and spacers are used to ensure proper alignment. A flexible form consisting of either a fiberglass jacket or corrugated metal pipe is placed around the pile and secured at the base. After the bottom of the form is sealed, concrete is pumped into the top of the form. After placement, concrete is sloped at the top to allow run off (Figure 1) [10]. In wet environments, cofferdams would need to be constructed around the base of the pile to allow the implementation of the repair method.

Figure 1. Concrete jacketing repair

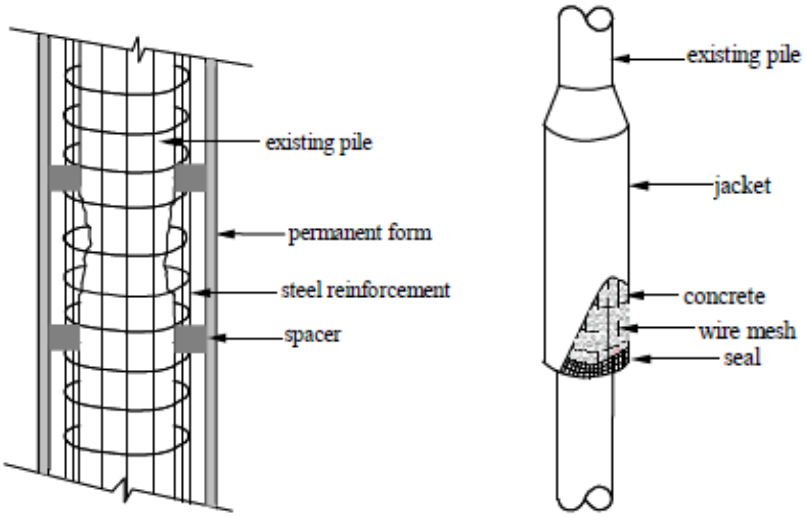

Should the concrete crack, the encased timber will continue to deteriorate. The ability to transfer load between the timber and concrete is considered questionable [11]. In confined spaces, placement of the rebar and jacketing can be challenging [10]. A cheaper version of this repair was reported as being $20 per linear foot not including labor cost [11].

Figure 2. Concrete jacketing installation

Posting/splicing (Figure 3) is utilized for repair of deteriorated piles at or above ground level [9]. It is very useful for badly deteriorated piles with extreme section losses because it completely removes the deteriorated section and replaces it with a whole pile. “Posted” piles can still transfer axial compression forces, but the pile may be weak in flexure [12]. Because of this, only half of the piles for a given bridge substructure can be repaired using this method [10]. AASHTO recommends that timbers on the end bents not be repaired with splicing because the overturning moment on the back wall could cause the splice to fail [1]. To complete a post repair, the area around the pile is excavated and a strut is installed using a hydraulic jack to support the pile cap. The damaged pile is removed below the permanent moisture line. A new treated post is installed in the place of the removed pile and secured [10]. The post section can be secured using a wide range of methods including concrete jacketing, drift pins, steel side supports, epoxy injection, and FRP wraps [13].

Figure 3. Posting/splicing

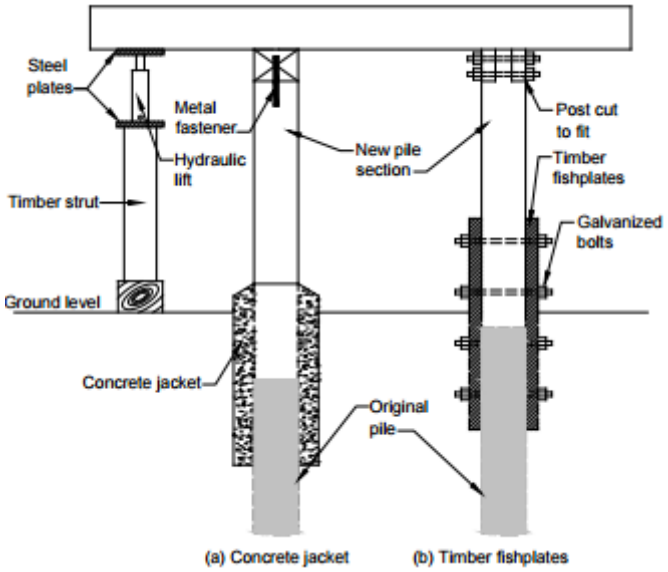

Bridge traffic must be rerouted during repair, while cutting out the damaged section and jacking up the bridge require extensive amounts of equipment. Installing a new post is also very difficult to utilize for spaces with limited clearance. Furthermore, discontinuous load distribution can take place throughout the pile due to the difference in cross section or variations in the timber between the new post and the original pile. Costs can vary for each post between $126- $252 depending on the material used for the splicing not including labor costs [11]. Service life will vary depending on the materials used to secure the posting.

Polyvinyl Chloride (PVC) wraps (Figure 4) utilizes plastic wraps (0.03 in. thick) applied around timber piles and tightened securely around the pile [9]. Piles with losses of up to 10 – 15% of the cross section can utilize this repair method [7]. The wraps can be utilized to protect the pile from abrasion and to prevent further degradation from biological influences such as marine borers and fungus. This is possible by isolating water inside of the wrap from fresh water creating an oxygen-starved environment preventing the spread of further decay [9]. The wraps are especially useful for piles at the splash zone as these areas most susceptible to biological decay.

Figure 4. PVC wraps

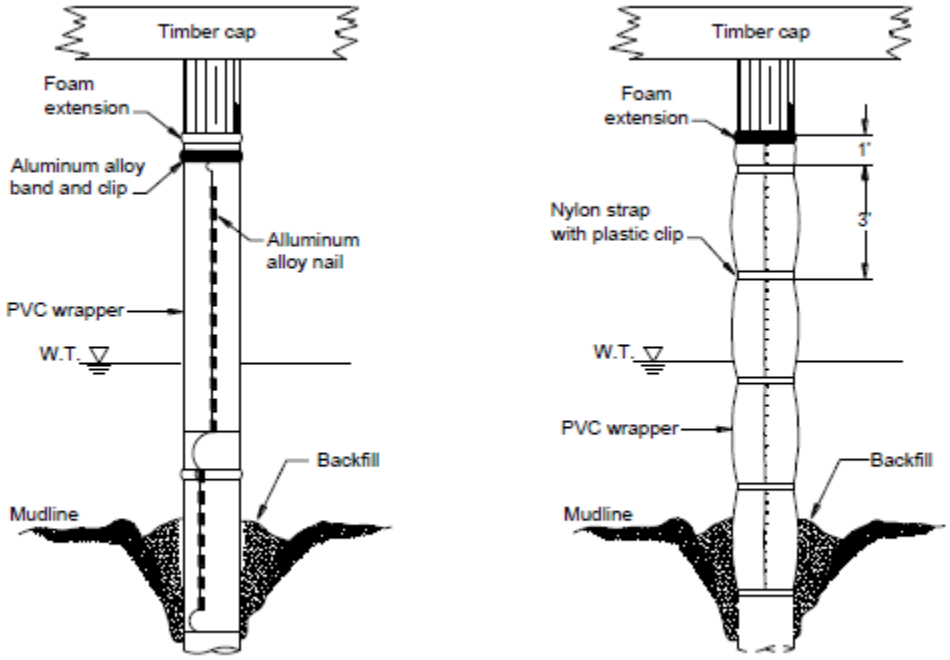

(a) Two-unit wrap (b) Single-unit wrap

For creosote-treated piles, a polyethylene film is wrapped first to prevent a reaction between the PVC and the creosote. Once that is in place, the halves of the PVC wrap are placed around the pile and secured then tightened. The repair method is inexpensive, but it does not restore any structural capacity to the pile, thus making it inappropriate for piles with larger section losses. PVC wraps used on rotting piles can increase the service life ~35 years [13].

Supplemental piles (Figure 5) should be used if the pile experiences section losses too great for other repair methods [9]. The supplemental piles are generally timber or steel columns [1] [13]. An opening in the deck is cut to allow for the placement of the supplemental pile and the pile is driven into the ground. Once embedded, it is laterally pulled to alignment under pile cap and shimmed. For timber piles, a drift pin is installed; for steel piles, expansion bolts are utilized [13]. The repair method is very expensive and requires bridge closure, so it should be considered as a last resort only.

Figure 5. Supplemental pile

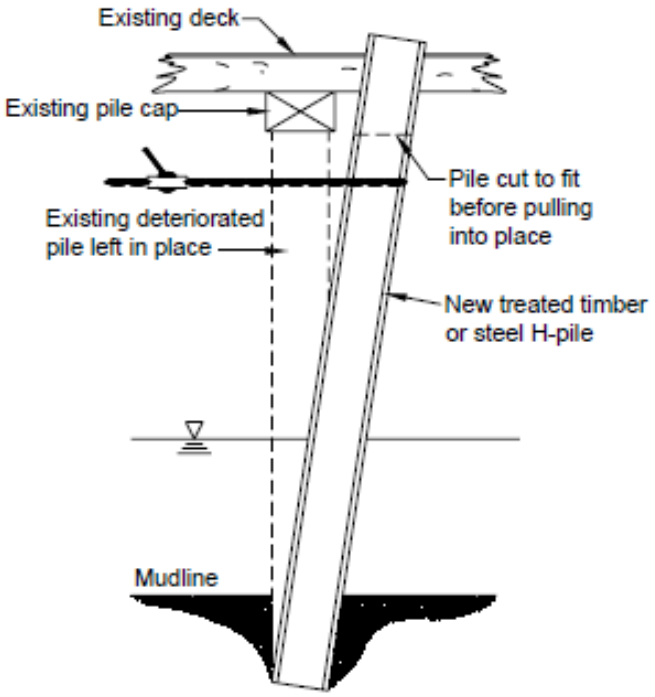

FRP shells with grout (Figure 6) are used in situations that require both structural strengthening and protection from further biological decay. The primary example would be a deteriorated marine wharf pile infested with marine borers. The damaged wood around the pile is removed and the remaining timber treated to ensure the decay does not continue under the repair. The FRP shell is placed around the pile and secured at the base, but an opening remains at the top of the pile. Utilizing this opening, grout (cementitious/epoxy with aggregate) is pumped into the shell. Once cured, the rehabilitation process is complete [13].

Figure 6. Prefabricated FRP shells

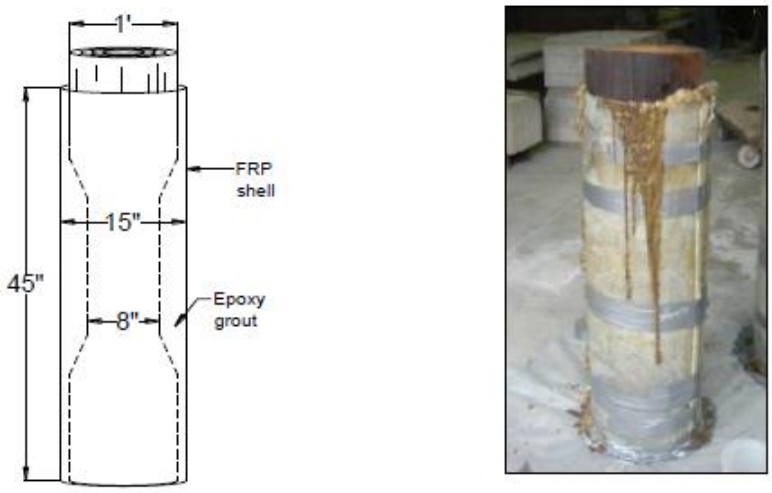

The repair time is relatively quick and typically does not interfere with the daily traffic of the road system. Furthermore, the shell serves the same purpose as the PVC wrap and effectively protects the pile. The repair method is more expensive than other methods, one source citing $600 for linear foot [11]. Additionally due to the higher stiffness provided by the grout, stress concentration could develop above and below the repaired portion of the pile due to the differential stiffness between the two materials [14]. This can result in premature bearing failure.

In a study in Nova Scotia at Halifax Cable Wharf, marine timber piles experiencing severe deterioration from freeze/thaw cycling and marine borers were rehabilitated using glass FRP prefabricated shells (Figure 7). The prefabricated shell consisted of multiple laminates of Tyfo® SHE-51 (E-glass unidirectional laminates) in vertical and horizontal orientations, wherein glass laminates were used to repair the sections with the most damage. The prefabricated FRP shells were placed around the piles and underwater grout was pumped into the shell. The prefabricated shells with grout provide local compressive strength [15].

Figure 7. FRP shell with filler

FRP wraps are utilized in situations that require protection as well as strengthening. Typical practice in marine environments is to remove damaged and decayed portions of the pile and the area is thoroughly cleaned to remove all remaining fungi. Once dried, a filler material (typically resin mixed with wood particles or expanding wood filler) is placed into the void and secured with shrink-wrap until cured. Once the filler has cured and set, the surface is then primed with a coupling agent to improve bonding. After this, the pile is carefully wrapped and smoothed to ensure no voids are present. Typical wrap layers vary from two to five wraps [13]. Once cured, the wraps protect the piles and increase their load carrying capacity. Good strengths, efficient labor utilization, limited traffic disruption, load transfer optimization, and costs make this repair method desirable [16]. One source listed costs as low as $10 - 50 dollars per square foot [11]. WVU-CFC utilized this technique for timber railroad bridge members that were repaired in 2001 [17], 2004 [18], and 2010 [19].

The Oklahoma Department of Transportation investigated the use of FRP wraps coupled with epoxy injection on the Cotton County Bridge. Once the area around the pile excavated, the damaged portions of the piles were removed and cleaned by vacuuming, flushing, and sawing then allowed to dry. The piles were then treated with preservatives. After treatment, aggregates were placed in the voids and two wraps were applied to provide containment. After the wraps cured, holes were drilled and the epoxy resin mortar was injected into the pile and allowed to cure. Exact wrap details and configuration were not supplied, but it appeared to be for confinement purposes. This method was later implemented on 120 piles at 12 different bridges. The Oklahoma DOT has utilized the repair method since 1999 and estimates that the service life of the structure is extended by about 10 to 15 years [6].

In a study in Nova Scotia at Halifax Cable Wharf, marine timber piles experiencing severe deterioration from freeze/thaw cycling and marine borers were rehabilitated using glass FRP wraps and prefabricated shells. The wet layup consisted of Tyfo SHE-51 with saturated with Tyfo SW-1S, an underwater epoxy, and were used primarily just for protection from future decay. However, it was found that the wet layup wraps increase shear capacity and provide confinement [15].

Due to the weakened flexural capacity of posted pile repairs, FRP wraps can be incorporated into the spliced repair to provide stiffness and provide added axial compression capacity (Figure 8). Additionally, the wraps provided protection to the otherwise exposed section [12]. This method has only been evaluated in the lab and has currently not been field tested to the authors' knowledge.

Figure 8. Hybrid method

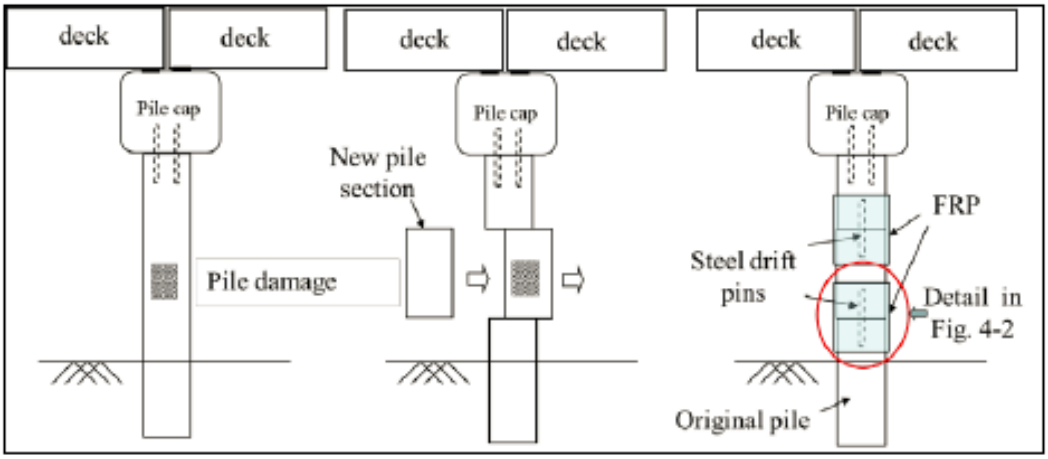

Recommendation

Compared to the other repair methods, FRP wraps are less intrusive, provide strengthening as well as protection from biological decay, and can be more cost effective than other methods such as pile posting and supplemental pile placement. Additionally, placing the wraps is far less labor intensive than moving a very heavy section of wood and replacing it with another section while simultaneously maintaining the original geometric configuration of a bridge superstructure. For these reasons, FRP wraps are a good choice for rehabilitation of deteriorated timber piles.

FRP Design Methodology

FRP Systems

FRP systems are composed primarily of two elements: 1) a fabric made up of fibers that provides the bulk of the strength and 2) a resin system that binds the fibers together and ensures transfer of forces including shear forces. FRP systems may also have additives and fillers, with wrap systems using an appropriate primer to ensure good bond. Selection of the proper FRP system is crucial to design work. E-glass fabric with phenolic resins has been previously utilized by WVU-CFC for pile repair because of its cost and compatibility with creosote-treated timber [19]. The primary fiber types are:

- Carbon: Carbon is utilized for high-end applications such as airplanes. It has high tensile strength to weight ratio, low coefficient of thermal expansion, and good weathering characteristics. They are expensive and have a low strain to failure [20].

- Glass: Glass is the most widely used of the fiber types. It is relatively inexpensive, has good chemical resistance, lower stiffness than carbon, and a high tensile strength [20].

From an economic standpoint, glass is better than carbon due to its cost and widespread use. The primary resin types are:

- Epoxy: Epoxy is a common high strength resin widely used in FRP manufacturing.

- Vinyl ester: A less expensive derivative of the epoxy family, vinyl esters (VE) have been used in the past because of their costs and good strength characteristics.

- Phenolics: Normally used as a wood laminating adhesive, they have shown to perform well with creosote systems. This family includes phenol formaldehyde (PF), resorcinol formaldehyde (RF), and phenol resorcinol formaldehyde (PRF).

- Urethanes: Urethanes typically cure quickly and have superior tensile strength compared to vinyl ester resins. These resins also do not emit styrene fumes. However, they require more work to mold compared to other resins.

The resins system selection is based upon bonding performance considering factors such as moisture, preservative treatments and heat. Material properties of the resin systems will be expanded upon for the final report.

Manufacturing Methods

Prepreg is the pre-impregnation of a fiber matrix with a partially cured resin, usually an epoxy or urethane. It allows for more control over the final fiber distribution and eliminates the need for time-consuming field operations. Because it is a prefabricated material, it is more expensive than wet layup. As the resin is already partially cured, the material has a limited shelf life. Although it has a higher fiber volume fraction and a uniform resin wet-out than wet layups, the higher costs and limited shelf life make it less attractive for field use [21].

Wet lay-up or hand lay-up is the simplest and most widely used FRP manufacturing method. Fabrics are soaked in resin, applied to the timber, and rolled flat using a hand tool. For proper application, the fabric has to be carefully wrung after soaking in resin. Less desirable elements include fumes, labor utilization, non-uniform resin distribution, and longer curing rates. Wet lay-up is the least expensive FRP wrapping method [21].

Filler Materials

The use of filler materials varied among researchers. In a few of the rehabilitation cases, cementitious grout was utilized with the wrapping repair [9], [13], [14]. While the stiffness of the pile increased, such designs caused increased bearing stresses on the sections above and below the repair. As such, it was recommended that bearing areas above and below the repaired area be strengthened with additional wraps and epoxy injection [14]. Another researcher utilized an expanding wood filler epoxy resin mixed with sawdust, which produced fumes and gave off high amounts of heat while curing and is no longer manufactured [9]. For the repair of utility poles, an off-the-shelf wood filler was used to repair gaps and provide a smooth surface for bonding [22]. WVU-CFC has utilized a phenolic resin combined with sawdust to fill large voids [17], [18], [19]. ASTM C881 Epoxy-Resin-Base Bonding Systems for Concrete provides standard grades and types of bonding systems that are likely suitable for timber repair [23].

Design Methodologies and Codes

The AASHTO LRFD Bridge Design specifications state that the nominal axial compression resistance for timber piles is based upon the strength of the pile in compression parallel to the grain, calculated as per Section 8.8.2 [24]. This calculation includes a reduction based on the Euler buckling strength of the pile, which is specified in 10.7.3.13.4 to include the depth under the soil to fixity, but is otherwise based on the adjusted compression strength parallel to the grain multiplied by the area of the pile [24]. The allowable compression strength can be found in Section 8.4.1.4, which lists the same values found in the *American Wood Council's National Design Specification* (NDS). AASHTO specifies various adjustment factors based on the size, condition and time effects. AASHTO specifies that timber piles must conform to the AASHTO M168, which references ASTM D25 for timber piles [25].

Further design information can be found in the following:

- ASTM D25 provides general pile specifications for new timber piles, including straightness, cutting and peeling requirements and minimum butt and tip sizes for different lengths and classes of piles [25].
- ASTM D2899 discusses how to establish the allowable stresses in round timber piles [26].
- The *Timber Pile Design and Construction Manual* (TPDCM) combines information from the NDS and ASTM standards into one complete guide for the design of new timber piles [27].

All of the above sources are developed on the basis that the pile is sufficiently braced. If not properly braced, a pile must be designed according to AASHTO 8.10.2 for loads subjected to both flexure and compression [24].

The information from these various codes and standards will be modified slightly to incorporate simple design calculations for determining the enhancement needed by the FRP wraps.

Currently, no design codes have been established for the wrapping of timber members. In light of this, design philosophies can be modified from the code for FRP wrapping of concrete substrates, ACI 440.2R-08 [28]. These were developed for general use and provide useful requirements on the storage, handling, installation, inspection, and maintenance of FRP wraps in Chapters 5-8. AASHTO also has developed a code FRP repair of concrete members, "Guide Specifications for Design of Bonded FRP Systems for Repair and Strengthening of Concrete Bridge Elements" [29]. The AASHTO manual, in addition to design guidelines for FRP systems, also includes surface preparation and inspection information. The design information is not currently directly applicable to timber structures, but some of the material will be useful for developing design guidelines for timber FRP wraps.

Compressive Strengthening

As FRP wrap is applied to an existing structure, the wood component carries the entire existing dead load from the structure, and the FRP only engages when live load is applied. The strength enhancement provided by FRP wraps for timber columns is not defined in the literature from a mechanics-based approach, but from limited observational data of repaired piles. The only consensus provided is that fully wrapped members with more wraps enhance the compressive capacity of members. The required number of wraps were calculated based on an iterative process not from a design approach. These studies are discussed in more detail below.

Song et al. tested 20 Douglas fir cylinders reinforced with unidirectional carbon fiber wrap. Specimens with one, two, and three wraps were evaluated under compression. During testing, samples with three wraps showed higher stress and strain values than those with fewer wraps [30]. From this study, it can be seen that more wraps increase compression capacity, but this trend does not continue proportionate to the number of wraps.

Najm et al. [31] evaluated 40 poplar timber samples in compression with carbon fiber reinforcement. All samples were short columns to avoid buckling. The carbon fiber reinforcement utilized included unidirectional fabrics and continuous strands wrapped in spirals with varying spacing. Unidirectional sheets were tested in one and three layers each. Evaluating the different configurations revealed that the columns with full confinement from the unidirectional sheet performed well, but those with three fabrics showed even higher performance levels [31]. From this evaluation, it can be seen that fabrics provide higher compression enhancement than strands, and more fabrics are even more advantageous.

Zhang et al. [32] conducted a unique study on cracked columns using different fiber materials (carbon, glass, and basalt) and filling applications for rehabilitation. Seventeen specimens were tested under axial compression, two of them used as undamaged control specimens, three of them damaged by inflicting a longitudinal crack, and the remaining specimens were manually cracked and repaired using different material. Different sections of the retrofitted columns were wrapped along their length at different spacing configurations in order to determine which fiber material and wrap design worked best as shown in Figure 9 [32].

Figure 9. Cracked column with staggered FRP wrap

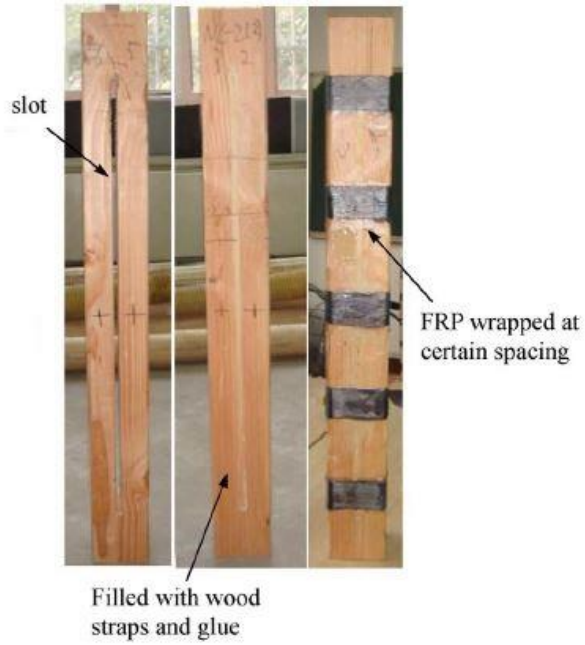

Three wrapped specimens remained unfilled, while the remaining wrapped columns had their cracks filled with glue and wood straps. After testing, it was determined that smaller spacing between wrapped sections of the column yielded a more efficient retrofitting effect. It was also shown that the retrofitting effect of the FRP sheets become stable with more than three layers of FRP applied over the full length of the timber columns. Carbon yielded the most effective repair out of the three different fiber material tested. It was determined that applying CFRP at a spacing of 60 mm, plus filling the crack, can increase the axial capacity of the cracked column by more than 20%. It is also recommended to chamfer the edges of the square column in order to avoid stress concentrations on the wrap [32]. Carbon wraps however at not generally used for bridge pile repairs due to their cost.

Hagos utilized unidirectional glass FRP wraps for the rehabilitation of damaged columns using grout as filler material (Figure 10). For his testing, he assumed that the grout carried

most of the load. Based on this assumption, he calculated the number of wraps to be used based on concrete confinement theory. While not directly applicable because of the grout, he determined that two wraps provided more strength than one [14].

Figure 10. Hagos wrapping scheme

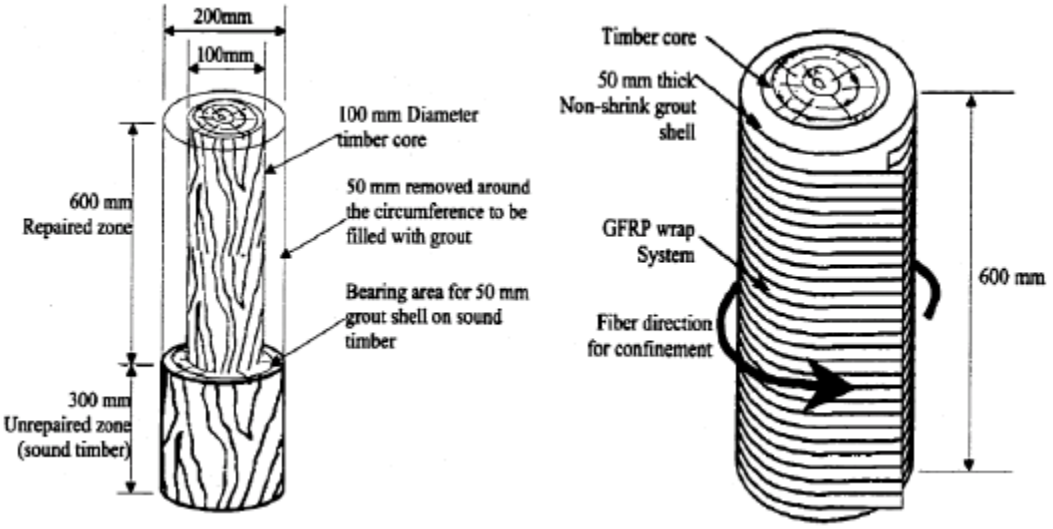

The Illinois Transportation Center used FRP wraps to enhance the capacity of piles repaired with posted sections. Members were evaluated in compression and compression-flexure. The number of wraps required to obtain strengths greater than the un-retrofitted capacity was determined by trial and error. The number of wraps used varied from 9-10, with the wrap restraining and preventing expansion at the joint between the old pile and the new post. The axial capacity was already significantly enhanced by the new pile section [12].

Field repaired sections from the Oklahoma DOT study [6] used to repair 11 piles at the Cotton County Bridge were removed from service and tested under axial compression testing with the transverse reinforcement. The repaired core showed the best results as shown in Figure 11. Comparing the axial compression test values to the published design values from the *National Design Specification for Wood Construction* revealed that all of the strengthening methods exceeded the published design values as shown in Table 1.

Table 1. Comparison of experimental values to published design values

	Design
Repaired Core without Reinforcement	+50%
Transverse Reinforcement with wood Core	+91%
Transverse Reinforcement with Repaired Core	+237%

Figure 11. Load vs. deflection graph of piles tested

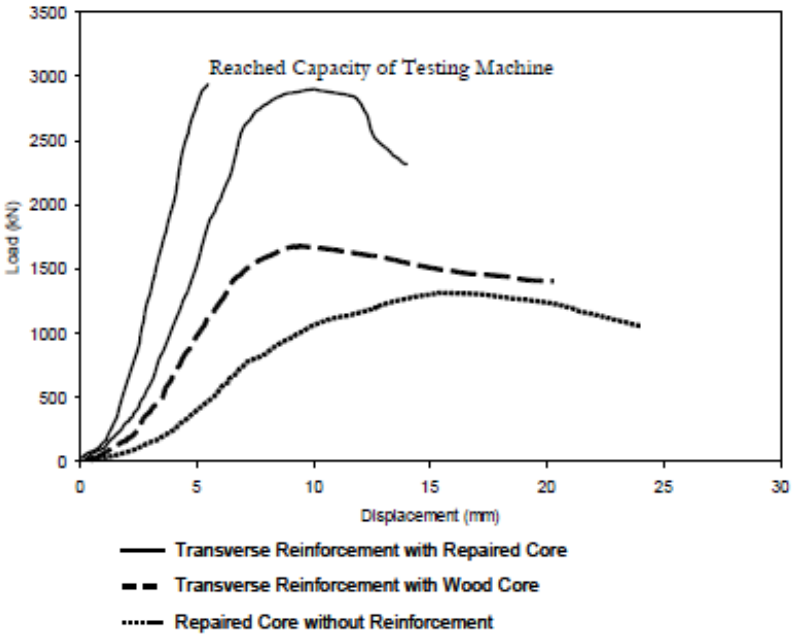

Field-testing was carried out by Iowa State University and WVU-CFC to determine the strength of restored piles. In this method, the force transferred to piles is measured before and after repair, using strain gages, and the decrease in strain indicates if the load is being more evenly distributed to the repaired section. Iowa State used three different loading configurations to the bridge shown below (Figure 12) and the load transfer among the piles was measured. In this particular bridge, concrete encasements were used to repair two of the damaged piles. The strains on the concrete and the piles were measured under the load configurations shown. It was discovered after testing that the strain in the concrete was less than the strain in the timbers. It was assumed that this was due to the greater cross-sectional area and modulus of elasticity of the concrete. Two other load configurations were used. From these readings, it was determined that the concrete encasements took 50 and 70 percent of the load imposed on the respective piles [13].

Figure 12. Example of strain gage placement on piles

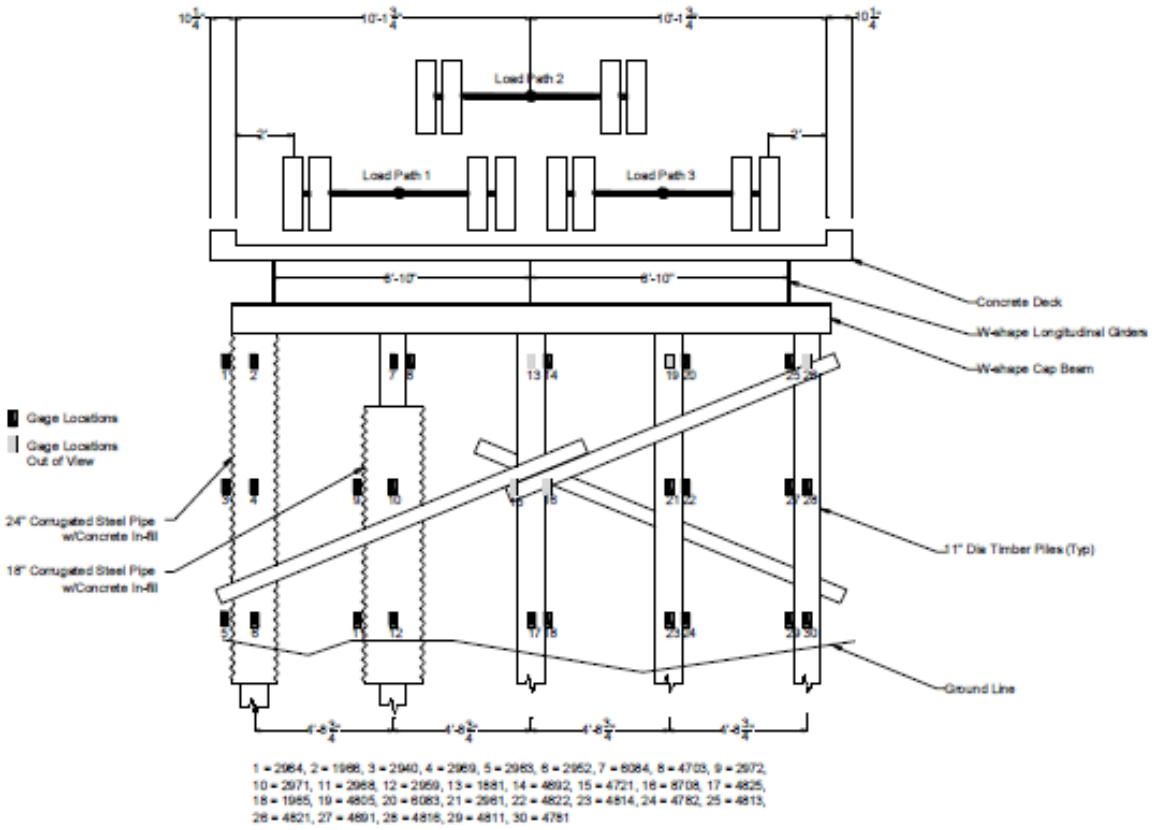

WVU-CFC utilized a similar method when testing their repair of railroad bridges. An 80-ton locomotive was used to apply dynamic and static live loads to the bridge before and after the piles were repaired. If the overall strain readings were decreased throughout the various piles, the repair was considered adequate. Such tests were done on Bridge 568 and Bridge 574 along the South Branch Valley Railroad (SBVR) owned by the West Virginia Department of Transportation (WVDOT).

Bridge 568 contained a pile bent that had undergone severe decay as shown in Figure 13. Previous rehabilitation efforts to restore pile capacity had failed; therefore, FRP wraps were used to rehabilitate the piles [18].

Figure 13. Bridge 568 repaired pile bent

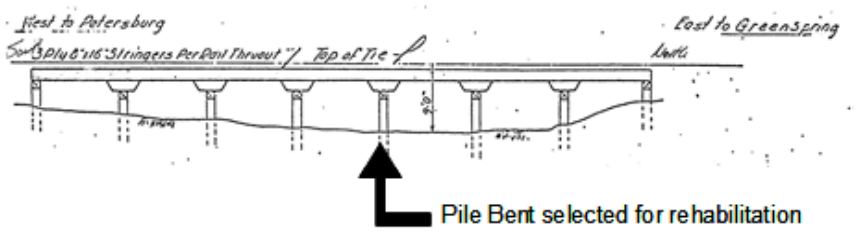

For Bridge 568, the locomotive was used as a static load directly over the pile and as dynamic load with speeds of 5, 10, and 15 mph. Strain gages were placed as shown in Figure 14 before and after rehabilitation. After the repairs were completed, the same loading was applied on to the piles and readings were retaken.

Figure 14. Strain gage locations at Bridge 568

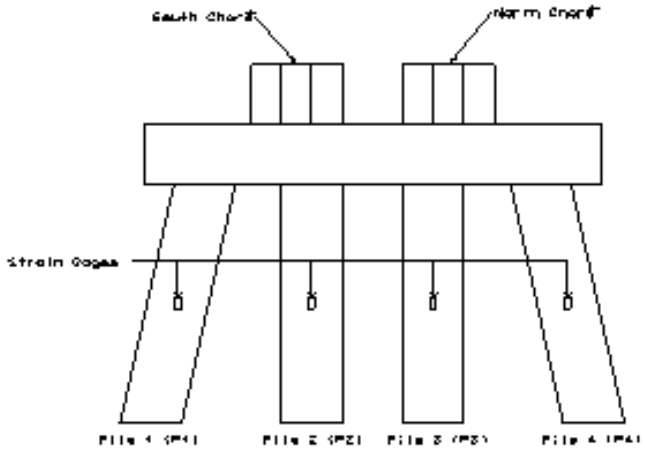

As shown in Table 2, the rehabilitated members displayed a more even load distribution between the piles indicating an increase in the overall capacity of the members.

Table 2. Change in strain following rehabilitation for Bridge 568

	Static	5 mph	10 mph	15 mph
Pile 1	28%	29%	42%	41%
Pile 2	52%	75%	83%	75%
Pile 3	78%	78%	81%	80%
Pile 4	14%	20%	0%	20%

Bridge 574 contained submerged pile bents that required rehabilitation as shown in Figure 15. A cofferdam was placed to divert the flow of water and piles were repaired using FRP wraps [33].

Figure 15. Rehabilitated section of Bridge 574

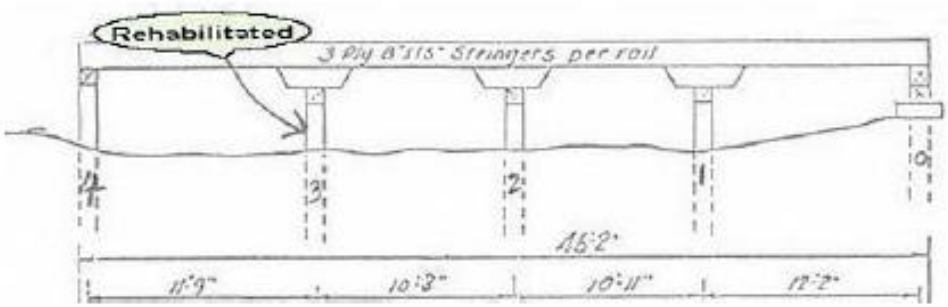

Strain gages were placed on all the piles including the un-retrofitted one as shown in Figure 16. An 80-ton locomotive was used to apply various load configurations before and after the repair to determine the enhanced strength provided by the wrapping. Readings on pile four were not readable before the repair took place and have been neglected.

Figure 16. Strain gage placement on Bridge 574

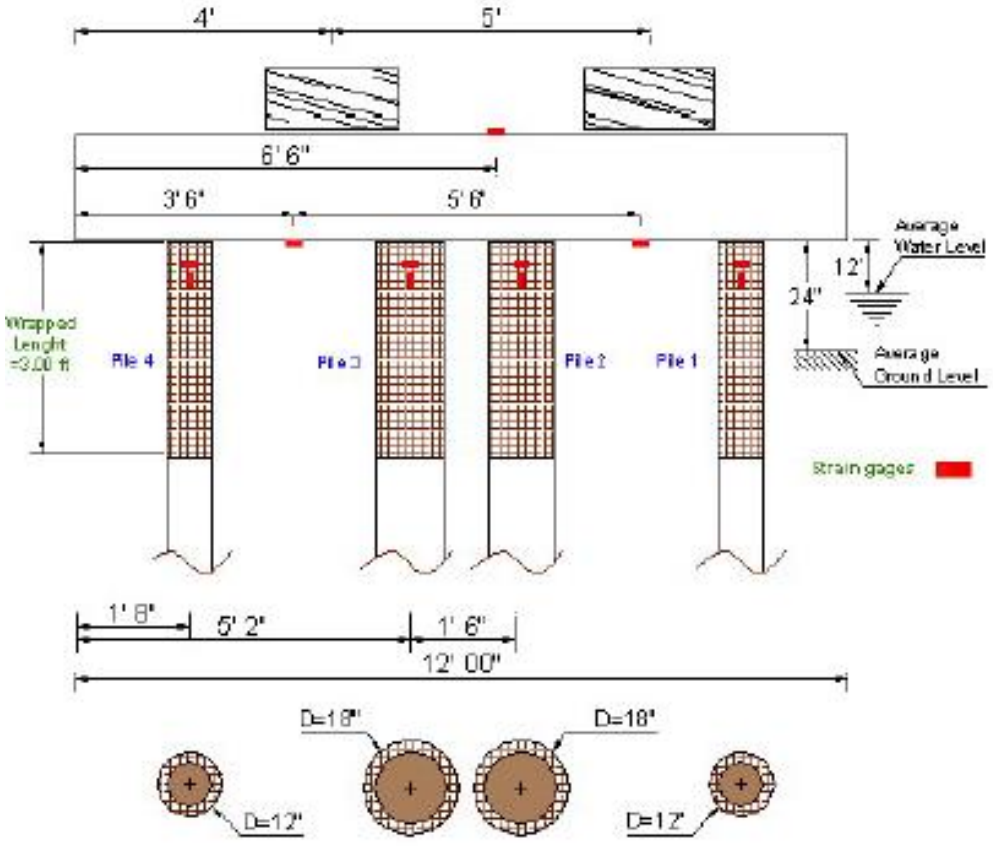

From the evaluation, it was found that the piles strains (Table 3) were reduced indicating a more even load distribution between the piles.

Table 3. Change in strain following rehabilitation for Bridge 574

	Front Wheel	Rear Axle	Front Axle	3rd Wheel	2 mph	15 mph	**Average**
Pile 1	26%	29%	16%	21%	38%	57%	**31%**
Pile 2	0%	12%	2%	18%	14%	11%	**9%**
Pile 3	21%	43%	27%	38%	33%	37%	**33%**

From the review, it would appear that two to three wraps are reasonable for even load transfer to the piles, but further testing is needed to determine the most cost-effective solution.

Poles under Bending

FRP flexural repairs are not directly applicable to the repair of piles, as FRP repair intended to primarily restore flexural capacity is much different from the one to restore axial capacity in terms of the bond strength required and fabric layout. However, this information could be useful for the limited flexural loads seen in a braced pile system.

Electrical poles up to 30 years old were repaired with epoxy/E-glass FRP wraps in tandem with off the shelf wood fillers as shown in Figure 17. The Tyfo S fluid epoxy was used to impregnate the FRP and as a primer on the timbers. Tyfo SHE-51A fabric was used with three 0° unidirectional layers in the axial direction and one 90° layer in the hoop direction. More wraps in the axial direction provided more stiffness under bending loads. Bending tests indicated that the repaired piles returned to approximately 85% of their original capacity. The report recommended for flexural strengthening that 80% of reinforcement should be orientated in the axial direction with the remaining 20% used for confinement. Additionally, the report recommended the length of wrap to be the full length of the damaged area plus one diameter of the pole on either side [22].

Figure 17. Electrical poles with FRP wraps

FRP Timber Bonding

The bond between the FRP and timber is critical to transferring the forces over a repaired area. In concrete members reinforced with FRP wraps, the overall strength gain is through the additional strength in the concrete gained via confinement [28]. However, it is not clear if this effect would be the same with repaired timber members, as decay mechanisms in timber cause voids in the cross section, reducing confinement effects. Thus, a perfect bond between the FRP and timber is needed, thus sealing the timber away from the decay mechanisms. While in theory such an assumption is reasonable, obtaining a perfect bond can be difficult. The bond strength is impacted through various factors including surface preparation, curing rate, curing pressure, moisture, resin/primer combinations, preservative treatments, chemicals, and aging.

Surface Preparation and Bonding Procedures

From the literature review, it was discovered that strong bonds depend upon surface preparation, surface moisture, installation pressure, curing time, and resin/primer type including its compatibility to the substrate.

Before applying the FRP wrap, free or loose material should be removed from the surface of the wood so adhesion will be directly with the main wood surface. After the removal of loose material, the pores of the wood surface should be opened to allow the adhesive to enter increase interlock. Methods commonly used in factories settings include sawing, sanding, or cutting by knife [34]. While cutting with a knife produces the most desirable finish and leaves open pores without residue, sanding would be most reasonable preparation method for field applications. Like planning with a knife, sanding opens up the pores of the wood, increasing wettability. Well-sanded surfaces are flat, allowing an even spread for the adhesive which improves the bond. Despite these benefits, sanding intensely can abrade portions of the wood substructure weakening the surface. Furthermore, sanding can leave a layer of dust in the pores that inhibits bonding [34]. Because of this, it is recommended that the surface should be lightly sanded with high grit sandpaper. Once a surface is sanded, it should be cleaned or vacuumed to remove the sanding dust, then the adhesive should be applied immediately to prevent the collection of contaminates on the surface [35]. For field installation, the most imperative issue would be creating a smooth surface and removing loose material. Therefore, despite its drawbacks, sanding would still be a reasonable surface preparation method. AASHTO provides information about surface preparation for concrete included in 1.2.2 that are helpful [29].

For factory bonding, it is recommended that the wood be conditioned to the same moisture content that the wood will be subjected to in the field [33]. This is done to minimize the

development of hygrothermal stresses as the wood swells. Elements that were preconditioned showed better durability than those that were dry and later exposed to moisture [36]. That said, too much moisture prevents bonding because the pores are filled with water, preventing the adhesive from entering the pores. If the surface is over dried, resin or oil extracts can diffuse to the surface of the wood [35]. For field applications, it would be more important to have a dry surface to create strongest bond than to be concerned about moisture cycling as this will occur at the water line. It would be more reasonable to select a moisture compatible resin. For many resin types, the surfaces should be dry, which requires diverting the water and drying the wood if possible.

Proper application of pressure is important because it forces out entrapped air, brings the adhesive into contact with wood, squeezes the adhesive into a uniform film, and holds curing FRP in place. For cold curing applications typical for fieldwork, it is suggested to apply pressure for 15 minutes to 24 hours [35]. Failing to apply uniform pressure results in weaker-than-expected bonds between the wood and FRP [37]. Manufacturers have specific pressure ranges for their adhesives, which should be followed to the best of the contractors' ability during field installation of FRP wraps.

While a more detailed discussion on the performance of primers and coupling agents will be conducted in the following sections, they are important for the improved bonding of plastics to both treated and untreated wood. Common coupling agents (primers) found [38] in the literature are hydroxymethylated resorcinol (HMR), resorcinol formaldehyde, and polyurethane. HMR was developed in the 1990s to improve bonding of epoxies, vinyl esters, and phenol resorcinol formaldehydes with CCA-treated and untreated wood [38], [39]. Resorcinol formaldehyde as discussed previously is a wood adhesive. Polyurethane has shown to produce good bonds between plastics and wood [38]. The performance and application of these primers will be discussed in detail below and their application generally improves bond strength [39].

Bond Evaluation Methods

Bond effectiveness can be determined destructively by evaluating shear strength under compressive loads, delamination under cyclic aging, and pull-off strengths under tension.

To characterize the bond between FRP and timber, several different ASTM tests have been utilized. Bond strength is often characterized by shear strength, bond delamination, and pull-off strength.

ASTM D-905 titled "Standard Test Method for Strength properties of Adhesive Bonds in Shear by Compression Loading" was originally designed to evaluate wood-to-wood

adhesion, but has been modified to evaluate FRP to wood adhesion [40]. The specimens with adhesive sandwiched between two wooden plates are tested in a shearing apparatus until failure. Adhesive performance is based on the shear capacity of the bond and the percentage wood failure obtained [40]. The American Institute of Timber Construction specifies 1075 psi for shear capacity and an 80% wood failure for dry samples. The majority of the literature presented utilize the two criteria for their shear evaluations [41].

ASTM D2559 titled ”Standard Specification for Adhesives for Bonded Structural Wood Products for Use under Exterior Exposure Conditions” is used to mimic exterior exposure conditions for laminated materials. The testing specifics include delamination testing under accelerated aging conditions as well as shear testing on “stair step samples” and creep evaluation under static loads. Most of the research presented below that utilized this standard, did so for the accelerated exposure test. Laminated samples are soaked in water under vacuum-pressure cycling for two cycles after which they are oven dried, ending the first cycle. The samples are returned to the pressure vessel at which point they were exposed to steam then pressurized water. After both treatments, the samples are oven dried, ending the second cycle. The first cycle is then repeated again. The samples are visually examined for bond delamination as indicated by a gap between the two laminates. The percentage delamination is expressed as the total delaminated length around the entire specimen divided by the total bond length multiplied by 100. The standard specifies that delamination for soft woods and hard woods should not exceed 1% and 1.6% respectively [42].

ASTM D7522 titled “Standard Test Method for Pull-Off Strength for FRP Bonded to Concrete Substrate” has been successfully utilized by WVU-CFC to evaluate the bonding strength of FRP wraps to concrete piles. By modifying this method for timber with FRP wraps, valuable comparative data can be gathered. This test method uses 2-in. diameter carrier that is bonded to the FRP surface on an area previously (hole) cut to create a distinct test area and then pulled off using a calibrated tester [43].

Moisture Influence on FRP/Timber Bond Durability

Moisture negatively affects the bond between FRP and wood due to the hygrothermal stresses developed by the swelling of the wood [44]. Researchers have evaluated the shear and delamination of various combinations of FRP, resins, primers, and timbers under dry and moist conditions to determine which systems produce effective bonds. Table 4 summarizes the most effective resin systems as evaluated by the respective researchers (listed by the first author only).

Table 4. Summary of most effective resin systems evaluated in literature[1]

Researcher	Wood	Treatment	FRP	Primer	Resin
Gardner	Poplar	None	Pultruded VE	None	RF
Raferty	Spruce	None	Pultruded VE	None	PRF
Ghasemzadeh	Red Oak	None	None	None	RF
Talakanti	Red Oak	None	Wet Layup	RF	Epoxy
Davalos	Red Oak	None	Wet Layup	HMR	Epoxy
Lopez-Anido	E. Hemlock	None	Pultruded VE	HMR	VE
Raferty	Spruce	None	Pultruded VE	Yes	Epoxy
Herzog	Yellow Pine	Creosote	Vacuum Bag	HMR	Epoxy
Laosiriphong	Red Oak	Creosote	Wet Layup	PRF	RF
Anegunta	Red Oak	CCA	Wet Layup	HMR	Epoxy
Lyons	Yellow Pine	CCA	Wet Layup	HMR	Epoxy

[1]Most effective resin from each study.

To demonstrate the effects of moisture on FRP wood bonding, Gardner et al. evaluated the shear capacity and delamination durability of yellow poplar bond to pultruded vinyl ester FRP with resorcinol formaldehyde, emulsified polymer isocyanate (EPI), and epoxy under wet conditions. From the testing, RF was shown to provide the best bond under wet conditions. Epoxy and EPI performed poorly. Epoxy in dry conditions did produce the greatest percent of failure in the wood substrate. Delamination testing of polyester FRP bonded with RF showed 100% and 80% in dry and wet conditions [44].

In another study, five adhesives including melamine urea formaldehyde (MUF), polyurethane (PU) and phenol resorcinol formaldehydes (PRF) were used to bond three different types of pultruded FRP composites to untreated Sitka spruce specimens under dry and wet condition. RF was excluded due to cost at the time. Shear and delamination testing revealed that PRF produced the most durable bonds of the resins evaluated [45]. As shown in Table 5, different formulations of phenolic adhesives have different effects on the strength loss.

Table 5. FRP-wood shear strength

Resin		Dry (psi)[1]	Moist (psi)[1]	Strength loss
PRF1		1175	1146	2%
PRF2		1160	899	23%
MUF		928	0	100%
PU		1305	1175	10%
EPI		870	841	3%

[1]Estimated Values from Charts

Similar results were found by Ghasemzadeh et al. in his evaluation of wood-wood bonding of untreated red oak. ASTM D905 shear testing was conducted on dry and soaked samples. The resins evaluated included epoxy, urethane, RF, PRF, Bi-epoxy, and polyester. Upon testing, epoxy and urethane were found to have the highest strengths under dry conditions (<19%) but performed poorly when soaked. Consistent with the other research, the RF showed superior wet shear performance to other adhesives as shown in Table 6 [46].

Table 6. Wood-wood shear strengths

Resin	Dry[1] (psi)	Wet[1] (psi)	Strength Loss[1]
Epoxy	2750	450	84%
Urethane	2150	450	79%
RF	1750	1200	31%
Phenolic	1150	750	35%
Bi-Epoxy	1000	100	90%
Polyester	750	50	93%

[1]Estimated Values from Graph

Using an aging method modified from Chow et al. to accelerate the aging of wood [47], Talakanti evaluated epoxy, polyurethane, polyester, RF, and PRF in shear testing according to ASTM D905. The fabric used was E-glass, and the timber was untreated red oak. Epoxy displayed the highest shear strength unaged but had lower strengths when aged as consistent with other research. The polyurethane FRP failed in the fibers. Such failure occurred because the resin did not fully saturate the fibers due to its high viscosity. The phenolic adhesives evaluated both had lower strengths in the unaged and aged conditions but retained roughly half of their strength after aging (Table 7). Compared to other phenolic adhesives evaluated in other studies, these values are drastically lower for dry conditions because during curing no pressure was applied, a step crucial to bond development [37].

Table 7. Shear performance of resins used to bond FRP to red oak

Resin	Un-aged (psi)	Aged (psi)	Strength Loss
Epoxy	1400	150	89%
PU	575	300	48%
Polyester	225	150	33%
RF[1]	250	150	40%
PRF[1]	175	75	57%

[1]No Clamping Pressure Applied

While phenolic adhesives on untreated timber showed good bonding, epoxies were badly affected under moisture exposure. However, the application of primers improved the performance of epoxies in moist conditions.

Using resorcinol formaldehyde as a primer, epoxy and polyurethane samples were evaluated under wet and dry shear conditions. Compared to unprimed values, epoxy showed increased strengths while polyurethane with the RF primer performed poorly [46].

Using the RF as a primer, Talakanti evaluated epoxy with and without the primer using a severe aging process. With a properly cured RF primer, the epoxy shear strength was enhanced in aged conditions [37].

Table 8. Epoxy shear strengths with RF primer

Resin	Primer	Un-Aged (psi)	Aged (psi)	Strength Loss
Epoxy	None	1400	150	89%
Epoxy	RF[1]	1200	600	50%
Epoxy	RF[1]	2000	1000	50%

[1]Pressure not applied to primer

Davalos evaluated the wet and dry shear strengths of epoxy with RF and HMR primers and phenolic adhesive on red oak. Table 9 shows that epoxy/HMR had higher wood failures and strengths under wet and dry conditions than the epoxy/RF combination and the phenolic adhesives [48].

Table 9. Comparison of HMR and RF primers

Resin	Primer	Dry (psi)	Wet (psi)	Strength Loss
Phenolic	None	1033	976	6%
Epoxy	HMR	1396	1030	26%
Epoxy	RF	1279	732	43%

Davalos et al. later evaluated the facture toughness of FRP wood samples bonded with phenolics against epoxies with primers. Under wet and dry conditions, epoxies with HMR displayed higher fracture toughness than phenolics and epoxy/RF samples [49].

Lopez-Anido demonstrated that HMR improved the bonding between vinyl ester and eastern hemlock in both dry and wet conditions via ASTM D905 as shown in Table 10 [50].

Table 10. HMR enhancement for vinyl ester resin

Resin	Primer	Dry (psi)	Wet (psi)	Strength Loss

PRF	None	967	614	37%
VE	None	605	289	52%
VE	HMR	861	645	25%

Raferty also confirmed that epoxies with primers improved moisture performance by evaluating three different epoxies under delamination testing, but the primer applied is one not commonly used in the United States [51].

Alexander examined wood to FRP bond durability through chemical kinetics. The phenol resorcinol formaldehyde (PRF) and epoxy/HMR adhesives tested were projected to undergo 30 percent bond strength degradation after 57 and 34 years respectively. Control wood-wood laminates were projected to display 30 percent bond strength reduction after 12 years. During shear testing on the bond interface, epoxy/HMR exhibited strengths 23% greater than PRF. Both systems were deemed acceptable for outdoor use [52].

Creosote negatively affects the bond performance of the system, and without primers, successful bonding was not achieved or bond strength is significantly reduced. While various adhesives have been evaluated, epoxy with HMR primer and resorcinol formaldehyde with a phenolic-based primer have been most successful.

An example of creosote's negative affects was presented by Tascioglu et al. who evaluated the performance of FRP wood bonds using PRF using oil-based creosote preservatives. Creosote can penetrate the resin matrix and create inter-laminar shear stresses in the bond, reducing the strength [53]. The results (Table 11) indicated that without a primer, bonding with creosote is very difficult.

Table 11. Negative effects of preservatives

	Untreated	**CDDC**	**Cu-N**	**PCP**	**Creosote**
Pre-treated	2.8	26.5	48.4	55.4	45.7
Post-treated	2.8	16	12	23.9	11.9

To verify successful resins for bonding with creosote, Herzog evaluated creosote-treated yellow pine bonded to epoxy, polyurethane, and vinyl ester glass FRP and vinyl ester carbon FRP. An HMR primer was applied to all wood samples to improve bonding. ASTM D905 shear and ASTM D2559 delamination tests were conducted on treated and untreated wood samples under dry and wet conditions. As indicated by the results, epoxy/HMR showed high strengths in shear with wood failures in the 90% range for both wet and dry conditions. Vinyl ester also showed good results but failed in wet shear. Polyurethane produced very poor bonds (this agrees with finding by Ghasmezadeh [46]). Under ASTM 2559, the epoxy/HMR

and vinyl ester delamination were 42% and 21% respectively (Table 12) and the delamination was deemed too severe [54].

Table 12. Performance of FRP with various resin types

Treatment	Resin	Primer	Dry (psi)	Wet (psi)	Strength Loss
Creosote	VE/Glass	HMR	1461	1153	21%
Creosote	Urethane	HMR	817	678	17%
Creosote	Epoxy	HMR	1475	1315	11%
Creosote	VE/Carbon	HMR	2133	1888	11%
None	VE/Glass	HMR	1656	1086	34%
None	Urethane	HMR	1634	941	42%
None	Epoxy	HMR	2148	1026	52%
None	VE/Carbon	HMR	3149	217	93%

Laosiriphong evaluated the shear strength of adhesive bonds between creosote-treated wood and glass fabrics in aged and un-aged conditions by using shear block samples prepared according to ASTM D-905. This study also utilized the modified aging method created by Chow et al. [47]. Different resin/primer combinations were used. PRF with RF primer, RF with PRF primer, PRF with phenol formaldehyde primer, and epoxy with phenol formaldehyde. Under aging, the epoxy samples completely separated and were deemed inadequate. The resorcinol formaldehyde adhesive with the phenol resorcinol adhesive primer produced the highest shear strengths under aged conditions. While low, the values as shown in Table 13 were deemed acceptable [55].

Table 13. Performance of FRP/timber bonds on creosote-treated wood

Resin	Primer	Un-aged (psi)	Aged (psi)	Strength Loss
Epoxy	PF	Debond	Debond	Debond
PRF	RF	1325	566	57%
PRF	PF	985	530	46%
RF	PRF	2041	614	70%

To expand the study beyond the coupon level, half scale creosote-treated red oak ties were aged using the same procedure. At the time of the study, PRF was unavailable for purchase so a resorcinol primer was utilized instead due to similar properties. Three-point bending tests were conducted on unwrapped and wrapped samples before and after aging. Wrapping improved the flexural rigidity and shear modulus by 13%-44% and 9%-18% respectively. Strength reduction of 17% under aging for both non-wrapped and wrapped samples were assumed to indicate that bond degradation under aging was limited under fully wrapped conditions [55].

Two researchers loosely evaluated the effects on creosote on the stiffness of beams in three-point bending. Houshmandyar used a polyurethane primer with a vinyl ester glass FRP to wrap creosote-treated beams. The testing compared beams flexural rigidity of beams with and without the polyurethane primer. Testing showed that beams with polyurethane had twice the flexural stiffness of those without, which was attributed to the creosote negatively affecting bond [56]. Talukdar tested creosote-treated Douglas fir beams reinforced with polyester glass spray layup technique with HMR and a two-part polyurethane primer. The flexural rigidity and ultimate load of the beams treated with HMR were lower than the ones treated with the polyurethane primer [57]. Both tests, while useful for demonstrating the effectiveness of polyurethane, do not provide enough evaluation to verify its performance using standard adhesive evaluation methods.

Table 14. Creosote-treated beam performance

Researchers	Primer	Improvement vs. none (%)
Houshmandyar	Polyurethane	183%
Talukdar	Polyurethane	17.9%
Talukdar	HMR	5.7%

The authors were unable to find any studies on the performance of FRP wrapped members subjected to water immersion. Laboratory research on concrete cylinders wrapped with epoxy-based GFRP wraps subjected to wet/dry conditions with seawater showed strength decreases up to 3% to 18% [58]. The result varied based on the type of epoxy used, and it is not clear if these results would be applicable to the resin systems used for timber. More research is needed in this area.

Conclusion

From the review, several conclusions can be gathered.

First, proper surface preparation and installation procedure are important to creating durable bonds. Surface preparations that open up the pores of the wood and increase wettability are most desirable. The surface must be adequately dried and primed. Proper pressure is needed to remove air voids.

Phenolic resins with primers performed very well on creosote wood specimens under aged conditions. Epoxy coupled with HMR primers performed better than those with RF primer or no primer in every application. Epoxy with phenol resorcinol primers on creosote-treated wood is not an effective solution. Resins with lower viscosity were more effective at saturating fabric fibers and penetrating wood pores. Two part systems showed higher overall strengths. Polyurethane performed poorly because its high viscosity prevents proper

saturation of the fabric during application. However lower viscosity polyurethane might produce improved results.

Field Implementation

Field implementation includes field installation techniques, quality control, assurance, and costs.

Field Installation Procedures

The following field installation procedures were followed for the majority of the pile repairs conducted by WVU-CFC with pictures from internal WVU-CFC files. Piles were repaired in 2001 [17], 2004 [18] & [59], and 2010 [19]. The steps involve site preparation, removal of decay, sanding of piles, priming piles, filler placement, fabric placement, pressure application, and sealing, as is detailed in the following sections using the references listed above.

1. Site Preparation

Debris and soil around the base of above ground portion of piles must be removed to allow for load transfer between the sound pile section underneath and the damaged section as shown in Figure 18. If the pile is submerged, a cofferdam or some other method for diverting water should be used (Figure 19). When the pile is exposed, it should be dried with a portable heater but at a low enough temperature to avoid creosote ignition (<130 °F).

Figure 18. Pile excavation

Figure 19. Removing excess water

2. Removal of Decay

Once the area around a distressed pile is clear and dried, the decayed portions of the pile should be removed and discarded (Figure 20).

Figure 20. Removal of decay

3. Sanding Pile

After removing the deteriorated material, the piles are then sanded down using hand sanders (Figure 21) to open up the pores of the wood for adhesion and to provide an even bonding surface. Sanding also helps remove loose portions of the wood that could create weak bonds.

Figure 21. Sanding pile

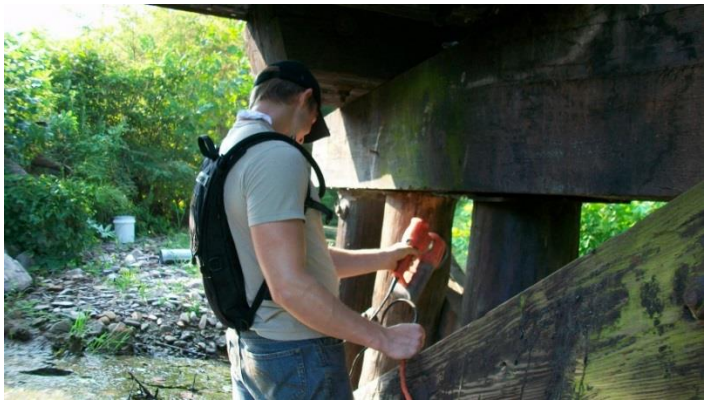

4. Priming Pile

Immediately following sanding, the piles should be primed. WVU-CFC has successfully used phenolic-based adhesives as primers in the past. Once the primer is placed, it should be cured as per manufacturer's recommendations.

5. Filler Placement

Any gaps, checks, or heart rot were filled with a sawdust/resin mixture (Figure 22). Depending on the consistency desired, the sawdust content could vary from 20% - 50%, which is determined by adding sawdust until the mixture is as thick as possible while still being able to be poured into the pile (roughly the consistency of honey). As resin flow depends on temperature, the amount of sawdust must be adjusted based on-site conditions.

Figure 22. Primed and filled pile section

6. Fabric Application

After the primer and the filler material dried, the FRP fabrics soaked in phenolic adhesive were applied to the piles. The widths of the fabrics were no more than 22 in. and lengths were limited to 2-3 layers around the pile based on pile degradation (for 3 layers wrapped around a 10 in. pile is around 94 in. in length). Starting at the bottom and wrapping upwards to avoid water pooling on fabric, the ends of the wraps were initially stapled to the woodpile to ensure a tight wrap and to avoid wrinkles.

7. Pressure Application

Shrink wrap was applied after the fabric was placed and voids were filled by pushing on the fabric by hand to remove wrinkles and ensure the fabric is in intimate contact with the timber. After curing for 24 hours, the shrink-wrap was removed.

8. Sealing

After wrapping, a phenolic-based adhesive was applied to the exterior of the wrap and around the edges to seal the surface and protect the bond from moisture (Figure 23).

Figure 23. Sealing with phenolic

For future work, the inspection processes provided in *ACI* [28] and *AASHTO* [29] design guides for FRP wraps for concrete piles could be utilized as a guide for quality control to the installation process.

Quality Control/Quality Assurance

As recommended by ACI [28], witness panels can be made according to ASTM D7565 to ensure that the FRP composite matches the material properties required [60]. Witness panels are made in the field using the same materials and techniques as the wrap installation on the piles. They are installed on a material that will not bond to the FRP, such as plastic sheeting. These panels can then be taken to the lab for testing to verify material properties using ASTM D3039 [61].

Once the FRP has been installed, it would be necessary to evaluate the in situ bond integrity. WVU-CFC in the past has used visual inspection, infrared thermography (IRT), digital tap hammers (DTH), and pull-off testing [62] as are recommended by ACI [28]. Both IRT and DTH are nondestructive methods while pull-off testing causes localized damage to the FRP that is repaired by patching.

Under visual inspection, the surface of the FRP is evaluated for signs of wear such a detachment or peeling. The wrap is also inspected by tapping it with a hammer and listening for hollow areas, but this is a highly subjective evaluation method [28].

Infrared thermography can be used to evaluate the FRP wrap as shown in Figure 24. Before evaluation, the area in question is heated to penetrate the material into wood, but too much heat causes damage to the resin. Immediately following heating, an image is taken with an infrared camera, which displays the surface temperature in different colors. On a fully bonded surface, the heat will dissipate freely, but if a debond is present, the gap will act as thermal insulator. As a result, an air-filled debonded area will have a higher temperature resulting in a brighter color. Using this method, voids and debonds can be easily detected.

Because of slight irregularities that are naturally present in FRP wrapped systems, it is recommended that the temperature difference be greater than 3-4 °C to qualify as a hot spot. This method has been used on timber and concrete structures [62].

Figure 24. Infrared testing

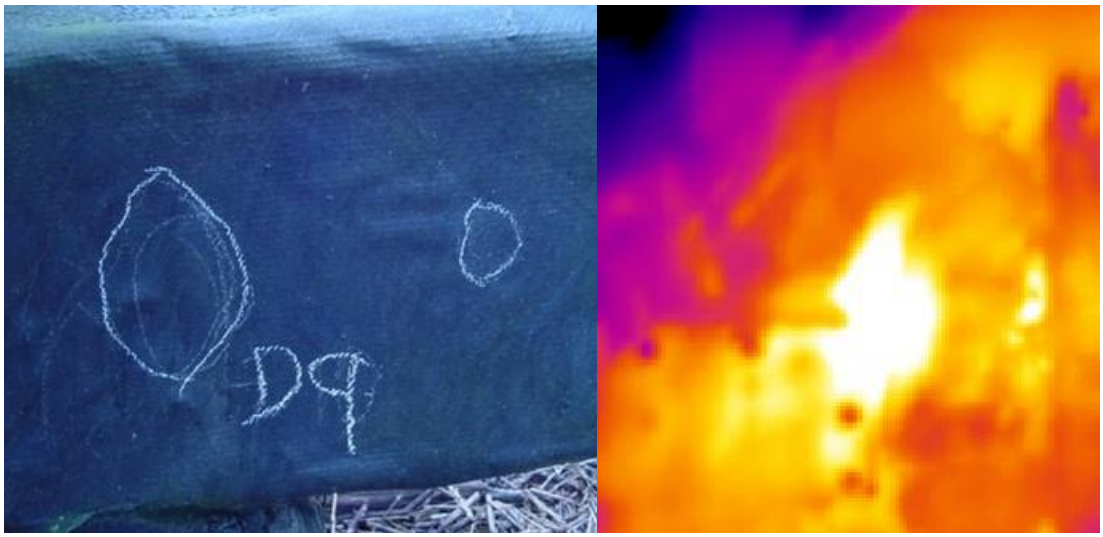

An ultrasonic digital tap hammer can be used as a quantitative evaluation compared to hammering and listening. Tap hammers display a calibrated number when a surface is hit which measures the time for an ultrasonic wave to reflect from the hammer to an accelerometer. Lower numbers indicate a stiffer surface while higher numbers indicate voids or de-bonds. Because the tap hammer is a localized measurement, examining large areas is time consuming. However, it can be helpful for confirming the infrared readings. This device has been successfully utilized on concrete and timber substrates by WVU-CFC [62].

As mentioned briefly in the bonding section, pull-off testing can be utilized to determine localized bond strength. The pull-off testing does cause localized damage to the FRP. The standard followed for pull-off testing that will be utilized is ASTM D7522 [43].

Cost Evaluation

In 2010, WVU-CFC repaired 57 piles with 1485 square ft. of wrap. The cost of materials and supplies totaled $5,203, and the total research project cost $53,000 including labor and overhead [19]. The repair technique used in Oklahoma is only for use on intermediate pile bents and not abutment piles and is estimated to cost between $2,000 to $3,000 per repair [6]. It should be noted that most of the projects done to date have been demonstration projects and likely do not accurately reflect high volume costs by outside contractors.

Summary of Literature Review

The following recommendations from the review are listed below:

Repair System: Due to the costs, rapid repair time, and lack of disruption, a wet-layup FRP wrap system is recommended.

Fabric: E-glass fabric is recommended because of lower costs, higher strengths, and good durability. Fabric configurations of 0/90 or unidirectional are recommended for pile wrapping.

Number of Wraps: Unlike concrete, which has a standard for calculating the strength of FRP-wrapped columns, the number of wraps for timber pile rehabilitation is not well defined. In most of the literature, a minimum number of two to three wraps was applied. Each additional wrap will increase the strength, but not proportional to the number of wraps, but it also increases the material costs. The data in the literature is insufficient to develop design guidelines for timber piles repaired with FRP.

Resin Systems: Phenolic based resins and primers have proven to be effective in previous situations so their continued application would be reasonable. From the review, it was indicated that lower viscosity resins (~100 centipoise) performed better as they were able to fully saturate the fiber and flow through gaps and pores of woodpile.

Filler Material: A commercially available filler of putty consistency could be utilized for smaller checks and splits, while a high viscosity resin mixed with a filler material could be used to fill larger voids. Fillers with the same stiffness as the original material are most desirable to limit bearing failure above and below repaired area. Because of this, cementitious fillers will be avoided. After applying the wrap, voids can develop leading to further debonding. A high viscosity resin, either vinyl ester or epoxy (~1500 centipoise), could be injected to fill these voids.

Protective Coatings: A protective finishing coat is recommended to protect the FRP wraps from moisture and abrasion. Phenolic-based adhesives have proven to satisfactorily protect FRP repaired pile. UV protective coatings are highly recommended if one is not specified by the manufacturer.

Failure Modes of FRP Wraps On Timber Piles

For FRP wrap repairs, four failure modes are possible: (1) compression failure in the timber, (2) loss of composite action between the FRP and the timber (i.e., bond slippage), (3) local compressive failure (crushing) of the FRP wrap, and (4) global buckling of the FRP wrap.

Timber Compressive Failure

In the field, degradation between timber piles can vary widely depending on the life of the pile and the environmental conditions in specific locations. Due to this variability of degradation, it is challenging to accurately predict the capacity of decayed timber from a design point of view. To eliminate such a large uncertainty, it is therefore most effective to assume that decayed portions of timber in zones of repair contribute zero compressive capacity. Any extra capacity will simply be in addition to that accounted for in the design. Compressive failure in timber outside the repair area would have been previously accounted for in the design of the timber pile and will not be considered.

Loss of Composite Action between Wrap and Timber (Bond Slippage)

For FRP wraps on columns, two types of strengthening mechanisms can be utilized: “contact critical” or “bond critical”. For concrete columns, FRP wraps are often used for “contact critical” application meaning the wraps provide passive confinement and do not fully engage until the concrete is dilated or cracked [28]. Alternatively, “bond critical” systems provide bending, shear, and axial enhancements from the start of external loadings.

For the purposes of design, FRP wraps on timber piles will be assumed to operate as bond critical systems since the behavior of the decayed timber under a contact critical application would be difficult to accurately predict. For bond critical systems, failure occurs when the timber and wrap separate from each other (bond slippage) resulting in the loss of composite action between the timber and the wrap. Such a slippage negates the additional strength provided by the wrap returning the pile to its original strength and behavior. In light of this, timber/FRP wrap slippage has been considered a critical area for evaluation in this study.

Much information is available on coupon size specimens related to FRP/timber bonding, but information on global FRP/timber bond slippage is limited. Therefore, to accurately determine the bond slippage strengths, full-scale bond evaluations were conducted on new, creosote-treated timber piles (to eliminate the irregularity present in decayed timber and to account for influences from preservatives). Ultimate bond slippage strengths have been determined for different bond development lengths to allow designers to comfortably specify bond lengths for field installations.

Tensile pull-off testing exists to determine bond strength adequacy in field installed wraps applied to concrete (ASTM D7522). For quality control purposes, it is reasonable to use a similar method to establish baseline pull-off strength values to correlate with field installed values in the field.

Compressive Failure of Wrap

In addition to bond slippage, FRP wraps can fail in compression through crushing based on compressive strength (load per area). The overall capacity increases based on the thickness of the composite (number of layers), while the strength plateaus quickly with additional layers. Should such a failure occur, the wrapped section immediately loses substantial strength, as the wrap can no longer resist any extra load.

While compressive design strengths for FRP products are provided by some manufacturers, they are based off small-scale specimens (i.e., less than 1 in. wide) evaluated by ASTM standards and these small coupon specimens do not necessarily predict the compressive behavior of full-scale repairs. Therefore, full-scale samples in the form of hollow tubes manufactured with different numbers of wrap were evaluated in axial compression until failure. By coupling compressive strength with wrap thickness (varying layers of wrap) and testing hollow tubes (neglecting timber capacity), the results provide designers with accurate strength values per number of wraps.

Buckling of Wrap

For global (Euler) buckling equation to be valid, the repaired FRP section must span a significant distance given the cross section of a pile, i.e., roughly 10 ft. without bracing for a typical 12-in. diameter hollow composite with ¼-in. thick walls with 50% of the fibers in the longitudinal direction. Thus, the crushing capacity governs the compressive strength of the FRP repair. Global buckling will be not considered as a failure mode for design purposes.

Objective

Design guidelines for load capacity and service life improvements are needed for full implementation of timber pile repairs using FRP wraps. Repairs with FRP must be safe and cost-competitive compared to traditional repair techniques. The research team proposes to provide a cost-effective and durable solution to timber pile repair in Louisiana.

The objectives of this research project were to determine the best FRP wrap materials and in-situ rehabilitation techniques to be used for repair through literature review and laboratory testing and to develop a simplified design methodology for the rehabilitation of timber piles. Strengths of both legacy splice mechanisms and FRP wrap splicing were analyzed to determine if FRP wrapping provides an adequate replacement in order to be implemented in the field.

Scope

The scope of the proposed work was as follows:

- Conduct a literature review of rehabilitation of timber piles
- Evaluate the axial load capacity of timber pile repaired with wet-layup FRP wraps assuming the timber does not contribute to the strength of timber piles
- Evaluate shear, bending, and axial strength capacities of pile systems using the FRP wrap splice and make comparisons to pile systems with traditional splice mechanisms
- Identify fillers that are suitable for repairing section losses in timber piles
- Develop a design procedure for repairing timber piles with FRP wraps
- Develop the following guide documents:
    - Construction specifications
    - Load rating methods
    - Field inspection techniques of FRP repaired timber piles
- Conduct workshops and field demonstrations to train personnel

Methodology

Materials

Timber Specimens

Timber specimens were used in bond evaluations, pull-off testing, and full-scale simulated rehabilitation. Testing was conducted on new timber piles to provide a uniform result. New timbers were selected due the variability present in deteriorated piles from the field that would influence the test results. Timber piles were provided in 8-ft. lengths and treated with creosote before shipping. Pile diameters varied from 10 in. to 12 in. A chain saw was used to cut the piles into the required portions for each tests as shown in Figure 25. While effective at cutting the pile into appropriate lengths, the hand held saw made it difficult to create straight cuts consistently. Therefore, on many of the timber specimens, surfaces are often non-parallel, which created small, amounts of eccentricities during testing resulting small amounts for column bending induced stresses. Any influences from these eccentricities are covered in the test discussions.

Figure 25. Cutting timber specimens

FRP-Wrap Systems

For this study, FRP systems using glass fibers were selected as these are relatively less expensive than other fabrics such as carbon or aramid, and have a similar elastic modulus to timber, which prevents stress concentrations. Furthermore, these systems have been previously used to rehab timber piles. A list of properties for each system is shown in Table 15.

Table 15. FRP system properties

Name	Fabric	Fabric Type	Fabric Density	Resin
Fyfe	SHE-51A	Unidirectional	27 oz/yd^2	Tyfo S Epoxy
Sika	Hex100G	Unidirectional	27 oz/yd^2	Sikadur Hex 300 Epoxy
Simpson Strong-Tie	CSS-CUGF27	Unidirectional	27 oz/yd^2	CSS-ES Epoxy
Phenolic	Vectorply	Bidirectional	18 oz/yd^2	Cascophen G-1131 Phenolic
Aquawrap	G-05	Bidirectional	22 oz/yd^2	Pre-impregnated polyurethane

Filler Materials

Fillers must be employed during rehabilitation to replace wood section loss due to deterioration and to prevent further decay. Prior to wrapping, external cracks on the pile must be sealed and exterior section loss must be repaired. These high viscosity fillers are intended to fill holes and cracks around the external surface of the pile. For this reason, the resin and putty must have sufficient resistance to flow to allow the fillers to cure in place, i.e., without flowing out of the cracks and holes. Thus, crack fillers must have high viscosities, thus fillers that meet ASTM C881 Grade-3 (non-sagging consistency) are considered ideal. For this project, the following external fillers were used:

- Sikadur 31 Hi-Mod Gel is a two component, non-sagging, epoxy paste that meets ASTM C881 Grade-3 specifications. It is tack free in 1.5 to 2.5 hours.
- Elmer’s ProBond Wood Filler is a water-based paste filler commonly used to fill voids in wood construction. It dries in 12-24 hours.
- Simpson Strong Tie ETR is a two-component epoxy paste with a non-sag consistency and quick cure times. Cure time is not known.

- Internal voids can be filled by pouring in a filler material, which should exhibit flow-ability, i.e., ASTM C881 Grade-1. Evaluation of these materials included both the resin itself and the resin mixed with sand to increase the yield.

- Sikadur 35 Hi-Mod LV is a two-component epoxy that meets ASTM C881 Grade-1 specifications for gravity feed of cracks. The viscosity is 375 cps and it will be tack free at 3-3.5 hours at 73°F.

- Cascophen G-1131 Phenolic resin is the same resin used for the FRP-wrap system, which WVU-CFC utilized as a filler on previous projects. It has a viscosity of 415-565 cps. It gels in 30-50 minutes at room temperature, with faster gel times at higher temperatures.

- Rimline SK 97014 is a polyol that when mixed with Suprasec 9701 iscocynate produces a polyurethane foam and is commonly used in resin transfer molding of structural composite products. WVU-CFC selected this product as it has a viscosity of 400 cps but expands as it cures, enabling it to fill the entire void area. The cured structural foam is not as rigid as the epoxy or phenolic resins, though quantifying the confined compressive strength is outside the scope of this project.

Finally, any voids found after wrapping the pile with FRP should be filled during construction to ensure a strong bond and aid in monitoring during later inspections. These fillers are injected with a syringe or adhesive dispenser (caulk gun) via holes drilled through the wrap. To ensure that the voids are filled, low viscosity resins should be used.

- Sikadur 35 Hi-Mod LV, previously described under bulk fillers, can also be injected. Injection was completed using a large syringe.

- Sikadur Crack Fix is a two-component epoxy with the same formulation as Sikadur 35 Hi-Mod LV, but it comes packaged in single tube cartridges that fit into standard caulk guns.
- Simpson Strong-Tie Crack-Pac Flex H_2O is a polyurethane injection resin that expands when exposed to water, and it is designed to work in wet environments. Depending on moisture and temperature, the foam will completely expand to 20 times the original size in as little as 3 minutes.

Bond Testing (Push Out)

The bond test concept is to apply a load to the timber and support the sample only with the FRP system, thus forcing the FRP/timber bond to carry the entire load. Due to the flexible nature of the fabrics during curing, it is difficult to create a uniform base without some form of mold that has the same shape as non-uniform timber pile. This issue is compounded by the fact that the mold must provide for a gap that does not resist any load, but is still capable of holding firm during wrapping. Finally, direct bearing of the composite on the loading surface could result in fiber crushing in the composite at the expected service bond load levels. While crushing of fibers is an issue because of the bearing on the steel plate, no such drastic change in stress will take place in the field, as the pile will be a continuous member. Therefore, the fiber crushing encountered is simply a test related issue.

After several test iterations, it was found that 6-in. and 12-in. bond lengths were realistic representations for short and long bond lengths. To prevent direct bearing failure or the FRP, a small piece of timber was used to provide a load transfer mechanism from the wrap to the loading platen at the bottom of the sample to prevent crushing of the fabric. A bond breaker was applied to create a controlled bond area accurately while accounting for the variability of hand lay-up. Figure 26 provides a visual representation of the components described above.

Figure 26. Testing schematic of pushout testing portions

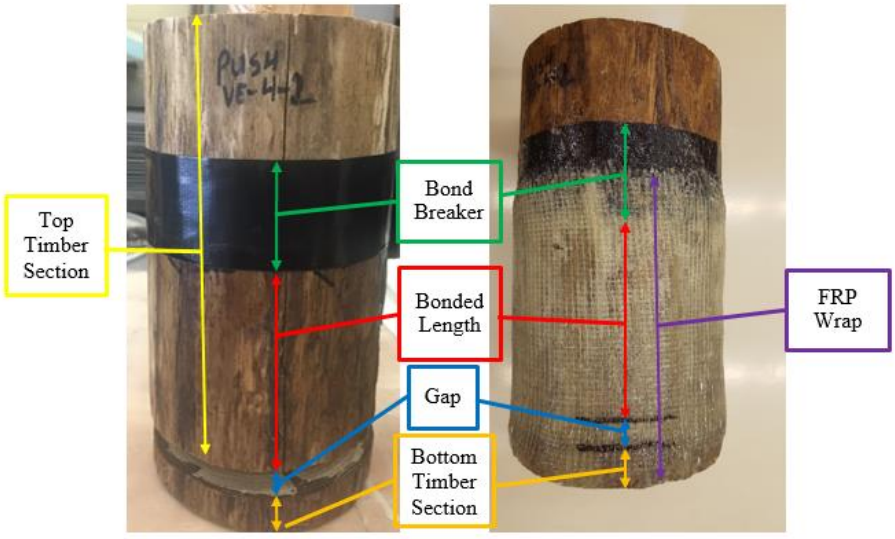

To create a gap between the timber sections, insulation was placed between the lower and upper portions of timber stubs to prevent the fabric from slipping into the gap and keep pooling resin away from filling the gap. It was further determined that additional layers of reinforcement around the base of the test specimens prevented the composite from buckling in the gap due to local discontinuities or crushing on the load platen. A gap of 1/2 in. was found to be adequate to allow slippage but not cause buckling in the gap.

From a design perspective, the primary concern was determining the axial load capacity per length of bond to be used in a design. Therefore, no strain behavior was evaluated.

In order to evaluate average bond strength of FRP composite wraps on timber, timber piles were wrapped with the FRP systems with 6-in. and 12-in. bond lengths. Three of each bond lengths were done for each commercial system (Table 16). Unidirectional fabric systems were wrapped with three layers to create a (0/90/0) laminate configuration with 0 indicating the longitudinal direction. Bidirectional fabric systems were wrapped with three layers, with the fibers being aligned in the longitudinal and hoop directions. Additional layers were applied around the base to provide additional buckling and bearing support.

Table 16. Bond strength testing iterations

FRP System	Short (6-in. Bond)	Long (12-in. Bond)
Fyfe	3	3
Sika	3	3
Simpson Strong-Tie	3	3
Phenolic System	3	3
Aquawrap	3	3

For the 6-in. bond length specimens, timber was cut at 10 in. with a 2-in. base portion. For the 12-in. bond length specimens, timber was cut at 16 in. with a 2-in. thick bottom. After cutting, the bond specimens were assembled with the ½-in. thick insulation sandwiched between the top (bond section) and bottom (2 in.) timber portions then screwed together with 3-in. screws. Insulation was later trimmed to match the circumference of the timber (shown in Figure 27) and putty was applied to fill any voids created during the trimming of the insulation.

Figure 27. Unwrapped timber bond specimen

Samples were then sanded on the surface with an electric palm sander to remove some of the creosote clogging the pores of the timbers to allow for resin penetration, which would improve the bond strength as shown in Figure 28. Wax paper was installed at the top of the specimen to provide a bond breaking material that ensured a consistent bond length during wrapping and ensured that the testing would apply load only to the timber.

Figure 28. Sanding of bond specimens

Samples were wrapped after sanding and the installation of the bond breaker. First, primer consisting of the saturating resin used was applied to the surface of the pile for the Fyfe, Sika, and Phenolic systems (Figure 29). Aquawrap did not provide a primer, but used water to activate the process; therefore, the piles were sprayed with a layer of water instead of applying a primer. Next, wraps with the dimensions shown in Table 17 were saturated by hand with the saturate resin (Figure 30) until the surface of the fibers were just beginning to show a coating of resin but not completely submerged with resin. The exception to this process was the Aquawrap, whose wraps were sprayed with water before applying them to the piles (shown in Figure 31). Once saturated (activating the prepreg resin) the wraps were wrapped tightly around the timber samples as shown in Figure 32 and secured in place with stricture wrap (shrink-wrap) to provide uniform pressure during curing. The stricture wrap was originally provided for the Aquawrap. It was also used for the other systems to provide consistent pressure application for each system. The pressure was critical in producing a strong bond between the timber and the wrap.

Table 17. Fabric dimensions for bond test

Type	Height (in.)	Length (in.)
6-in. Bond	10	38
1-in. Bond	16	38

Staples were used on the bottom 2-in. section of pile to provide additional load transfer to the 2-in. timber base. No staples were used in the upper bond test area as they would provide additional strength that is not realistic in the field as metal staples would rust and fail under field conditions.

Figure 29. Apply primer to smaller mock up sample

Figure 30. Apply resin to wraps for smaller mock up sample

Figure 31. Spraying of Aquawrap for bond testing

Figure 32. Wrapping smaller mock sample

After curing, the screws were removed and the ½-in. thick insulation was dissolved with acetone via holes drilled into the bottom of the base. The insulation and acetone were used exclusively for this particular lab test to create the gap required to allow for bond slippage, and it does not represent a procedure that would be utilized in field repairs. The loading surfaces were cleaned of any excess resin and the edges of the composite were trimmed flush with the timber at the base to ensure a uniform loading of both the wrap and the 2-in. base. Samples were allowed to cure for at least 7 days before testing. The resins cured within 24 hours, but 7-day cure was done to allow for full bond strength development.

Testing Apparatus

Specimens were evaluated under compression on WVU-CFC's Instron 1000HDX universal testing machine at a loading rate of 10,000 lbf per minute. To provide a large enough bearing surface for the 10-in. to 12-in. diameter piles, 2-in. thick steel plates were attached to the machines. The configuration for the test is shown in Figure 33. A typical bond test is shown in Figure 34.

Figure 33. Schematic of bond test

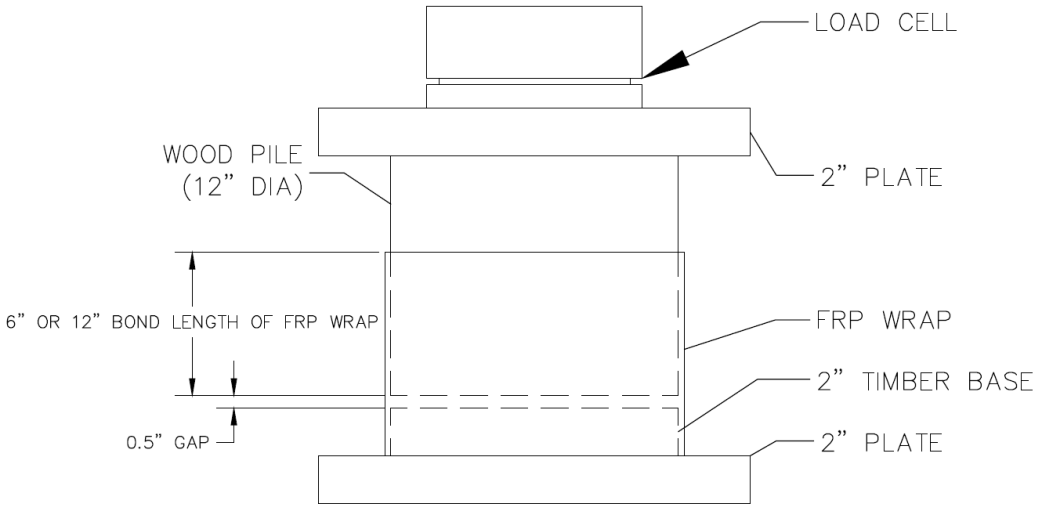

Figure 34. Testing configuration for bond test

The samples were loaded at a constant rate until slippage occurred. Slippage was determined based upon evaluating the load versus deflection plots obtained for the results similar to the example shown below in Figure 35. The point at which the bonded portion of the wood began to slip was identified to be the highest load on the graph. Notice in Figure 35 that substantial deflection occurred even after slippage at much lower than maximum loads; this indicates the top portion sliding down into the gap. Evaluating the graph of position versus time (Figure 36) clearly shows the point at which the bond slipped, as indicated by the rapid increase in deflection (horizontal) with very little increase in time (vertical). The samples

were evaluated after testing by cutting the wrap into two halves and separating it from the timber to assess the failure mode.

Figure 35. Example of pushout load vs deflection plot

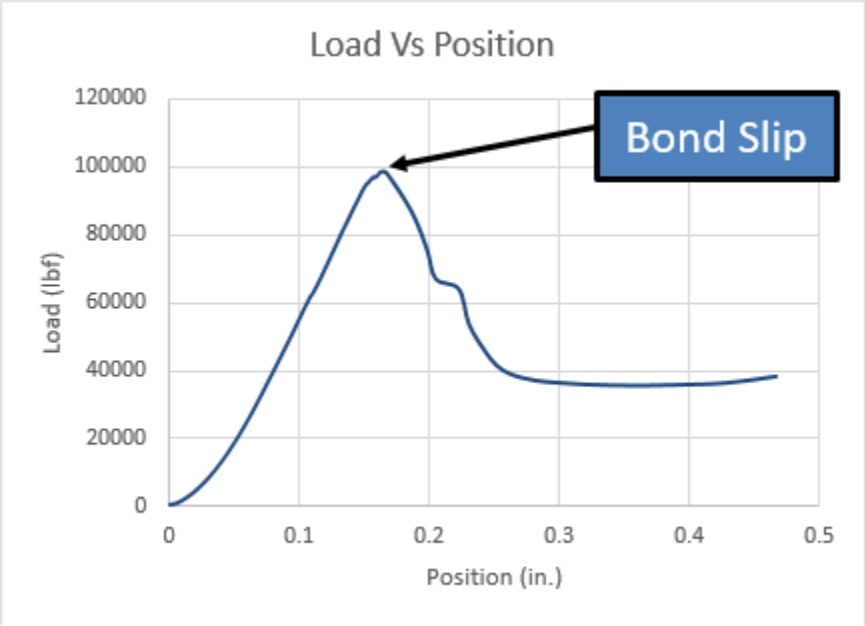

Figure 36. Example of deflection over time for pushout tests

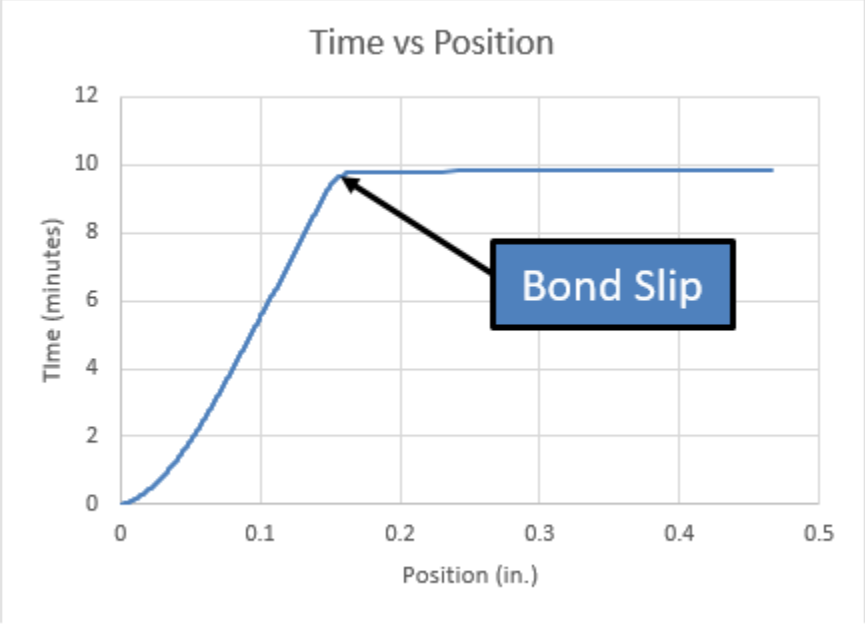

Aging Bond Tests

Aging tests were conducted to evaluate the effects of moisture through wet/dry cycles on bond strength and pile load capacity. Two 12-in. bond samples of each wrap system were prepared in the same manner as the bond testing and evaluated using two tanks. The samples were divided between the two tanks, and one of the tanks was filled with domestic water. Every 6 hours, a timer turned on a sump pump, which cycled the water to the other tank. Thus, half of the samples were submerged for 6 hours while the other half were dry. This process was conducted constantly for four months, from September 15, 2017, to January 15, 2018. Figure 37 shows the specimens in an empty tank after the aging simulation was complete. Figure 38 shows the specimens underwater during the saturated phase of the cycle.

Figure 37. Aging specimens in tanks

Figure 38. Saturated aging specimens

Once the samples aged, they were removed from the tanks and tested under compression in the same manner as the bond test samples as discussed previously.

Pull-Off Bond Test (Modified ASTM D7522)

Test Development

While the bond testing could provide a value of bond strength in laboratory conditions, evaluating installed FRP systems for proper bonding in the field is equally important. For concrete samples, ACI recommends using ASTM D7522 to establish the bond strength of FRP bonded to concrete. To use this test method, a 2-in. inner diameter core drill is used to cut into the FRP and concrete to a depth of 1/4 to 1/2 in. A 2-in. diameter-loading fixture (carrier) is bonded to the FRP using high strength epoxy. After curing, a tension force is applied to the carrier via a tester and the failure load and failure type is documented. However, there are no similar ASTM test procedures for FRP bonded to timber. In light of this, pull-off tests were conducted on the FRP systems bonded to creosote-treated timber piles using ASTM D7522 to provide a general range of values and to correlate these values to the bond values determined during bond testing.

Specimen Preparation

Pull-off testing specimens consisted of four timber pile portions (8 in. tall, 10 in. diameter) each wrapped with one of the composite wrap systems. Five pull-offs were used on each system. Before wrapping, the piles were gently sanded to remove loose splitters and to open up the pores of the timber for bonding. The timbers were primed by applying the resin used to saturate the fabric in a thin, even layer around the circumference of the pile. Exception to the priming process was the Aquawrap preimpregnated system and does not provide a primer resin for application. Three layers of saturated FRP wrap were applied using hand lay up around the pile's circumference. Stricture wrap was applied for all systems with uniform pressure around the wrapped portions to remove voids and prevent layers from experiencing delamination before the composites were fully cured.

After curing for at least 7 days, specimens were prepared for pull-off testing. First, the composite was drilled with a 2-1/8 in. composite hole-saw through the FRP. Next a 2-1/8 in. wood hole saw completed the cut 1/4 to 1/2 in. into the timber. This was done to ensure a localized bond strength was being tested and to prevent contributions from the rest of the bond area. Consistent cutting was ensured by a small wooden plate with a hole that matched the hole-saw diameter attached with screws as shown in Figure 39. The plate allowed the saw to cut in the same location on the specimen without any misalignment. After the holes were drilled and the plate removed, aluminum pull-off pucks with 2 in. diameters were attached to the composite with 2500-psi fast setting epoxy and secured by timber sheaths as shown in Figure 40.

Figure 39. Cutting of timber for pull-off tests

Figure 40. Pull-off puck attachment technique

Testing Apparatus

A Dyna Proceq Z16 pull-off tester was used to remove the pucks from the specimens. The apparatus consisted of three adjustable legs with a single testing shaft attached to the pucks, adjusted by a hand crank as seen in Figure 41. Tests were considered completed when the pull-off pucks achieved a peak load resulting from the FRP bond failing or exceeding the tensile strength of wood fibers along the specimen length.

Figure 41. Dyna Proceq Z16 pull-off tester

Compression Testing

Compression Test Development

To determine how to most efficiently evaluate the full sized (i.e., 9-in. diameter and 24-in. long) shells in compression, preliminary testing was conducted on 6-in. diameter, 10-in. long compression samples. These preliminary tests revealed that the samples tended to fail in bearing where the FRP material was in contact with the hardened steel testing platen. Several different methods of reinforcing the ends of the test samples were evaluated, but it was found that the simplest and most effective method was to provide at least three strips of FRP, effectively doubling the wall thickness for the top and bottom 6 in. of the samples.

Manufacturing methods for creating the shells were also developed through experimentation. Initially, specimens were found to be sticking to the PVC pipes used as molds after curing, and mold release agents were not found to be effective for full size samples although they were effective for smaller samples. As a solution, two layers of 3-mm plastic sheeting were placed around the molds allowing the shell to bond to one of the plastic layers while sliding off of the second layer underneath. Additionally, initial shells were found to shrink onto the molds as they cured, requiring over 20,000 lbf to remove the mold from inside the shells. To address these issues, PVC pipes were split lengthwise. The top of the molds were held open by set screws that were used to expand the molds and insert a ½-in. wide wood strip into the lengthwise cut in the pipe, thus expanding the diameter of the PVC pipe as shown in Figure 42. After the FRP was wrapped and cured on the mold, the wooden strips were removed and PVC mold snapped back to its original shape, allowing for easy removal. After these adjustments, successful shells for compression testing could be produced.

Figure 42. PVC mold for compression testing

Specimen Preparation

To evaluate compression, wet layup tube specimens were manufactured consisting of both three and five layers (three of each tube type). The tubes were manufactured on PVC molds to have a diameter of roughly 9 in. and height of 24 in. For Fyfe, Sika, Phenolic, and Simpson Strong-Tie, fabric was cut to 30 in. (transverse) by 24 in. (longitudinal) for a single layer. During wrapping, the resins were prepared as per the specifications and applied to fabric in order to saturate them fully as shown in Figure 43. For unidirectional Fyfe, Sika, and Simpson Strong-Tie fabric systems, the layers were oriented with the majority of fibers in the longitudinal directions in a (0/90/0) orientation for three layers and (0/90/0/90/0) for five layers of wrap. For the bidirectional fabric systems (Aquawrap and Phenolic), the wraps were simply wrapped with three and five layers as necessary. See Figure 44 for an example of wrapping shells.

Figure 43. Saturating fabric and spreading resin

Figure 44. Wrapping of compression test tubes

For the Aquawrap, 12-in. wide rolls were provided. The first and third layers were applied by laying 12-in. portions next to each other to create a 24-in. portion. The second layer consisted of one 12-in. portion in the middle and two 6-in. portions on either side. The same process was used with the five-layer specimens.

To prevent fiber crushing on top and bottom of the shells during compression testing, additional strips were placed on the top and bottom with a width varying from 4 in. to 6 in. After applying the extra reinforcement, the specimens were wrapped with stricture wrap to ensure proper bonding between layers and to keep the specimens from slipping off the forms. Specimens were wrapped and cured above 70°F. After curing the specimens, the ends of the specimens were cut with a commercial band saw to provide a reasonably square, smooth bearing specimen for uniform load distribution, preventing stress concentrations. However, this cutting method still leaves some undulations and out-of-square given saw blade wobble and operator errors. Many of the completed shells are shown in Figure 45.

Figure 45. FRP shell specimens

Testing Apparatus

The same Instron machine used for bond testing was used for the compression testing, with loading rates adjusted to achieve failure in 2 to 10 minutes. Loading rate for Sika, Fyfe, and Simpson Strong-Tie systems was 20,000 lbf per minute. For the Phenolic system, load rates were 20,000 lbf/min (A and B), 5,000 lbf/min (Phenol C and D), and 10,000 lbf/min (Phenol E & F). For the Aquawrap shells, loading rates were 20,000 lbf/min (Aqua A) and 10,000 lbf/min (Aqua B-F). Two-in. steel plates were used to supply a large bearing surface on the test machine. A schematic of the compression test is given in Figure 46.

Figure 46. Schematic of compression test

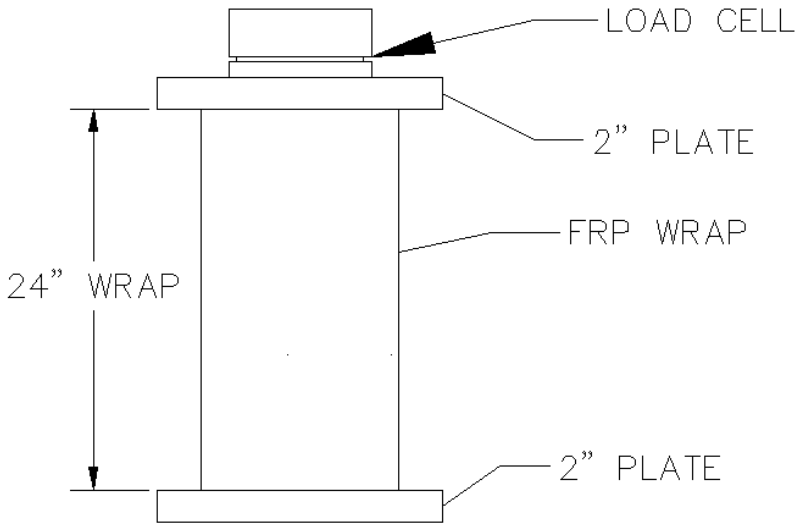

Full-Scale Rehabilitation Simulation

Rehabilitation Simulation Test Development

Once the bond strength and compression capacities of the systems were established separately, it was determined that evaluating the two failure modes together was needed to demonstrate rehabilitation capacities that might be encountered in the field. Because the capacity of decayed timber in the field is uncertain and difficult to determine, the deteriorated timber portion cannot be counted upon to provide any reasonable capacity and should be neglected. Thus, two 10-in. diameter timber sections separated by an 18-in. foam-filled gap were wrapped with each FRP system and tested under axial compression.

Specimen Preparation

To ensure the timber samples remained parallel to each other during testing, a steel pipe was used for alignment and to aid in handling. The two 16-in. portions of timber pile were drilled with a 2-1/4-in. vertical hole to place it on the 2-in. steel pipe. The ends were secured with plywood plates with 2-in. diameter holes to adjust the alignment of the two timber samples to account for drilling and cutting errors as shown in Figure 47.

Figure 47. Setting timber for rehabilitation

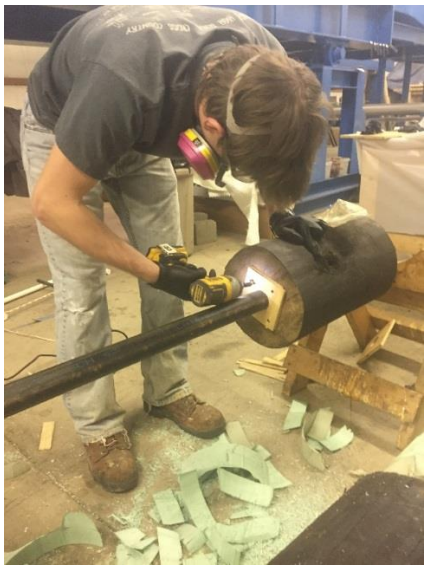

The two portions were separated by an 18-in. gap created by 9 pieces of 12-in. x 12-in. x 2-in. extruded insulation. The insulation was then trimmed with a hot wire to match the shape of the timber as shown in Figure 48. Figure 49 shows a sample ready to be wrapped.

Figure 48. Trimming insulation for simulated rehabilitation

Figure 49. Simulated rehabilitation specimen

Dry wall compound was utilized to fill any voids developed during the trimming process and provide a uniform wrapping surface. The timber specimens were then wrapped with the FRP wraps as shown in Figure 50. For the hand lay-up specimens, fabrics were cut to 42 in. (longitudinal) by 38 in. (transversely). After curing for 7 days, the pipes were removed from the specimens, and the insulation was melted away with acetone to produce a hollow core between the timber pieces.

Figure 50. Wrapping of rehabilitation specimens

Testing Apparatus

The configuration of the simulated rehabilitation testing is shown in Figure 51. Instron 1000HDX universal testing was used as shown in Figure 52. Failure was determined using the same methods for bond and compression testing. Loading was applied at a constant rate of 10,000 lbf/min until failure occurred in the specimens.

Figure 51. Schematic of simulated rehabilitation test

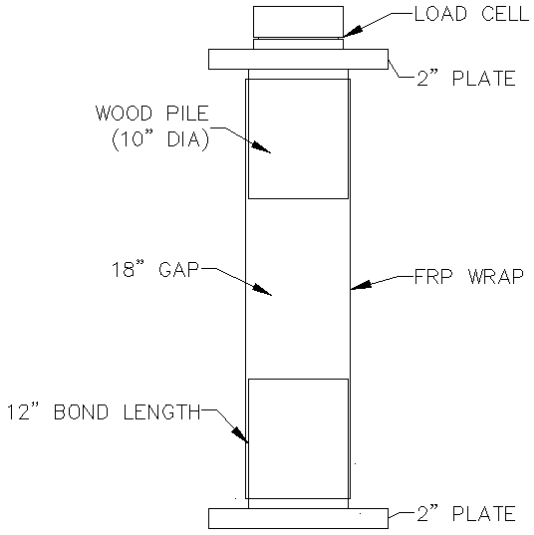

Figure 52. Simulated rehabilitation evaluation testing setup

Combined Axial and Bending Tests

As in-service piles are subjected to both flexural and axial forces, testing was completed to ensure that an FRP wrap has the same capacity under combined loading. To evaluate this, three 30 in. long Sika axial compression samples were instrumented with strain gages at the top, bottom and middle. The samples were placed in a test fixture (Figure 53) in the WVU-CFC Major Units Lab and subjected to an axial load equal to 75% of the maximum failure load as determined from the axial compression testing. With the axial load on the wrap, a bending load was applied to the center of the wrap, which was equal to 10% of the allowable flexural strength obtained from axial compression testing. The strain gages measured the axial strain (middle gage), combined axial and flexural compression (bottom gage), and combined axial and flexural tension (top gage).

Figure 53. Schematic of axial compression with flexure

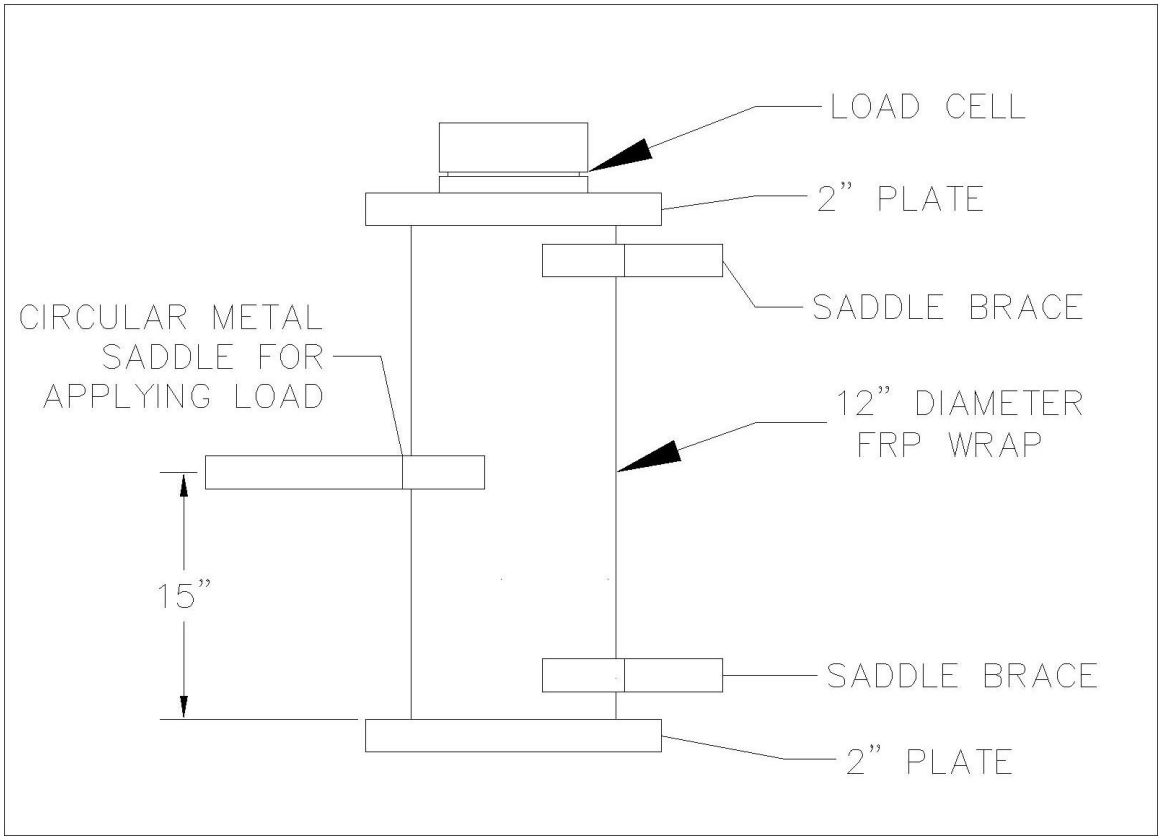

Filler Evaluation Methodology

To test crack and external void fillers, 4 in. nominal diameter, 6-in. long fence posts were hollowed out in a lathe to create an internal void. Three holes and two saw cuts of varying sizes were made into the sides of the voided area to simulate splits and holes as shown in Figure 54. A single sample was made for each filler consistently so that results could be compared. Each filler was then applied to a sample ensuring the filler completely sealed the cuts and holes and left to cure for 24 hours. The voids were filled with 10W-30 motor oil that has a similar viscosity of the bulk fillers and placed in a pan to catch any leaks. The oil levels in the samples were then monitored for 3 hours to assess for any leakage.

Figure 54. Crack filler specimen

To test the ability of bulk fillers to fill heart rot, 2 pieces of 4 in. nominal diameter, 6-in. long fence posts were hollowed out to a depth of 2 in. in the same manner as the crack filler samples (except without any cuts or holes in the walls). The actual diameter of the fence posts varied but averaged 3-3/4 in. Two different bits were used with a 1-15/16-in. diameter bit, resulting in 26% cross section loss. A 3-in. diameter bit was used to simulate 64% cross section loss, which was the largest section loss possible while leaving enough wall thickness on the smallest samples to avoid breaking during cutting and provide a glue surface for later fabrication. Two specimens were glued together with the voided areas abutting to create a 4-in. long void as shown in Figure 55. Silicone caulk was used to attach and seal the two sections together. To pour the resin into the void, a ½-in. diameter filling hole was drilled at a 30° angle into the top of the void. Similarly, a ¼-in. diameter hole was drilled at a 45° angle to allow air to escape, with the air hole coming out higher on the outside of the wood. A total of 9 samples were made for each filler material with 3 at 25% voided and 6 at 56% voided. Three 25% voided samples and 3 of the 56% voided samples were filled with only resin, while the remaining 3 samples at 56% void were filled with a mixture of resin and sand. The

ratio of sand to resin was determined by adding more sand until the mix would just flow through the ½-in. funnel opening into the void, i.e., maximizing the amount of sand. Phenolic was mixed at 1:1 sand to resin by weight, Sika at 1.5:1 sand to resin, and Rimline at 2:1 sand to resin. It is important to note that the viscosity of the resins changes significantly with temperature, thus these ratios may not apply to field conditions. Field ratios should be adjusted based on site-specific conditions including temperature and filler hole size at the time of rehabilitation of a timber pile.

Figure 55. Bulk filler specimen

The samples were filled using a funnel and allowed to cure for 24 hours. To assess the amount of fill, the samples were cut open and the amount of voided area was measured by determining the depth of the filler to the nearest $1/16^{th}$ of an inch and multiplying this by the diameter of the void.

To test injection filler effectiveness, voids of variable sizes were created in flat wood boards. Small voids were created using a 1-in. diameter Forstner bit drilling to a depth of 1/4 in. Medium voids were created using a 2-in. diameter Forstner bit to the same ¼-in. depth creating voids that exceed the typical limit of 2 in^2. To assess the ability for the filler to flow between interconnected voids, larger and more complex voids were created. As shown in Figure 56, a single 2-in. diameter void was drilled to a depth of 1/4 in. and two smaller 1.25-in. diameter voids were drilled to a depth of 1/8 in. in close proximity but not connected. The 1.25-in. voids were connected to the larger void by cutting down from the top to make a 5/16-in. wide channel, with 1 channel at 1/8 in. deep and the other 1/16 in. deep. In addition, a 5/16-in. hole was drilled to a depth of 3/8 in. and connected to the 2-in. void by a 1/16-in. hole connecting the two areas. Acrylic panels were glued and screwed over the holes to

simulate FRP bonded over the timber while still allowing investigators to see into the voids. Two holes were drilled through the acrylic, one 1/8-in. hole to fill and a 1/16 in. hole to allow air out, with the holes on opposite sides of the simulated voids. The injectable fillers were pumped into the holes and allowed to cure.

Figure 56. Large injection filler

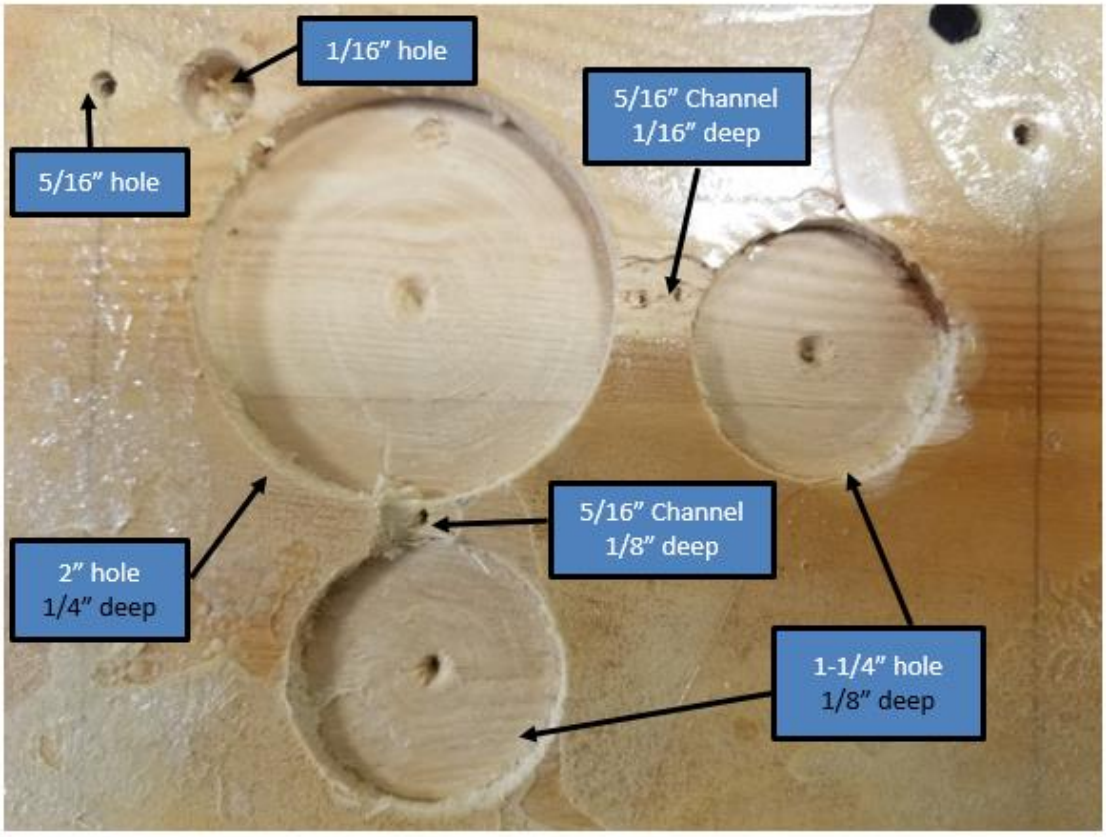

Traditional Timber Pile Splicing Repair

Splice repair was conducted by cutting out the damaged timber pile portion and replacing it with a new pile section of the same diameter as the original pile. The newly inserted pile section was secured to the preexisting pile using three different types of splicing methods: flat steel plate splicing, C-channel steel plate splicing, and wooden plate splicing. The effectiveness of splicing methods was evaluated by measuring the shear, bending, and axial strengths. In addition, splicing of the new pile section and the old (undamaged) pile section was done by wrapping with glass FRP fabrics overlapping the new and old (undamaged) pile sections. The following sections expand upon the outcomes of timber pile repair using the above splicing methods and through the strength analyses.

Assembly of Timber Piles

A total of 36, 12-in. diameter, creosote-treated, southern pine piles were tested under axial, shear, and bending forces with four splice configurations. The test specimen configurations for each loading condition are detailed in Table 18 below. Virgin piles were cut to desired lengths of 5 ft., 8 ft., or 16 ft. and were cut further at midspan for splicing, with specifications (directions and drawings) provided by LTRC. Timber pile diameter varied approximately ±1 in. in some cases. Therefore, the exact diameter of each pile was recorded for stress computation and reported herein.

Table 18. Pile splice configuration

		Splicing Method Used				
Test Type	**Pile Length (ft.)**	**Flat Steel Plate**	**C-Channel Plate**	**Wood Plate**	**FRP Wrapping**	
Axial	5	3	3	3	3	
Shear	8	3	3	3	3	
Bending	16	3	3	3	3	
Total:		9	9	9	9	36

The cut pile pieces were joined together with steel plates as shown in Figure 57. The steel plate and C-channel splicing methods used 18-in. long bolts of ¾ in. diameter (Grade B61). The wooden plate method used 24-in. long bolts of ¾ in. diameter (Grade B61) to accommodate approximately 3-in. thick timber splices. All joints were spliced with 54-in. long plates that were 5.5-in. and 6-in. in width for timber and steel plate splices, respectively. However, the C-channel splicing mechanism also included an 8-in. wide steel channel. Steel plate schematics are provided in Figure 58. An image of an assembled pile prepared for shear testing, using the steel plate splicing method is provided in Figure 59.

Figure 57. C-channel splice detail

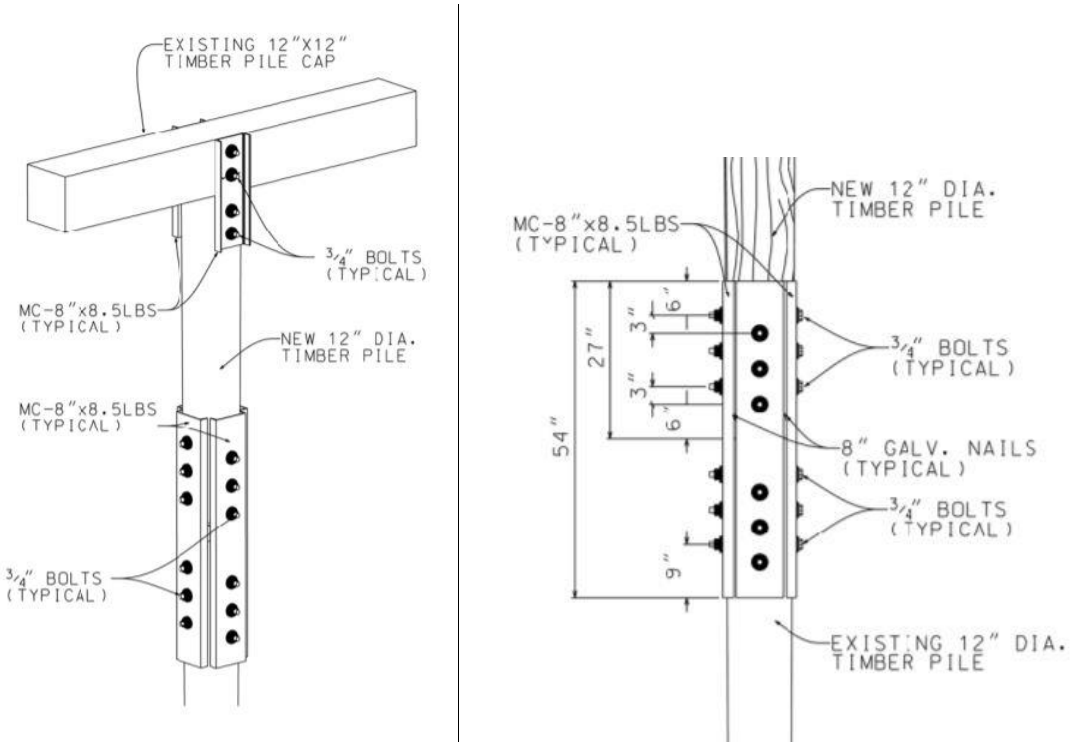

Figure 58. C-channel and flat steel plate detail

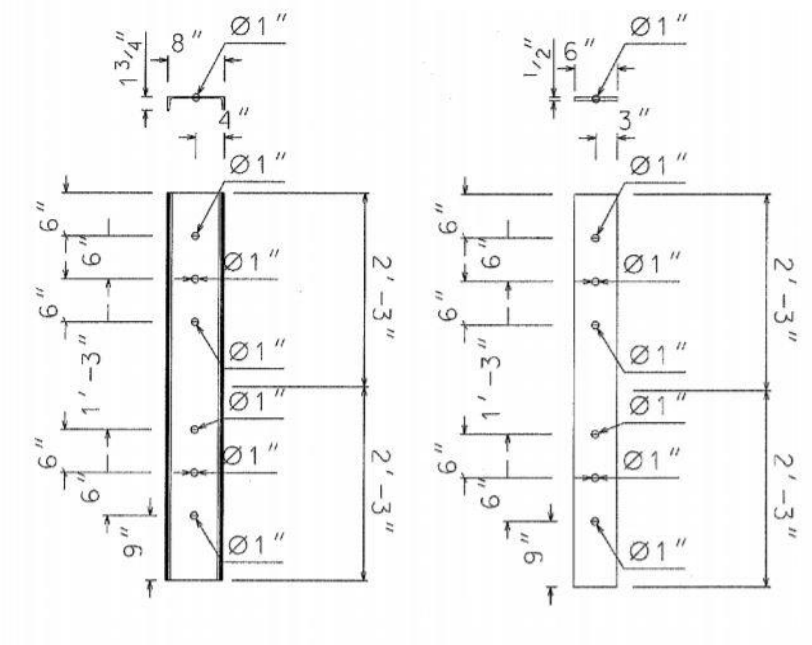

Figure 59. Steel splice specimen constructed in WVU CFC lab

Timber Pile Repair Using Fiber Reinforced Polymers

Timber piles may be repaired in several ways, but a potentially more efficient method to obtain comparable strength to the legacy splicing systems (from previous sections) is to use composite materials. Fiber reinforced polymer (FRP) composite was used to rejoin a pile cut into two parts. It was hypothesized that once the FRP was bonded to the pile, the wrap would act similar to the steel and wooden plates used to splice the samples and provide a confinement stress. FRP splicing method was tested for shear, bending, and axial compressive strengths and compared to other splice methods. These concepts were evaluated for the influence of FRP wraps for timber piles. The testing setup for this method remains the same compared to traditional methods of splicing.

Fiber reinforced polymers consist of fibers and resin, as shown in Figure 60. For civil structures, a variety of commercially available fiber and resin systems are used. The Sika system used in Phase 1 research of this project was used again herein, i.e., Sika Hex 100G, i.e., a unidirectional glass fabric, and Sikadur Hex 300, a two-part epoxy resin. Together it created a glass-epoxy composite that is bonded to the wooden pieces. Unidirectional refers to the orientation of fibers primarily within the matrix, in a single direction. Sika Hex 100G fabric has a density of 0.092 lb./in^3.

Figure 60. Unidirectional FRP composite orientation

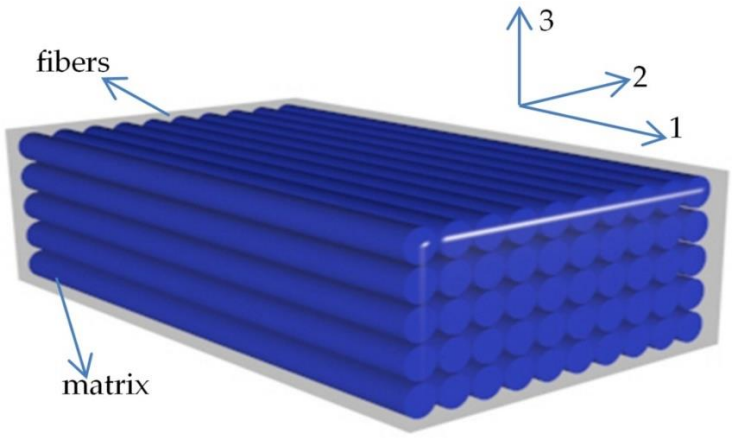

Assembly of Fiber Reinforced Polymer Splicing

Piles were cut to the desired length for each test, i.e., 16 ft. for bending, 8 ft. for shear, and 5 ft. for axial testing. The piles were cut in half before splicing with FRP wraps. Only three piles of each length were needed for this portion of testing to remain consistent with testing performed on piles with traditional splicing methods. The sections of each pile were nailed together to prevent pile separation or movement during wrapping. Sheets of fabric were cut to 4 ft. in length, creating a rectangular sheet of fiber with dimensions 48 x 51 in., where 51 in. was the width of the glass fabric roll supplied by Sika. The resin was prepared by mixing part A with part B as per the manufacturer's instructions. The contents were mixed using a mixer drill bit for five minutes. After thorough mixing of the resin, it was used to prime the pile and saturate the glass fabric sheets. Each pile tested was wrapped with three layers around its circumference. The pile was primed by thoroughly brushing the primer (resin) onto the surface of the pile and subsequently prepared by rolling resin onto both sides of the fabric, ensuring that the entire sheet was fully saturated. After the pile was primed, the fabrics were then applied (wrapped around) to the pile. The fabrics were stapled at the ends and pressed. While the fabric was wrapped around the pile, the resin saturated fabric was wiped and pressed by hand to remove voids and ensure a tight, void free wrap. After both sheets were applied to the pile, it was set aside to cure for at least three days before testing. An image of a finished FRP splice is provided in Figure 61.

Figure 61. Completed fiber reinforced polymer splice

Testing Methods and Setup: Shear, Bending, and Axial

Test Methodology

In order to compare FRP to the traditional splicing methods, certain tests were conducted; this section provides details on the test procedures for shear, bending, and axial loading. All tests were conducted in compliance with ASTM D198-15 for static tests of lumber components.

Shear Test Setup

The shear test was prepared by placing two concrete supports with clear span of 4 ft., 8 inches apart. To induce a shear mode of failure, l/d ratio ranging between 4 and 10 must be achieved. However, l/d < 6 is recommended as per ASTM D198-15. The test span (4 ft., 8 in.) for shear testing leads to l/d of 4.67.

An 8-ft. long pile was placed on steel saddles following splicing of the test specimen at the center of the span of the refurbished pile (Figure 62). A concentrated load was applied using a hydraulic actuator. The load was transferred from the actuator to a load cell that was placed on top of a spacer on the pile specimen. The load cell records the amount of force applied to the pile from the actuator. A linear variable differential transformer (LVDT) was placed at the center span to measure deflection. A shear test setup with wood plate splicing overlapping the pile joint is shown in Figure 63.

Figure 62. Shear test schematic

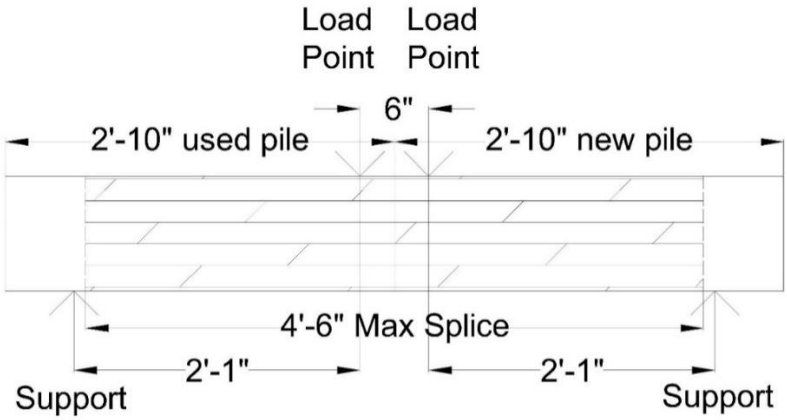

Figure 63. Shear test setup with wooden splice

Bending Test Setup

To obtain bending mode of failure the l/d ratio was taken as 15. Therefore, the test specimen was spanned at 15 ft. (clear span) between support saddles. Other instrumentation remained the same as in the shear test setup. With the pile in position, an I-beam shown in Figure 65 was placed on top to distribute the loading and create a test setup that generates a 4-point bending test. This I-beam distributed the actuator induced load at two points on the pile. The I-beam load was accounted for in the stress-deflection computations. A string pot was used to measure the downward deflection induced by the vertical load application. The string pot was placed directly underneath the center of the splice and was attached to the bottom of the pile using fishing line. All sensors were initialized (zeroed) before the I-beam was placed on the specimen. Figure 64 provides a schematic of the test setup under four-point bending loading

as per ASTM D198. Figure 65 gives additional details of the bending test setup with a C-channel spliced member.

Figure 64. Bending test schematic

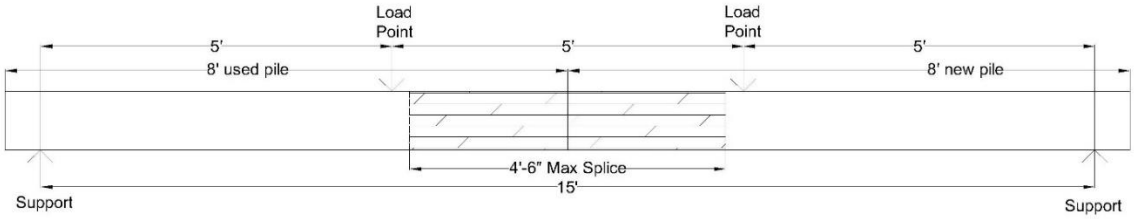

Figure 65. Bending test setup with C-channel splice

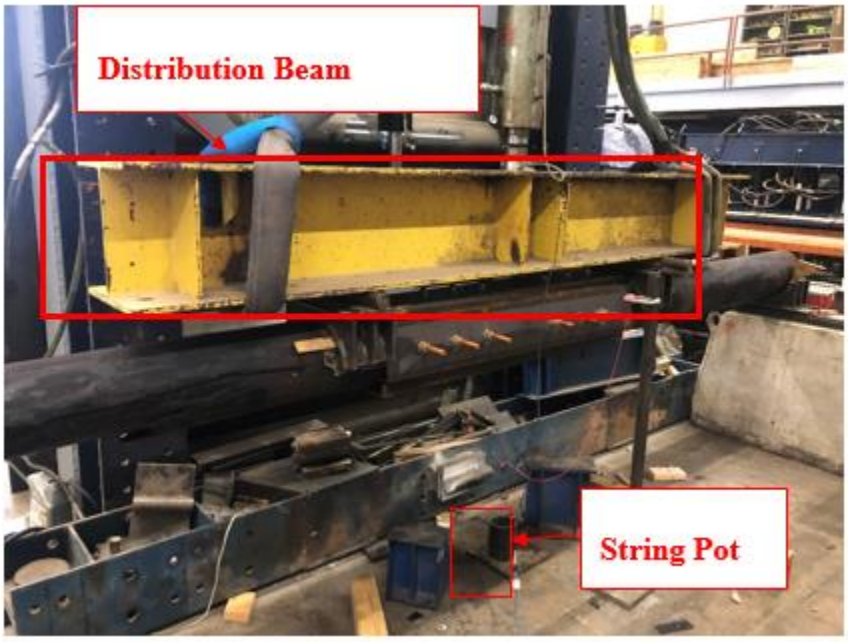

Axial Test Setup

The axial compression test was performed by placing the 5 ft. long pile sections in a compression test frame, which had a load capacity of 750 kips. Load was applied using a hydraulic jack applying load to a 16 x 16-in. steel plate, which in turn exerts axial force on the pile cross section. A LVDT was used to measure longitudinal displacement under compression. Figure 66 was a schematic of the axial compression test. Figure 67 provides an image of axial testing performed with C-channel splicing.

Figure 66. Axial compression test schematic

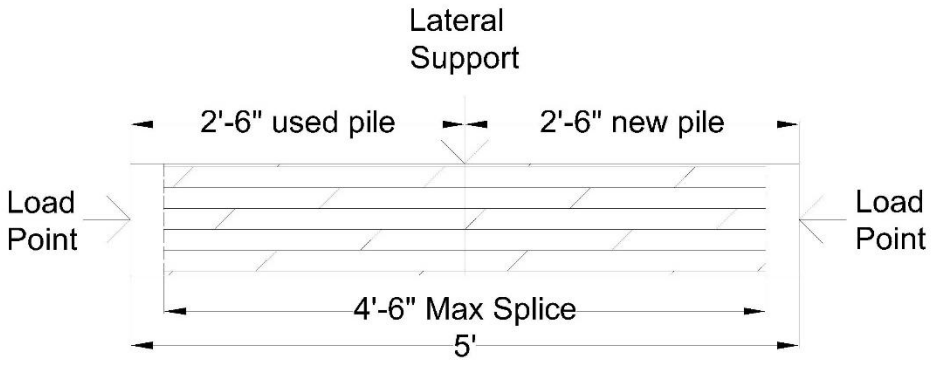

Figure 67. Axial test setup with C-channel splice

Discussion of Results

The data from the evaluations are presented for each system with discussions of the failure mechanisms. The significance of results for each of the tests is described for each test type.

Bond Testing (Push Out)

The bond pushout testing was conducted on the five systems for 6 in. and 12 in. bond lengths. The individual results for each system are presented first, with a summary of the complete results after.

Fyfe Bond Strengths

All specimens bonded with Fyfe resin failed due to timber failure. As shown in Table 19 and Table 20, the average bond strengths for 6 in. and 12 in. of lengths of bond were 284 psi and 235 psi. Capacities were 54,717 lbf and 90,541 lbf for 6 in. and 12 in. bond lengths, respectively. The 6-in. samples had a greater spread in the data, as indicated by a higher coefficient of variation (COV).

Table 19. Fyfe 6-in. bond length results

Sample	Bond Area (in^2)	Peak Load (lbf)	Peak Stress (psi)
Fyfe 6-1	195.00	53,233	273
Fyfe 6-2	189.75	69,067	364
Fyfe 6-3	195.00	41,853	215
Average		54,717	284
COV		25%	26%

Table 20. Fyfe 12-in. bond length results

Sample	Bond Area (in^2)	Peak Load (lbf)	Peak Stress (psi)
Fyfe 12-1	385.50	98,333	255
Fyfe 12-2	394.50	97,572	247
Fyfe 12-3	373.50	75,718	203
Average		90,541	235
COV		14%	12%

As shown in Figure 68, delaminated wraps contained large portions of timber ranging from 1/4 in. to 1/2 in. in thickness. Such behavior was indicative of failure in the timber substrate and not the resin used in the FRP system. From this visual evaluation, failure in timber was assumed to be the controlling failure mode for the majority of the specimens bonded with Fyfe resin. This indicates the epoxy resin was able to bond sufficiently to the creosote-treated pile and obtain a small degree of penetration into the timber.

Figure 68. Retained timber on Fyfe bond tests

The load versus deflection plots in Figure 69 show similar failure behavior of all the samples in which the sample reaches a maximum load at bond failure, before losing its resistance capacity. The 6-in. bond capacities (dashed) were typically lower than the 12- in. bond (solid) in terms of total load resistance, but higher in terms of bond stress to failure.

Figure 69. Fyfe bond test load vs. deflection

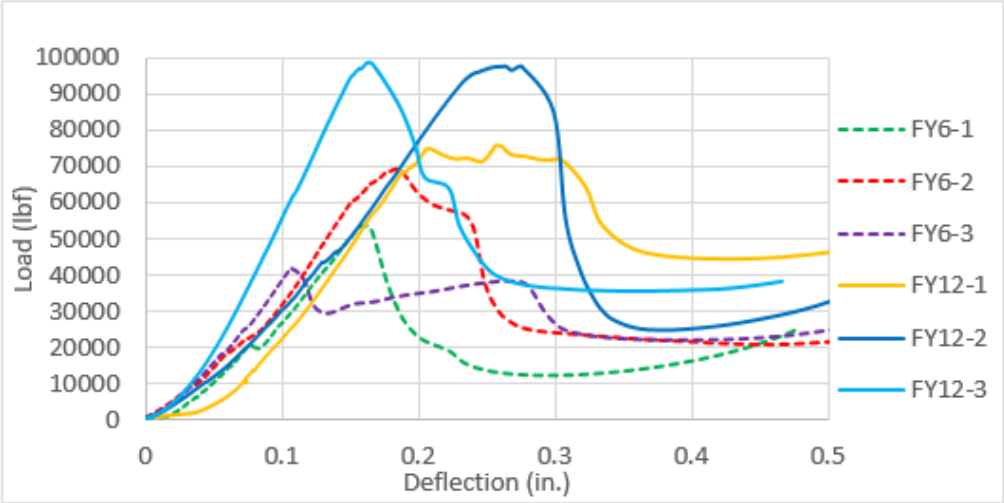

Sika Bond Strengths

All Sika bond specimens failed due to timber failure. Average bond strengths for 6 in. and 12 in. of lengths of bond were 353 psi and 212 psi. Capacities were 68,867 lbf and 80,010 lbf for 6-in. and 12-in. bond lengths, respectively. Results from the bond evaluations are reported for the 6-in. and 12-in. bond lengths. Sika bond lengths are shown in Table 21 and Table 22 respectively. The bond stress spread was similar to the Fyfe samples, and reduced as the bond length increased.

Table 21. Sika 6-in. bond length results

Sample	Bond Area (in^2)	Peak Load (lbf)	Peak Stress (psi)
Sika 6-1	199.50	50,953	255
Sika 6-2	193.50	81,343	420
Sika 6-3	193.50	74,305	384
	Average	68,867	353
	COV	23%	25%

Table 22. Sika 12-in. bond length results

Sample	Bond Area (in^2)	Peak Load (lbf)	Peak Stress (psi)
Sika 12-1	378.00	80,246	212
Sika 12-2	378.00	89,272	236
Sika 12-3	378.00	70,511	187
	Average	80,010	212
	COV	12%	12%

Visual inspection of the Sika samples showed the same timber failure mode as the Fyfe samples, as shown in Figure 70. This indicates the epoxy resin was able to bond sufficiently well to the creosote-treated pile and obtain the required degree of penetration into the timber, to prevent debonding at the glue line.

Figure 70. Retained timber on Sika bond tests

The Sika pushout test varied from the Fyfe tests as some of the 6 in. samples (dashed) reached similar loads to the 12-in. samples (solid) as shown in Figure 71. This indicates that the internal timber strength may be a limiting factor. Once maximum load was reached a sharp drop in load occurred.

Figure 71. Sika bond test load vs deflection

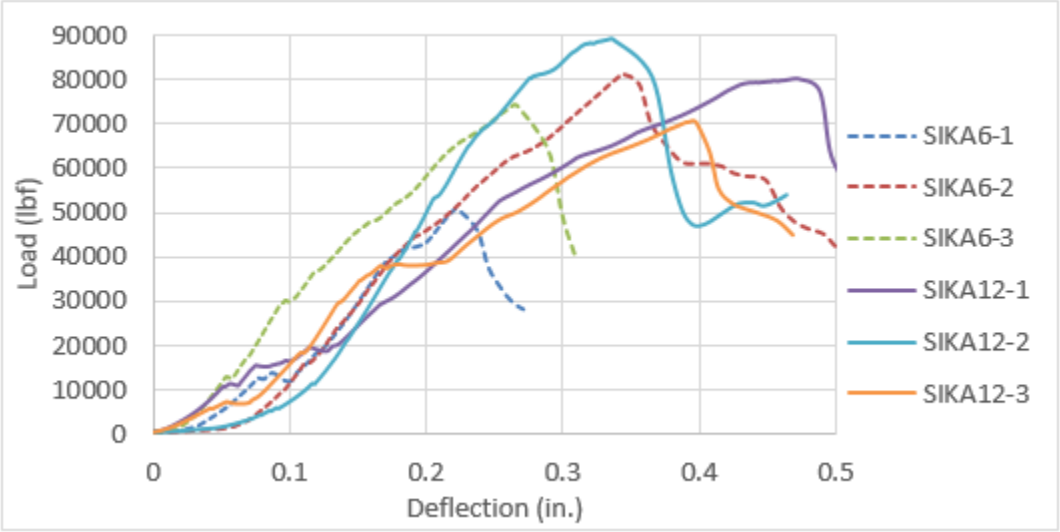

Simpson Strong-Tie Bond Strengths

All Simpson Strong-Tie (SST) timber bond specimens failed due to timber failure. Average bond strengths for 6 in. and 12 in. of lengths of bond were 279 psi and 199 psi, respectively. Capacities were 55,992 lbf for 6-in. bond lengths and 76,031 lbf for 12-in. bond lengths. The results for the 6-in. bond length are shown in Table 23 and for the 12-in. bond length in Table 24. The 6-in. bond samples had a greater spread (COV) than the Fyfe or Sika samples, but the 12-in. samples had a similar spread as the others.

Table 23. Simpson Strong-Tie 6-in. bond length results

Sample	Bond Area (in^2)	Peak Load (lbf)	Peak Stress (psi)
SST 6-1	195.75	51,161	261
SST 6-2	204.75	79,130	386
SST 6-3	198.00	37,685	190
	Average	55,992	279
	COV	38%	36%

Table 24. Simpson Strong-Tie 12-in. bond length results

Sample	Bond Area (in^2)	Peak Load (lbf)	Peak Stress (psi)
SST 12-1	387.00	68,940	178
SST 12-2	399.00	74,749	187
SST 12-3	366.00	84,405	231
	Average	76,031	199
	COV	10%	14%

Visual inspection of bond strength failure modes of Simpson Strong-Tie with timber substrate were similar to the Fyfe and Sika samples, with a large amount of timber still bonded to the wrap and the failure occurring in the timber itself. This indicates the epoxy resin was able to bond sufficiently to the creosote-treated pile and obtain a small degree of penetration into the timber.

Figure 72. Retained timber on Simpson Strong Tie bond test

As shown in Figure 73, the 6-in. bond capacities (dashed) were typically lower than the 12-in. (solid) capacities, though SST 6-2 had a very high load capacity to failure. As with previous systems, the load drops after bond failure and does not recover until the gap is closed.

Figure 73. Simpson Strong-Tie bond test load vs deflection

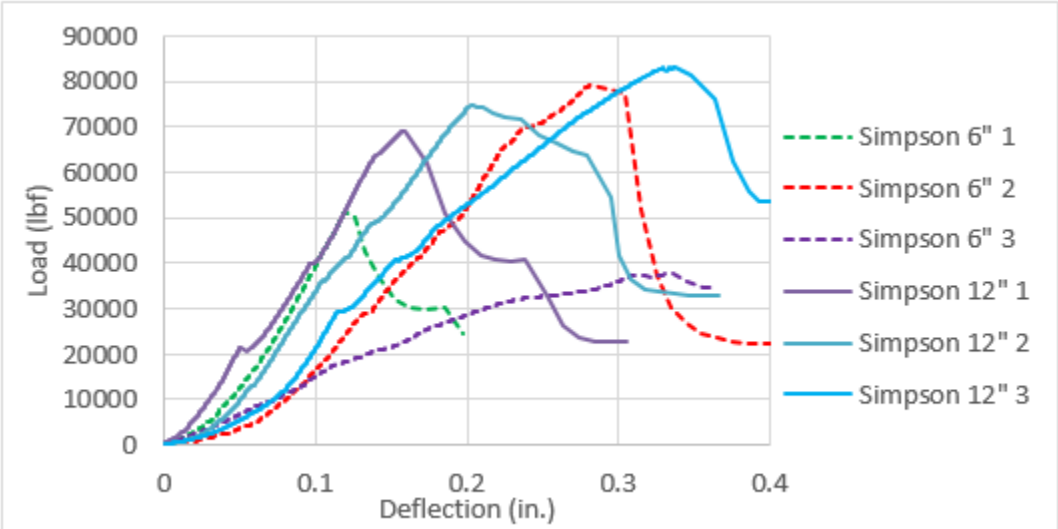

Phenolic Bond Strengths

Specimens with phenolic (PH) bond specimens failed in bond slippage between the FRP system and the timber substrate. The average bond strengths for 6 in. and 12 in. of lengths of bond were 112 psi and 64 psi, respectively 6-in. bond lengths provided an average capacity of approximately 24,107 lbf while 12-in. bond lengths averaged 25,997 lbf. Results from the bond evaluations are reported for the 6-in. and 12-in. phenolic bond lengths are shown in Table 25 and Table 26. Due to the limited increase in capacity from 6-in. to 12-in. bond lengths (only 7%), it is likely that the phenolic material has an optimum bond length between 6 in. and 12 in.

Table 25. Phenolic 6-in. bond length results

Sample	Bond Area (in^2)	Peak Load (lbf)	Peak Stress (psi)
PH 6-1	206	19,279	93
PH 6-2	221	28,518	129
PH 6-3	216	24,523	114
	Average:	24,107	112
	COV:	19%	16%

Table 26. Phenolic 12-in. bond length results

Sample	Bond Area (in^2)	Peak Load (lbf)	Peak Stress (psi)
PH 12-1	405	30,754	76
PH 12-2	381	23,756	62
PH 12-3	432	23,481	54
	Average	25,997	64
	COV	16%	17%

After unwrapping the glass fabric bonded with phenolic resin, it was found that no timber substrate adhered to the FRP. On the other hand, the creosote layer had been pulled off as shown in Figure 74. The few pieces of timber retained were superficial. This indicates that the phenolic resin was unable to make a sufficient bond beyond the outer layer of creosote.

Figure 74. Superficial retained timber on phenolic wraps

As shown in Figure 75, all the samples failed at similar loads and lost significant strength after reaching the maximum load. This indicates the phenolic bond strength was the controlling factor and that it does not increase with increasing bond area.

Figure 75. Phenolic bond test load vs. deflection

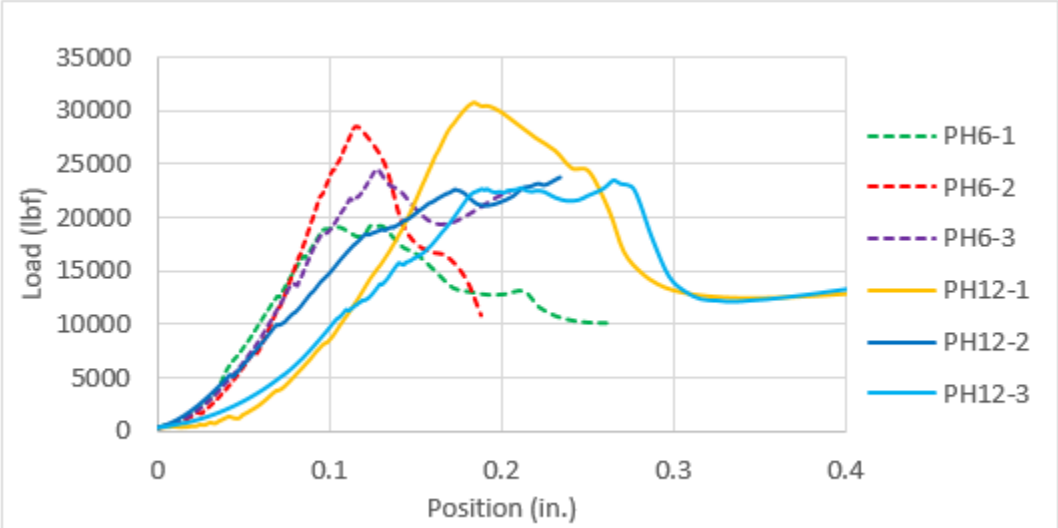

Aquawrap Bond Strengths

Failure modes varied from bond slippage for the 6 in. samples to crushing of the fibers in the base for the 12-in. samples as the Aquawrap (AQ) specimens were not reinforced in the base, as were the other systems. Average bond strengths for 6 in. and 12 in. of lengths of bond were 82 psi and 56 psi, respectively. When bonded to a 10-in. diameter timber, 6-in. bond lengths provided an average capacity of 16,836 lbf while 12-in. bond lengths averaged 22,336 lbf for the same approximate diameter. Results from the bond evaluations were reported for the 6 in. and 12 in. Aquawrap bond lengths are shown in Table 27 and Table 28. Failure modes are indicated by subscripts on the tables.

Table 27. Aquawrap 6-in. bond length results

Sample	Bond Area (in^2)	Peak Load (lbf)	Peak Stress (psi)
AQ6-1	219	22,783	104
AQ6-2	200	9,803	49
AQ6-3	192	17,921	93
	Average	16,836	82
	COV	39%	35%

Table 28. Aquawrap 12-in. bond length results

Sample	Bond Area (in^2)	Peak Load (lbf)	Peak Stress (psi)
AQ12-1[1]	409	28,412	69
AQ12-2[1]	373	16,394	44
AQ12-3	401	22,202	55
	Average:	22,336	56
	COV:	27%	22%

[1]Fiber crushed in gap

Evaluating the wraps after bond testing revealed that no timber remained as shown in Figure 76 on the wrap, suggesting that failures occurred in the bond line and not the wood. Failure in the bond line indicates a poor bond strength.

Figure 76. Limited retained timber on Aquawrap 6 in. and 12-in. bond specimens

The Aquawrap bond samples (Figure 77) showed extended deflections under peak loading, not sharp drops as with the other systems. Such load-deflection behavior suggests the bond was very weak and the system was responding more to frictional forces between the wrap and the timber.

Figure 77. Aquawrap bond test load vs. deflection

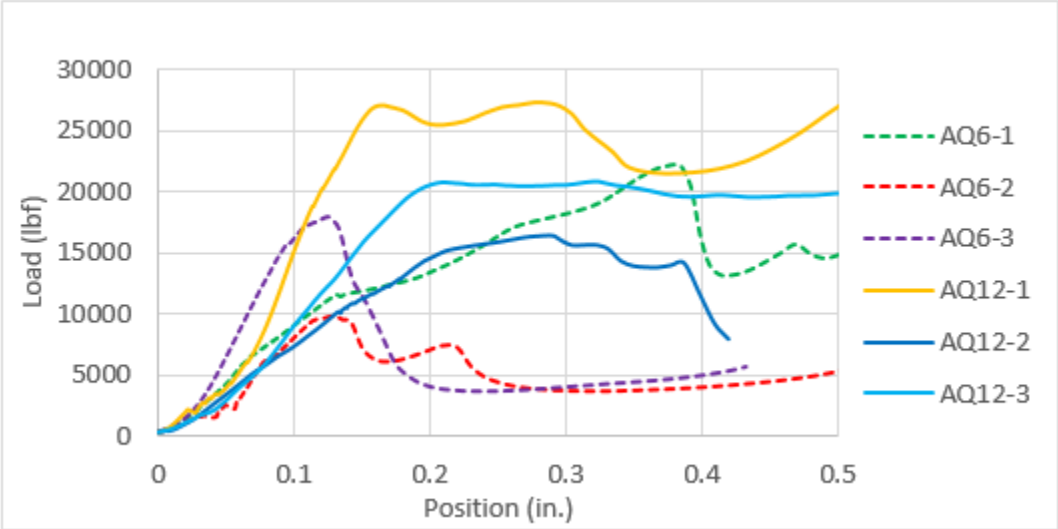

Bond Test Conclusions

The bond strengths and capacities for the Fyfe, Sika, Simpson Strong-Tie, Phenolic, and Aquawrap systems evaluated are included in Table 29. For the three epoxy-based systems, increasing the bond area increased the overall capacity of the bond, but the bond strengths were always reduced. Such behavior suggests a non-linear relationship between wrap length and bond strength. The Sika wraps provided the highest bond strengths and capacities for the 6 in. bond length, while the Fyfe system provided higher bond strengths and capacities for the 12 in. bond length. All of the epoxy systems performed similarly in terms of strength and capacity, though none reached the allowable strength of a new timber pile (94,000 lbf) without any wrap. For the phenolic wraps, the bond strengths were low and increasing the bond length did not significantly increase the bond capacity (≈ 7% increase). The Aquawrap systems displayed low average bond strengths and capacities.

Table 29. Summary of strengths and capacity by bond length

System	Strength (psi)		Capacity (lbf)	
	6 in.	12 in.	6 in.	12 in.
Fyfe	284	235	54,717	90,541
Sika	353	212	68,867	80,010
Simpson Strong-Tie	279	199	55,992	76,031
Phenolic	112	64	24,107	25,997
Aquawrap	82	56	16,836	22,336

Inspection of specimens after evaluations showed that epoxy-based systems failed predominately in the timber as there was significant timber still bonded to the wrap after cutting the samples apart. The phenolic samples only bonded to the creosote layer, while the Aquawrap specimens failed consistently in bond with no retained timber.

The epoxy based systems (Fyfe, Sika, and Simpson Strong Tie) all bonded well to the creosote timber as shown by the amount of timber still bonded to the FRP after cutting the samples apart. This was attributed to the use of epoxy resins that have longer pot lives (up to 6 hours) and longer cure time (up to 72 hours), which allow the resins to penetrate into the timber. The phenolic resin has a pot life of 45 minutes and cures in 8 hours, limiting the ability to penetrate into wood pores. Aquawrap cures with water, which forms a barrier layer on the creosote, and cures in 1 hour. In addition, it was noted that the pre-impregnated Aquawrap system did not want to conform to the undulations in the timber surface creating numerous gaps as shown in Figure 78.

Figure 78. Gap between Aquawrap and pile

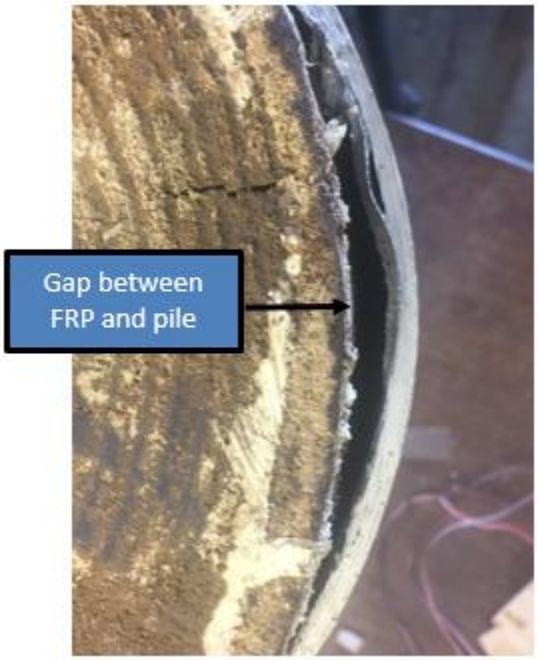

Based on similar performance from three manufacturers and high capacities of epoxy-based systems, epoxies are recommended for future use by DOTD. The design methodology will be based only on these systems, and rating methodologies and inspection techniques will be provided for all systems based on the expectation that all of them are already in use.

Aging Bond Tests

After being subjected to wet/dry cyclic conditions for 4 months, the aged samples with 12-in. bond length aged samples were tested using the same method as the other bond tests. The peak loads and stresses are shown in Table 30 including the difference between the aged samples and average load and stress for the unaged samples. Overall, the peak stress was 15% higher for the aged samples compared to the unaged samples. Prior to wrapping, the pile samples were stored indoors, which reduced the moisture content compared to outdoor storage. After the 4 months of wet/dry cycles, the piles were left indoors for 24 hours to dry prior to testing. The increase in bond strength was attributed to the timber expanding due to the increase in moisture content of the wood compared to the time when the pile was wrapped. This shows that if in-service piles are in a wet environment, drying them to reduce the moisture content will result in slightly higher bond strengths. This testing also shows that the wet/dry cycles did not exhibit any negative effects to the wrap or bond, which is based on the limited number of cyclic tests that have been completed under this program.

Table 30. Aged bond strength compared with average bond strength

Sample	Peak Stress	Stress Difference
Fyfe 1	293	25%
Fyfe 2	241	2%
Sika 1	202	-5%
Sika 2	224	6%
Simpson 1	283	42%
Simpson 2	209	5%
Phenolic 1	81	27%
Phenolic 2	68	6%
Aqua 1	75	34%
Aqua 2	58	4%

Pull-Off Bond Testing (Modified ASTM D7522)

Pull-off testing is typically conducted on FRP-wrapped concrete to assess the in-situ bond strength, thus similar testing was undertaken herein with wood as the substrate. Bond pull-off testing was conducted on five systems with five pull-off tests for each system in addition to a baseline pull-off test on unwrapped timber.

Fyfe Pull-off Bond Strength

Fyfe bond pull-off specimens failed in the timber with large thicknesses of timber attached to the wrap, as shown in Figure 79, thus showing that the FRP to timber bond in tension exceeds that of the underlying wood. The average pull-off strength was ~353 psi as shown in Table 31. The wood fibers for these tests displayed a large amount of variability (knots, grain changes) which contributed to the large variation between pull-off tensile strengths.

Table 31. Fyfe pull-off bond capacity and strengths

Sample	Force (lbf)	Stress (psi)	Failure Mode
FY 1	1133	360.65	Timber
FY 2	660	210.08	Timber
FY 3	1471	468.23	Timber
FY 4	1682	535.40	Timber
FY 5	596	189.71	Timber
Average	1108.4	352.81	43% (COV)

Figure 79. Fyfe pull-off carriers (timber failure)

Sika Pull-off Bond Strength

Similar to the Fyfe bond pull-off specimens, Sika pull-off samples all failed in the timber with large thicknesses of retained timber as shown in Figure 80. Again, the strength of the FRP to timber bond in tension exceeded that of the underlying wood. Sika 2 is not included in the analysis as the sample was taken over a crack in the timber, which resulted in a very low strength. Sika 5 failed in the glue line between the dolly and the FRP, which is attributed to failure of the test procedure and is not presented in Table 32. The average pull-off strength was 316 psi as shown in Table 32.

Table 32. Sika pull-off bond capacity and strengths

Sample	Force (lbf)	Stress (psi)	Failure Type
Sika 1	934	297.30	Timber
Sika 2	Excluded	Excluded	Cracked timber
Sika 3	1016	323.40	Timber
Sika 4	1033	328.81	Timber
Average	994.333	316.51	5% (COV)

Figure 80. Sika pull-off carriers (timber failure)

Simpson Strong-Tie Pull-off Bond Strength

Simpson Strong-Tie bond pull-off specimens all failed in the timber, but as shown in Figure 81, the amount of timber retained was less than the amount of timber retained in previous tests. This was attributed to a shallow drilling depth used in these tests. Since the failure was in the timber, the FRP to timber bond in tension exceeds that of the underlying wood. The average pull-off strength was 191 psi as shown in Table 33.

Table 33. Simpson Strong-Tie pull-off bond capacity and strengths

Sample	Force (lbf)	Stress (psi)	Failure Mode
SST 1	397	126.37	Timber
SST 2	479	152.47	Timber
SST 3	584	185.89	Timber
SST 4	975	310.35	Timber
SST 5	572	182.07	Timber
Average	601.4	191.43	37% (COV)

Figure 81. Simpson Strong-Tie pull-off carriers (timber failure)

Phenolic Pull-off Bond Strength

Phenolic pull-off specimens exhibited timber failures, as shown in Figure 82, with a thin layer of timber retained on the FRP wrap. This failure shows that the FRP to timber bond in tension was greater than that of underlying timber, but that the resin did not penetrate deeply into the timber. Average pull-off strength was 173 psi as shown in Table 34.

Table 34. Phenolic pull-off bond capacity and strengths

Sample	Force (lbf)	Stress (psi)	Failure Type
Phenolic 1	514	163.61	Timber
Phenolic 2	549	174.75	Timber
Phenolic 3	426	135.60	Timber
Phenolic 4	613	195.12	Timber
Phenolic 5	613	195.12	Timber
Average	543	172.84	14% (COV)

Figure 82. Phenolic pull-off pucks (timber)

Aquawrap Pull-off Bond Strength

The pull-off tests for the Aquawrap displayed failure in the bond line indicating poor resin penetration into the wood substrate (Figure 83). Aquawrap 3 is excluded from the average as the load was below the acceptable range of the test fixture, and Aquawrap 4 is excluded as excessive epoxy adhered to the pile beyond the 2-in. pull off puck invalidating the test. The average pull-off strength was 34 psi as shown in Table 35.

Table 35. Aquawrap pull-off bond capacity and strengths

Sample	Force (lbf)	Stress (psi)	Failure Type
Aquawrap 1	141	44.88	Bond line
Aquawrap 2	99	31.51	Bond line
Aquawrap 3	Excluded	Excluded	
Aquawrap 4	Excluded	Excluded	
Aquawrap 5	105	33.42	Bond line
Aquawrap 6	82	26.10	Bond line
Average	106.75	33.98	23% (COV)

Figure 83. Aquawrap pull-off carriers (bond line)

Unwrapped Timber Pull-off Capacity

Pull-off testing was completed on various locations of unwrapped creosote-treated timber piles to obtain baseline pull-off values. For well-bonded FRP systems, the timber should fail in pull-off testing, so it is important to know the average timber capacity along with the variability in the results. The outside of the pile was sanded before attaching pull-off dollies. As shown in Table 36, the average capacity of the timber under pull-off was 241 psi, but varied from 130 psi to 383 psi. Timber 3 failed in the bond line, which is a failure of the test procedure and was excluded from the results.

Table 36. Pull-off bond capacity

Sample	Load (lbf)	Stress (psi)	Failure Type
Timber 1	508	162	Timber
Timber 2	666	212	Timber surface
Timber 3	Excluded	Excluded	Bond line
Timber 4	753	240	Timber surface
Timber 5	689	219	Timber
Timber 6	1203	383	Timber
Timber 7	1092	348	Timber
Timber 8	525	167	Timber
Timber 9	409	130	Timber
Timber 10	981	312	Timber
Average	758	241	36% (COV)

Pull-off Testing Conclusions

Results from the pull-off evaluations are summarized in Table 37. The Fyfe and Sika systems displayed the highest pull-off strengths. The coefficient of variation for the tests was high due to 4 of the 5 systems failing in the timber, which had higher variations when tested without wrap. Therefore, field test data should be evaluated by recognizing that bond failure in timber substrate results in larger coefficient of variation in the bond test data.

Table 37. Summary of pull-off strengths

System	Strength (psi)	COV	Failure Mode
Fyfe	353	43%	Timber
Sika	317	5%	Timber
Simpson Strong-Tie	191	37%	Timber
Phenolic	173	14%	Timber
Aquawrap	34	23%	Bond line
Timber	241	36%	Timber

Note that the pull-off strengths for these systems were higher than the timber itself. Two possible explanations are: First, the timber used in the Fyfe and Sika tests may be stronger than the un-bonded timber samples. Second, it is possible epoxy resin penetrated deeply into the timber, increasing the pull-off strengths.

The two bond tests conducted in this study evaluated two different bond properties: (1) shear (bond tests), and (2) tension (pull-off). The bond tests were conducted from a design point of view to determine the axial capacity based on bond length. Pull-off tests were conducted to determine any correlations between the two tests, as pull-off tests are likely to be used to verify proper field installation. For comparison purposes, the average pull-off and bond strengths (for both 6-in. and 12-in. bond tests) are provided for each system in Table 38.

Table 38. Comparison with pull-off and average pushout bond strengths (psi)

System	Pull-off Tests		Bond Tests	
	Strength (psi)	Failure Mode	Strength (psi)	Failure Mode
Fyfe	353	Timber	260	Timber
Sika	317	Timber	282	Timber
Simpson Strong-Tie	191	Thin Timber	239	Timber
Phenolic	173	Thin Timber	88	Thin Timber
Aquawrap	34	Bond	69	Bond

The average pull-off and bond strengths are generally similar, and the failure modes for all systems are similar except for the Simpson Strong-Tie samples. In those samples, the pull off strength is lower than the bond strength, which is attributed to an insufficient drilling depth for the pull-off samples. This testing shows that pull-off testing can be an effective method of verifying the in-situ bond strength of FRP systems bonded to timber following ASTM D7522. Further discussion is provided in the inspection guide documents.

Compression Testing

Compression testing was conducted on the FRP shells without any timber to determine the strength of the FRP spanning over timber that has experienced 100% section loss. Wrap thicknesses were varied between three layers and five layers. The results for each system are presented individual followed by summary conclusions for all systems.

Fyfe Compression Results

The Fyfe specimens generally failed in compression initiated by layer separation leading to highly localized buckling of the fabric as shown in Figure 84. The white areas in Figure 84 show areas of matrix failure wherein delamination between fabric layers was noted. Once the matrix fails, the fibers loose lateral support and buckle on a fiber-by-fiber basis, further tearing away from the matrix. The matrix failure rapidly spreads around the entire circumference of the member. This is a typical compression failure mechanism of thin walled composite members and results in permanent, irreversible damage to the sample, which is readily visible as a white cloud.

Due to a misalignment error, Fyfe A which failed in compression and bending only on one side of the sample and is excluded from the averages and further analysis. The maximum compressive loads and stresses of the Fyfe shells are presented in Table 39 for three layers wrap and Table 40 for five layers of wrap. The maximum average stress for three layers was 14,510 psi, and 14,689 psi for five layers.

Table 39. Fyfe three-layer compression results

Specimen	Area (in^2)	Load (lbf)	Stress (psi)
Fyfe A[1]	Excluded	Excluded	Excluded
Fyfe B	4.11	70,600	17,183
Fyfe C	4.17	49,324	11,838
	Average	59,962	14,510
	COV	25%	26%

[1]Off-center positioning (neglected in average)

Table 40. Fyfe five-layer compression results

Specimen	Area (in^2)	Load (lbf)	Stress (psi)
Fyfe D	7.45	106,130	14,252
Fyfe E	7.45	125,490	16,851
Fyfe F	7.45	96,546	12,965
	Average	109,389	14,689
	COV	13%	13%

Figure 84. Typical Fyfe compression failure (Fyfe E)

Figure 85 shows the load versus deflection response for the Fyfe samples. The response was typical to composites wherein there was an initial nonlinear area as the load builds and distributes through the fibers, and any irregularities in the cut ends are evened-out. This was followed by a linear response until sudden failure, resulting in sudden drop in the applied load. The slope of the load versus deflection curves are relatively similar for a given number of layers, which indicated a consistent modulus of elasticity (stiffness) of the wrap. The failures displayed abrupt drops, which are due to the failure in the fibers.

Figure 85. Plot of Fyfe compression load vs deflection

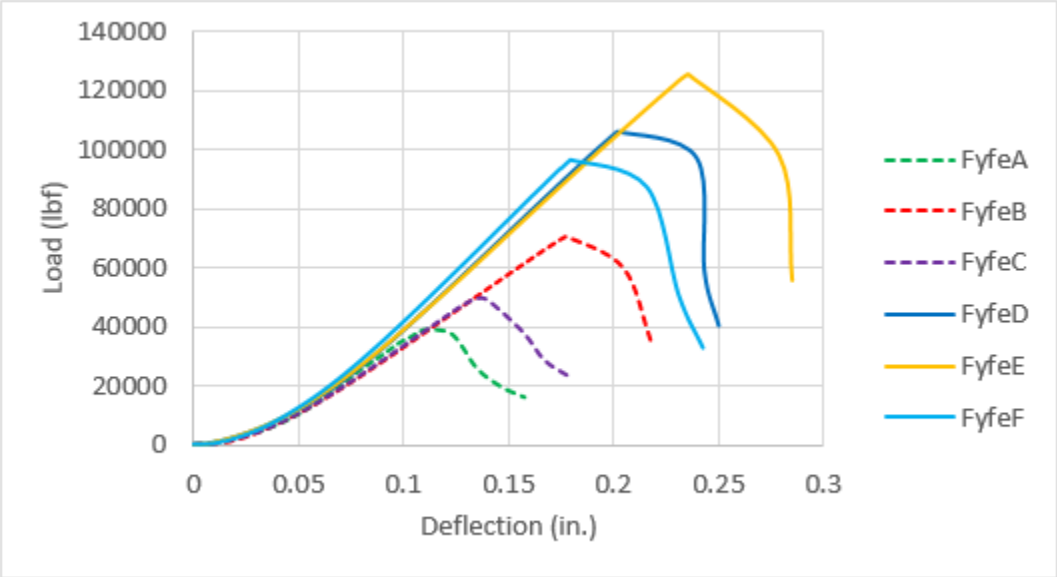

Sika Compression Results

The Sika wraps also failed due to micro buckling in the fibers after resin failure, similar to the Fyfe system, as seen in Figure 86. The maximum compressive loads and stresses of the Sika shells are presented in Table 41 for three layers wrap and Table 42 for five layers of wrap. The maximum average stress was 13,809 psi and 14,096 psi for three and five layers, respectively. The ends of Sika B were not cut perfectly parallel, which resulted in bending forces being induced during the testing, Therefore Sika B was excluded from the analysis.

Table 41. Sika three-layer compression results

Specimen	Area (in^2)	Load (lbf)	Stress (psi)
Sika A	3.43	48,957	14,279
Sika B[1]	Excluded	Excluded	Excluded
Sika C	3.43	45,734	13,339
	Average	47,346	13,809
	COV	5%	5%

[1]non-parallel testing surfaces (Average neglects Sika B)

Table 42. Sika five-layer compression results

Specimen	Area (in^2)	Load (lbf)	Stress (psi)
Sika D	7.36	91,674	12,457
Sika E	7.36	112,690	15,312
Sika F	7.36	106,850	14,519
	Average	103,738	14,096
	COV	10%	10%

Figure 86. Typical compressive failure of sika system (Sika C) in the fibers

Figure 87 shows a similar behavior in the load and deflection response as the Fyfe samples, with a linear response for most of the loading and a sudden drop off near the peak load. The initial slopes are also consistent for a given number of layers.

Figure 87. Sika compression capacities

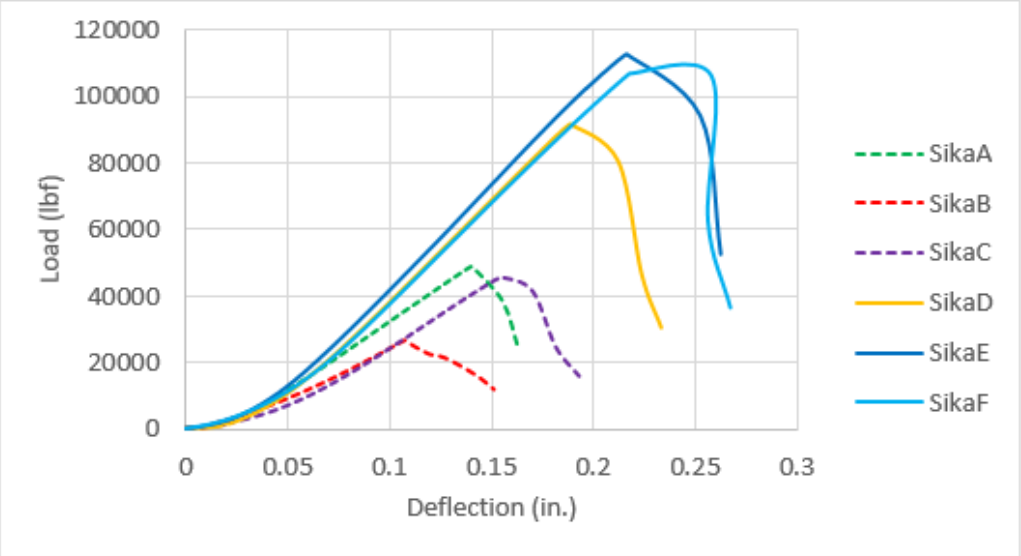

Simpson Strong-Tie Compression Results

The Simpson Strong-Tie wraps yielded similar results as the other epoxy systems with micro buckling of the fibers after matrix failure. The results for the three and five layer shells are presented in Table 43 and Table 44 respectively. The maximum average stress for three layers was 11,482 psi and 16,590 psi for five layers.

Table 43. Simpson Strong-Tie three-layer compression results

Specimen	Area (in^2)	Load (lbf)	Stress (psi)
Simpson A	4.20	49,518	11,778
Simpson B	4.91	57,949	11,797
Simpson C	4.64	50,421	10,870
	Average	52,629	11,482
	COV	9%	5%

Table 44. Simpson Strong-Tie five-layer compression results

Specimen	Area (in^2)	Load (lbf)	Stress (psi)
Simpson D	9.02	139,730	15,494
Simpson E	6.99	124,280	17,786
Simpson F	7.15	117,910	16,490
	Average	127,307	16,590
	COV	9%	7%

Plots of the load versus deflections of the Simpson wraps are shown in Figure 88. The Simpson Strong-Tie wraps displayed very similar behaviors as to those of other epoxy resin-based wraps.

Figure 88. Simpson Strong-Tie compression capacities

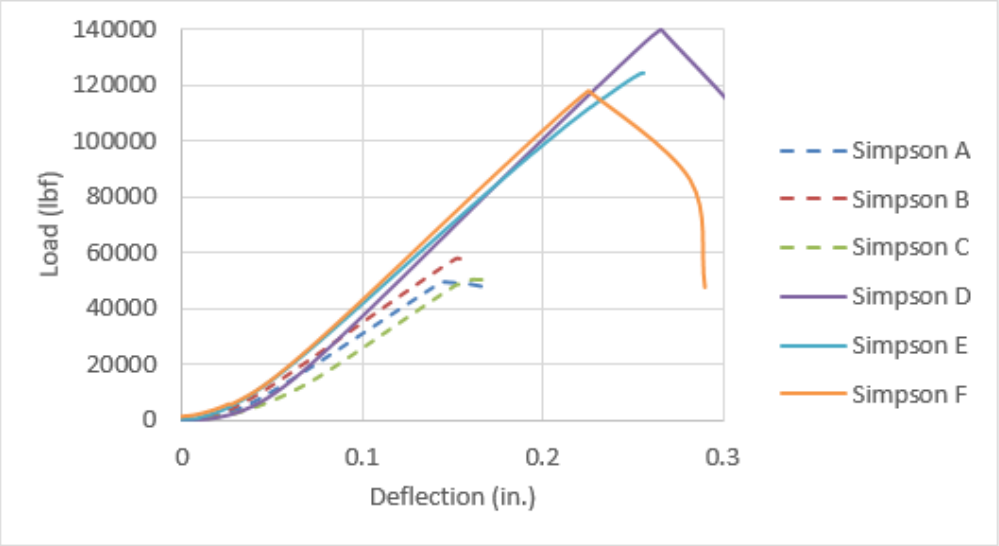

Phenolic Compression Results

Phenolic wraps all failed in a different manner than the epoxy systems. The vertical fibers appear to have torn as the layers separated, with minimal lateral movement of the fibers as shown in Figure 89. The lack of visual damage was attributed to the lower energy at failure due to the small failure loads (~30% of the epoxy systems). The maximum compressive loads and stresses of the phenolic shells are presented in Table 45 for three layers of wrap and Table 46 for five layers of wrap. The maximum average stress for three layers was 4,716 psi and 7,660 psi for five layers.

Table 45. Phenolic three-layer compression results

Specimen	Area (in^2)	Load (lbf)	Stress (psi)
Phenolic A	2.98	11,462	3,843
Phenolic B	2.88	15,004	5,210
Phenolic C	2.96	15,091	5,095
	Average	13,852	4,716
	COV	15%	16%

Table 46. Phenolic five-layer compression results

Specimen	Area (in^2)	Load (lbf)	Stress (psi)
Phenolic D	4.98	37,390	7,515
Phenolic E	4.98	36,380	7,312
Phenolic F	4.98	40,563	8,153
	Average	38,111	7,660
	COV	6%	6%

Figure 89. Typical compressive failure mode in the phenolic shell (Phenolic A)

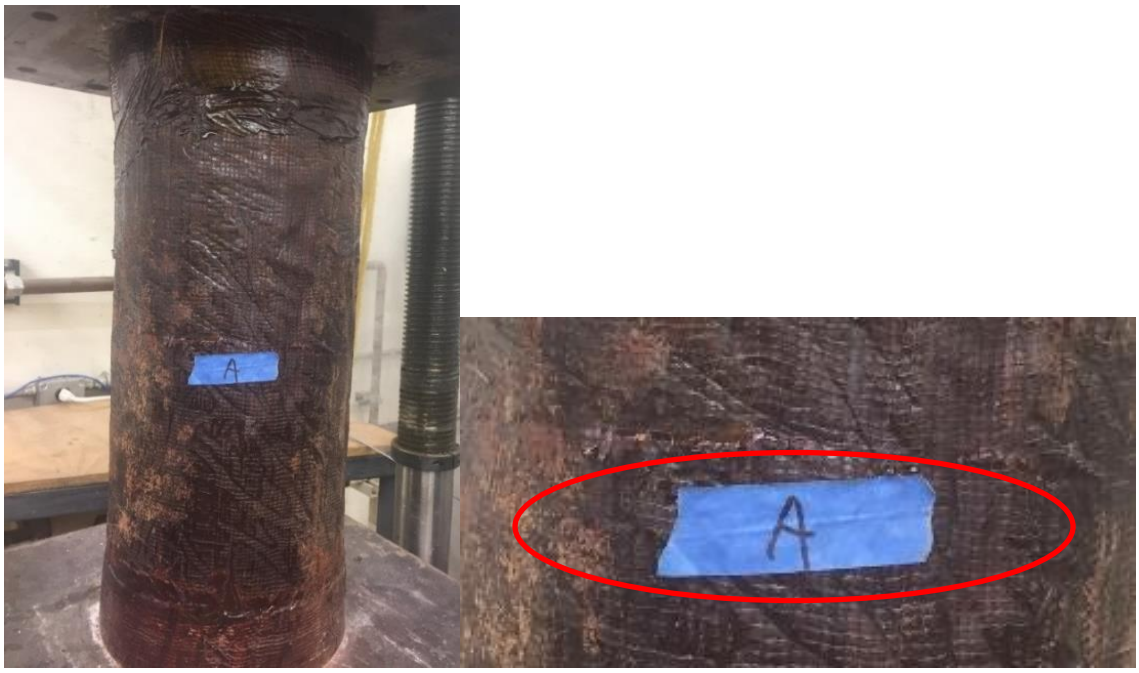

Plots of the load versus deflection behavior of the phenolic wraps are shown in Figure 90. The plots display the similar stiffness and failure behavior as the epoxy systems, but at much lower loads. The damage would be difficult to detect visually under normal inspection practices. This can be a critical flaw in early detection of failure as the samples have significantly lower capacity following failure.

Figure 90. Phenolic compression capacities

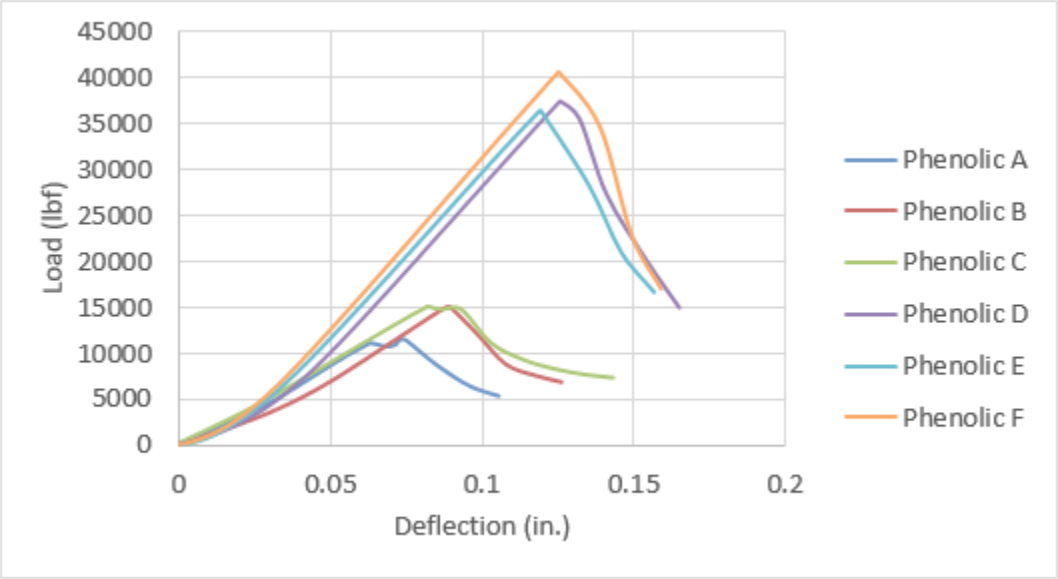

Aquawrap Compression Results

Wraps manufactured from the Aquawrap system displayed classic local buckling failure as shown in Figure 91. The layers debonded from each other at failure, which allowed for lateral movement of the layers without damaging the fibers. Once the load was removed, the shells returned to their original shapes. The maximum compressive loads and stresses of the Aquawrap shells are presented in Table 47 for three layers wrap and Table 48 for five layers of wrap. The maximum average stress for three layers was 4,243 psi and 4,018 psi for five layers.

Table 47. Aquawrap three-layer compression results

Specimen	Area (in^2)	Load (lbf)	Stress (psi)
Aquawrap A	4.86	20,307	4,175
Aquawrap B	4.86	14,102	2,899
Aquawrap C	4.93	27,882	5,655
	Average	20,764	4,243
	COV	33%	33%

Table 48. Aquawrap five-layer compression results

Specimen	Area (in^2)	Load (lbf)	Stress (psi)
Aquawrap D	8.26	16,362	1,981
Aquawrap E	7.92	35,399	4,468
Aquawrap F	8.04	45,049	5,606
	Average	32,270	4,018
	COV	45%	46%

Figure 91. Local buckling failure of Aquawrap

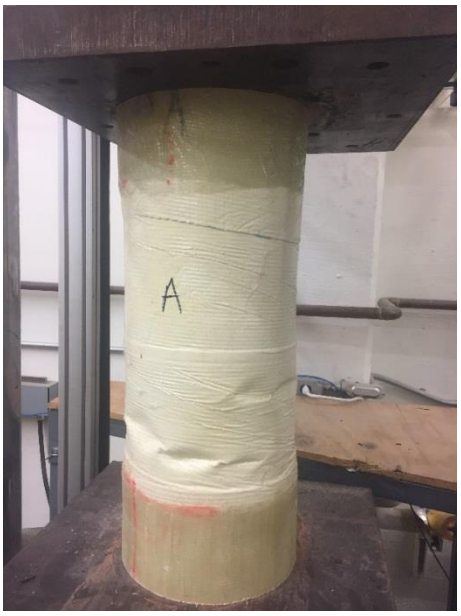

Plots of the load-deflection behavior of the Aquawrap shells are shown in Figure 92. The local buckling failure resulted in a more rounded peak load at failure, but a significant decrease in load after failure.

Figure 92. Aquawrap compression capacities

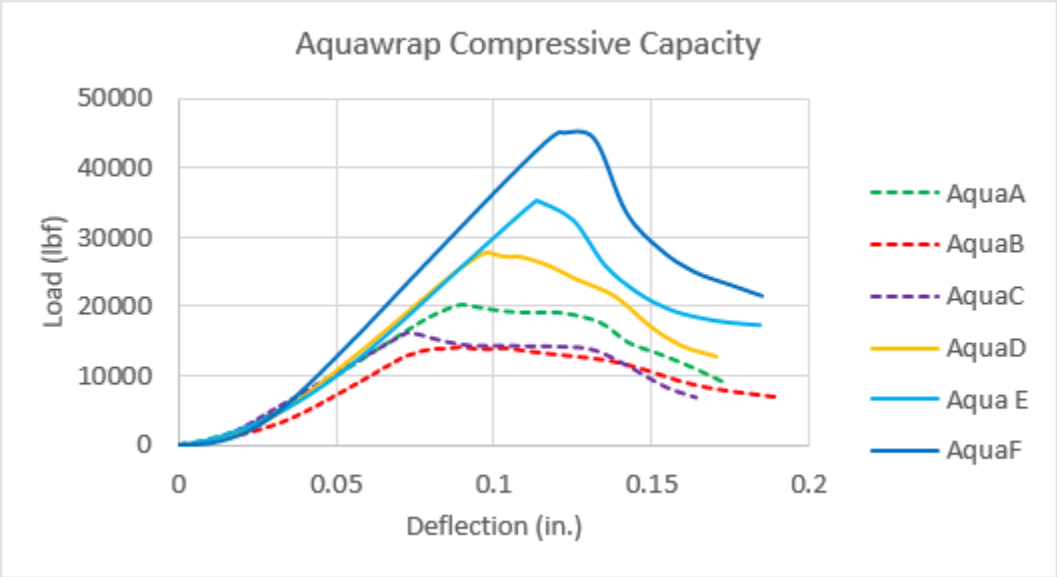

Compression Testing Conclusions

Compression evaluations showed that the epoxy systems (Fyfe, Sika, and Simpson Strong-Tie) provided the highest load capacities and strengths and were reasonably consistent between systems as shown in Table 49 and Table 50. Increasing the number of wraps also increased the strength and capacity of the shells, i.e., more layers leads to higher strengths. The strengths of the Fyfe and Sika systems did not vary with the number of wraps, while most of the other systems showed significant increases in strength with additional layers. This suggests that three layers may be insufficient for the Simpson Strong-Tie and Phenolic systems to reach their design potential. The compressive strength was reduced by 5% with the Aquawrap system showing the strength between layers is a controlling factor.

Table 49. Average compressive load capacity by number of wraps (lbf)

System	Three wraps	Five wraps	Percent Difference
Fyfe	59,962	109,389	82%
Sika	47,346	103,738	119%
Simpson Strong-Tie	52,629	127,307	142%
Phenolic	13,852	38,111	175%
Aquawrap	20,764	32,270	55%

Table 50. Average compressive strength by number of wraps (psi)

System	Three Wraps	Five Wraps	Percent Difference
Fyfe	14,510	14,689	1%
Sika	13,809	14,096	2%
Simpson Strong-Tie	11,482	16,590	44%
Phenolic	4,716	7,660	62%
Aquawrap	4,243	4,018	-5%

For the Fyfe, Sika, and Simpson Strong-Tie systems, the shells failed consistently due to resin failure between layers resulting in highly localized buckling of the fibers in pure compression. The phenolic samples do not appear to have buckled but rather have torn following layer separation. The failure mode for the Aquawrap shells was entirely in elastic local buckling due to poor adhesion between the layers.

When the load versus deflection behavior of the shells is plotted, the differences between failure modes are even more distinct, as shown in Figure 93. The plots for the Fyfe (purple), Sika (blue), and Simpson Strong-Tie (green) shells display consistent linear deformation until maximum capacities were reached. After the maximum capacities were reached, a sharp drop occurs in the plots, which corresponds to the failure of the fibers. The phenolic samples (red) show similar abrupt peaks and loss of capacity but at much lower loads. The Aquawrap samples (yellow) peaked in a rounded way due to the elastic buckling as opposed to sudden fiber failure.

Figure 93. Load vs. deflection for five layers of wrap

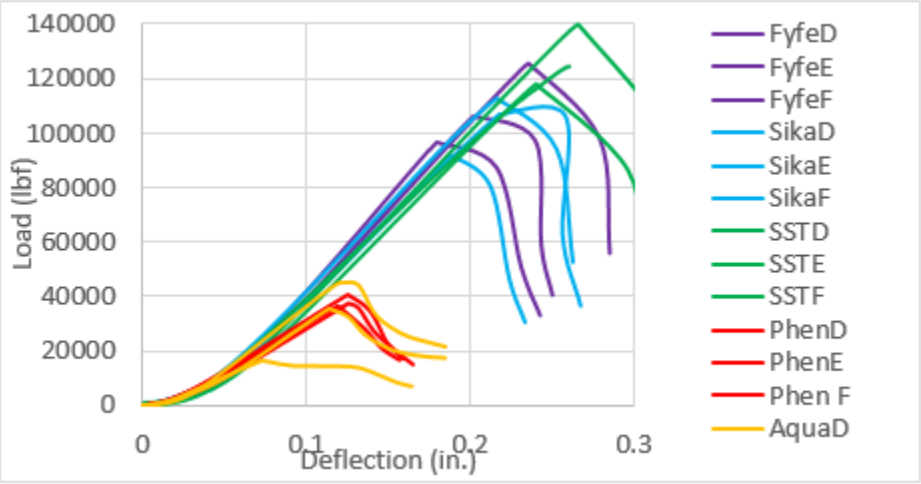

Only one manufacturer publishes compressive strength values, as these FRP systems are typically used with the fabric under tension. The compressive strengths from the testing herein are much lower than published tensile strengths due to a variety of expected reasons:

1) Composites tend to be much stronger in tension than compression. Tension failures primarily occur due to fiber rupture, whereas compression failures tend to occur in the weaker matrix or debonding of layers due to Poisson's effect.

2) Tension samples were tested with all fibers oriented longitudinally, while the testing herein required a third of the fibers in the hoop direction to provide lateral strength.

3) Tension samples are coupons (typically 1 in. wide and 10 in. long) while the samples tested herein are much larger.

4) The hand lay-up of the samples tested herein resulted in samples that mimic the approach used in the field, which is significantly less precise than the coupon prepared by manufacturers.

Based on the above reasons, it was decided not to use manufacturer suggested tension or compression design values in the development of the design guides or guide documents instead relying on the values from the testing conducted herein.

Full-Scale Rehabilitation Simulation

Full-scale rehabilitation simulation tests were conducted using one sample from each system. Three layers of wrap were used to create a repair that incorporated 12 in. bond lengths on each timber pile and an 18 in. gap filled with non-load bearing foam. The main purpose of this test was to simulate a full repair, and demonstrate that testing under axial and bond loads individually is appropriate. Table 51 shows the ultimate loads, stresses, and failure modes for each sample. The comparable failure stress for compression failures was the average failure stress for the three-layer compression tests, while the comparable failure stress for bond was the average failure stress from the bond tests. Most systems failed in compression, with load deflection responses (Figure 94) and loads similar to the compression tests. As these were large samples, fabrication was difficult and eccentricities were present in the completed samples, which resulted in failure primarily on one side of the sample as shown in Figure 95. The lower failure stresses of the Fyfe, Sika, and Phenolic samples were attributed to the eccentricities present in these samples. Only the Aquawrap sample failed in bond, and the failure was significantly lower than any other bond test data corresponding to other manufacturers.

Table 51. Summary of simulated rehabilitation

System	Ultimate Load (lbf)	Failure Stress (psi)	Failure Mode	Comparable Failure Stress (psi)
Fyfe	49,733	11,629	Compression	14,510
Sika	44,330	10,842	Compression	13,809
Simpson Strong-Tie	64,604	12,819	Compression	11,482
Phenolic	20,953	4,844	Compression	4,716
Aquawrap	7,198	18	Bond	56

Figure 94. Combined failure load versus deflection

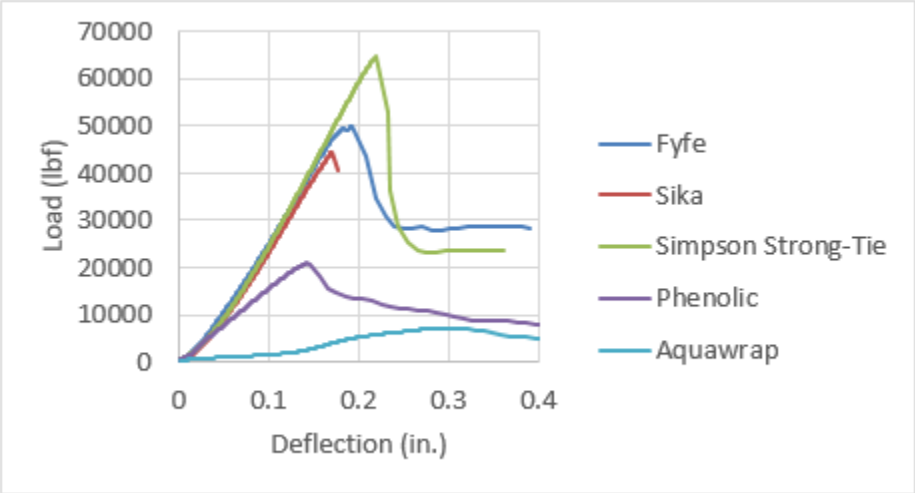

Figure 95. Typical simulated rehab failure

The simulated rehabilitation testing suggests that the individual compression and bond tests are suitable test methods to replicate the field conditions. The individual tests are much easier to prepare than the simulated rehabilitation tests, resulting in fewer experimental errors. In addition, the individual tests use less material and thus are more economical to conduct additional tests.

Combined Axial and Bending

Three 30-in. long samples composed of three layers of the Sika system were tested under combined axial and bending loads. Strain gages were installed to measure the axial strain (middle gage), combined axial and flexural compression strain (bottom gage), and combined axial and flexural tension strain (top gage), with negative strain indicating compression. First an axial load was applied, then a side load was applied until failure. The axial load was applied until it reached 75% of the average failure of load of the three-layer compression tests, until cracking was heard, or ultimate failure load was reached. Axial loading for sample 1 was halted at 17,021 lbf when significant cracking was heard, and sample 2 failed in axial load at 25,935 lbf as shown in Table 52. The test fixtures did not allow for adjustment due to uneven cuts, thus the initial axial loads likely had a bending component as well. The uneven loading was evident in the strain readings, which should be equal under axial loads as these gages were placed along the loading direction, but at opposed faces of the test specimens. However, the gage readings varied from one location to another. Sample 3 was the only sample with similar strain readings on all sides under axial load, and it was the only sample to reach 75% of the axial compression failure load.

Table 52. Loads and strains under initial axial load

Sample	Max Axial Load (lbf)	Axial Stress (psi)	Strain at Max Axial Load		
			Bottom	Middle	Top
1	17,021	5,207	-257	-959	-475
2	25,935	7,980	-1053	-4080	-2029
3	35,412	9,013	-1674	-1799	-1973

Side load was applied to samples 1 and 3 to generate bending forces. As shown in Table 53, flexural behavior was observed as the bottom strain gage recorded higher compressive strains due to the combined axial and flexural compressive stresses. The top strain gage recorded lower compressive strains due to the combined axial and tensile compressive stresses. However, the middle gage located at the neutral axis should have not changed in strain values, but instead saw larger reductions in compressive strain than the top gages. Failure of both samples was due to local crushing of the sample at the edge of the curved saddle used to apply the side load. Additional details of failure under combined loads can be seen in Figure 96, which was not indicative of a typical flexural failure. Thus, no inferences on the combined axial and bending can be made using the work carried out herein. Future testing should use longer samples to induce greater flexural moments.

Table 53. Loads and strains under combined axial and bending loads

Sample	Max Side Load (lbf)	Strain at Max Side Load		
		Bottom	Middle	Top
1	2,382	-1365	-166	-98
3	761	-1941	-945	-1439

Figure 96. Failure of combined axial and bending

Crack, Bulk, and Injection Fillers

Crack fillers were evaluated for their ability to fill cracks and external voids to prevent internal fillers from leaking out. The crack filler was applied with a putty knife onto the timber samples and allowed to cure. The Sikadur and Simpson Strong-Tie fillers hardened within a couple hours, while the Elmer's took a full day to cure. After 24 hours, the specimens were filled with 10W-30 motor oil, which simulates the flow properties of many bulk fillers. The specimens were observed for three hours. At that time, the oil level in each sample dropped by a maximum of 1/4 in., no leaks were present, and no oil was observed on the pan underneath the samples. This indicates the oil was soaking into the wood and all of the fillers were performing as intended. After three hours, the bulk fillers would have gelled, meaning that the crack fillers were sufficient for the task. It was important to apply the fillers in a manner that deeply fill the holes and cracks.

Figure 97. Prepared crack filler specimens

Bulk fillers were evaluated by how well they filled the manufactured voids in the samples. Since the samples were all drilled to the same depth, they could be cut just above the void and the degree of fill measured with a ruler. Table 54 shows the percent of the volume filled for each system and for each void percent. The phenolic system flowed slower than the other systems, which led to the voids not being topped off as well. The Sikadur epoxy flowed very easily, but it was thin enough to leak out of a small crack in the bottom of two of the 75% void samples. The addition of sand to the Sikadur resin eliminated this problem. The expanding Rimline polyurethane completely filled the voids in every case, with the foam expanding up the fill holes and onto the surface of the timber. The cured foam was not as hard as the rigid phenolic or Sikadur product. It is a structural foam that should be able to support some amount of compressive loads in a confined environment (such as a wrapped

timber pile), but establishing the strength is outside the scope of this work. It was observed that the sand tended to settle to the bottom of the mixing cups in all of the resins, but this was not considered to be a detrimental issue.

Table 54. Bulk filler fill percentage

System	Void Percent	Void Volume Percent Filled
Phenolic	25%	98%
Phenolic	56%	90%
Phenolic with Sand	56%	83%
Sikadur	25%	100%
Sikadur	56%	74%
Sikadur with Sand	56%	98%
Rimline	25%	100%
Rimline	56%	100%
Rimline with Sand	56%	100%

The assessment of the effectiveness of injecting filler into voids was the most subjective. Each filler was easy to apply, and the store-bought syringe worked well for the Sikadur 35 resin, which allows for the same material to be used for bulk and injection filling.

Figure 98 shows the small voids, Figure 99 shows the medium voids, and Figure 100 shows the large interconnected voids. In each photo, the tests were labeled 1-9 with 1-3 referring to Sikadur Crack Fix injected with a caulk gun, Sikadur 35 injected with a syringe in samples 4 through 6, and the blue Simpson Strong-Tie foam in tests 7 through 9. Overall, the Simpson Strong-Tie polyurethane did an excellent job filling the voids in every test, with the foam expanding into every hole in the larger, interconnected void tests. However, the foam was quite soft upon curing, thus it was not clear if this would create false positives during later inspections. The Sikadur resins performed similarly regardless of the applicator wherein there was always a small air bubble left up to 1/2 in. diameter. These air bubbles were a consequence of the need to have a filling hole which the resin flows back after being pumped in (the samples were filled in the vertical position to replicate a repaired pile). However, the voids were smaller than the typical nonconforming void area (2 in^2), so this is not considered a failure of the filler. The syringe had a smaller tip than the caulk gun, which did not fit in the predrilled holes as tightly. Thus, they could not be pumped under pressure into the smallest holes in the large interconnected test with the syringe (tests 4-6), while the pressure applied with the caulk gun filled the small holes in tests 2 and 3.

Figure 98. Small voids (1 in. diameter)

Figure 99. Medium voids (2 in. diameter)

Figure 100. Large interconnected voids

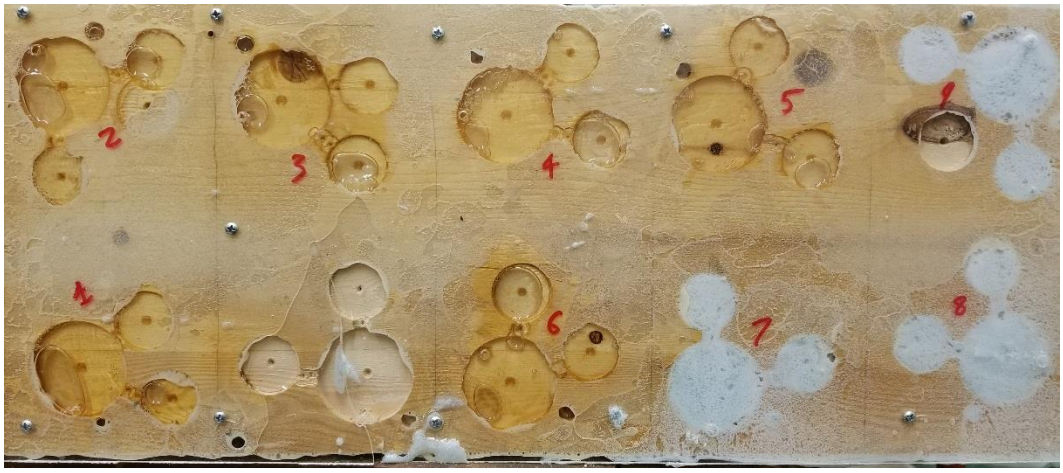

Overall, the Simpson Strong-Tie foam had the best filling ability, but the soft nature of the cured foam might hinder later inspections by creating false positives. The Sikadur resins performed well, though the caulk gun injection allowed for more pressure to be applied resulting in better filling of smaller voids.

Design Methodology

A design methodology was proposed herein based on standard timber design practices and the data generated through this experimental program. The proposed methodology was expected to be conservative due to the limited number of samples tested while providing a high factor of safety until additional testing and evaluation could be completed. Based on the failure modes, the design methodology focuses on the two primary limit states: axial capacity and bond strength. The design methodology does not take into account bending as the test data was not conclusive. Repaired piles should be sufficiently braced to prevent flexural effects. The loads were assumed to be equally distributed between piles.

Design Methodology – Axial Capacity Limit State

The experimental testing completed for this project revealed that the axial capacity of a FRP rehabilitated timber pile was controlled by compression failure initiated by layer separation leading to localized buckling of the fabric. Therefore, the limiting factor was the compressive strength of the FRP system. Imperfections in the FRP shell can lead to premature failures due to additional stress build up from bending and/or twisting under compressive loads and other local stress concentrations due to voids, fabric kinks, and inclusions. Design of FRP is assumed to be wrinkle and void free. Due to difficulties of installation, voids/wrinkles are impossible to avoid in practice, so an added factor of safety was applied into the design equation. Of the five systems tested, the epoxy-based systems had exhibited consistently higher strengths and were chosen for the design methodology development. The shells tested were representative of real-world application where the deteriorated timber contributes no strength, as per the scope of this work.

The compressive strengths and axial capacities for only the epoxy-based systems (Fyfe, Sika, and Simpson Strong Tie) are listed in Table 55. The five-layer compression shells showed higher strength than the three-layer shells. The average compressive strength increased from 13,012 psi for three layers to 15,125 psi for five layers. It is noted that the increase in layers does not linearly increase the strength, but rather shows a diminishing effectiveness. Rajappa found that with more FRP layers the axial strength goes up, but the effectiveness per layer will eventually reach a peak and then start to decline [63]. Rajappa accredits this occurrence to shear lag between the resin and the fiber. Since the testing program was limited to only two different configurations, it is not known when diminishing returns start with additional layers, thus the total thickness should be limited to 0.5 in. maximum to arrive at cost effective solutions.

Table 55. Compression testing results

	Compressive Strength (psi)		Capacity (lbf)	
	Three Layers	**Five Layers**	**Three Layers**	**Five Layers**
	10,870	12,457	45,734	91,674
	11,778	12,965	48,957	96,546
	11,797	14,252	49,324	106,130
	11,838	14,519	49,518	106,850
	13,339	15,312	50,421	112,690
	14,279	15,494	57,949	117,910
	17,183	16,490	70,600	124,280
		16,851		125,490
		17,786		139,730
Average	**13,012**	**15,125**	**53,215**	**113,478**

Based off the experimental testing data given in Table 55, the compressive strength increases with shell thicknesses but shows a diminishing return of compressive strength with shell thickness. A natural log function was used as a trend line as shown with the dashed line in Figure 101 and presented as equation (1). A natural log was chosen as it best represents the diminishing return found in both the data herein and reported by Rajappa.

$$\sigma = \varphi(2615 * \ln x + 18356) \quad (1)$$

To arrive at a design equation, two sets of adjustments were made. First, a reduction factor was derived using Section 3.5.1 of the *Timber Pile Design and Construction Manual*, which provides equation (2). If this equation was applied to the experimental data presented herein, the working axial stress of the FRP should not exceed 5,654 psi. It was decided this limit should apply to a wall thickness of 0.5 in., which is double the max wall thickness tested. A modification factor of 0.35 was found to produce a stress of 5,790 psi with a 0.5 in. wall thickness. The constants and coefficients in equation (1) were rounded to further adjust the predicted stress, resulting in the axial strength design equation (3). The reduction factor also accounts for the lack of redundancy in the event of failure under axial load; once the FRP has crushed, the strength is effectively reduced to zero.

$$\sigma = (AVG - 1.645SD) / 1.88 \quad (2)$$

Where,
σ = compression strength for compression parallel to the grain on timber piles (psi),
AVG = average of the test results (psi), and
SD = standard deviation of the test results (psi).

Figure 101. Compressive strength plot

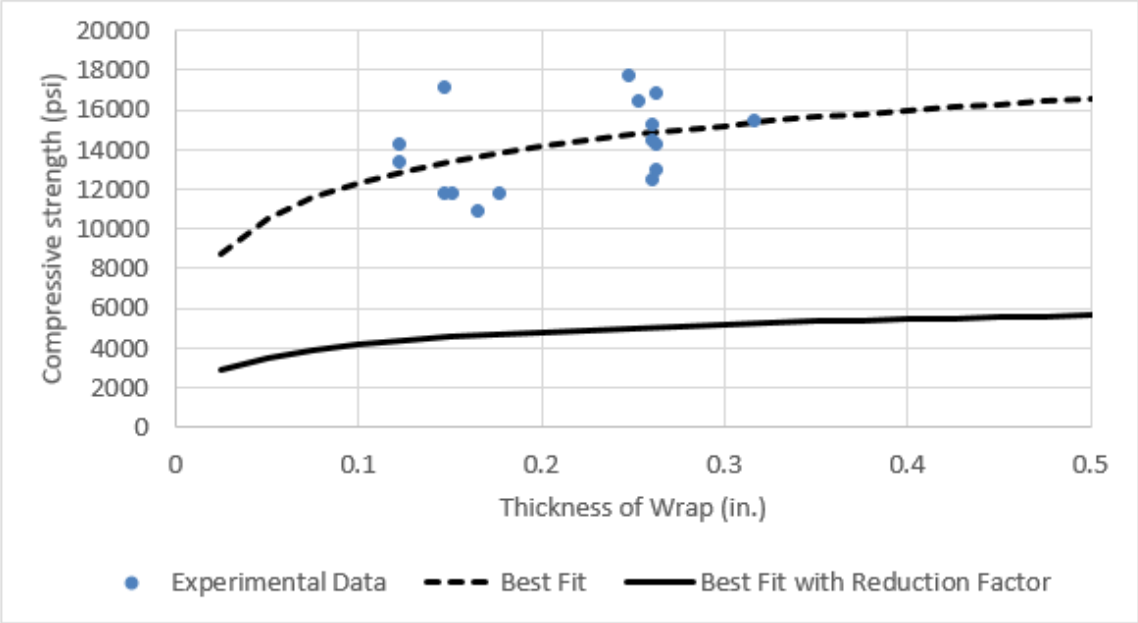

The axial strength design equation is

$$\sigma = \varphi(2650 * \ln x + 18000) \quad (3)$$

Where,

σ = compressive stress (psi),
φ = reduction factor (0.35), and
x = shell thickness, max of 1 inch (in.).

Using the axial design equation (3), the maximum capacity can be calculated using the diameter of a pile, which in this case was taken as 10.4 in. diameter to match the average experimental pile diameter value. To obtain a strength similar to the 94,000 lbf capacity of a 10-in. diameter southern yellow pine pile, a shell thickness of 0.5 in. is required, or ~10 layers using the epoxy-based systems tested. The predicted capacity at 0.15 in. of thickness (~3 layers) is 22,573 lbf and at 0.25 in. (~5 layers) it is 41,941 lbf using a 10.4 in. diameter.

Figure 102. Axial strength plot

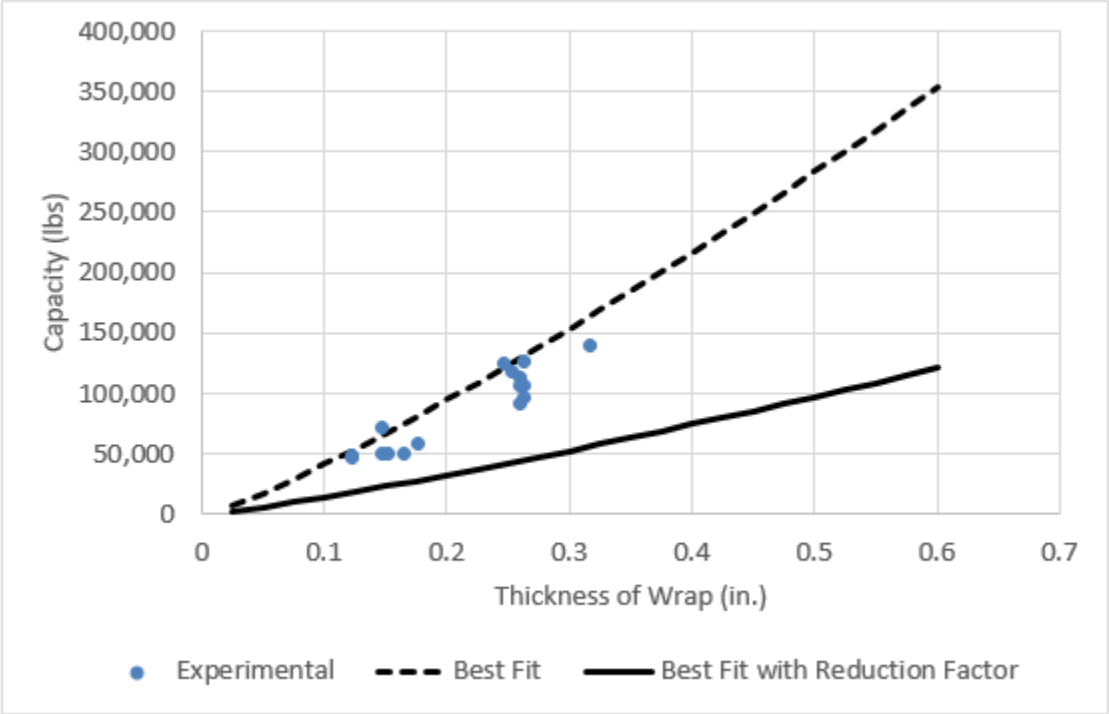

Design Methodology – Bond Strength Limit State

For this project, new timber piles samples were wrapped with FRP and tested under controlled conditions to determine the bond strength between the FRP wrap and the creosote-treated timber piles. The compression testing subjected the samples to loading conditions that isolated the bond shear strength of the completed repair through the axial compression tests discussed in depth in the full report. Visual inspection of the failed test samples for the epoxy based systems (Fyfe, Sika, & Simpson Strong Tie) revealed that large portions of timber were still bonded to the FRP after failure which is noted in the wood (the other systems are not included as their axial capacity was insufficient). As shown in Table 56, increasing the bond length from 6 in. to 12 in. did not maintain the bond stress/strength capacity, but instead the bond strength reduced from an average of 306 psi to 215 psi. This phenomenon is well understood and also has been documented. For example, the bond strength decreased from 1869 psi to 343 psi when the bond length increased from 0.59 in. to 7.0 in. [64]. The combination of timber delamination onto the wrap and decreasing capacity indicates that the FRP-timber bond strength for this application is controlled by the timber substrate in terms of timber peel strength parallel to the grain. In addition, the 12-in. bond samples aged in wet-dry conditions for 12 months did not show any decrease in bond strength as the timber controlled the failure and no failure is noted at the glue line FRP wrap and timber substrate. These test results are included in further analysis to provide additional data to arrive at a design equation through curve fitting process.

Table 56. Experimental bond strength

	6-in. bond		12-in. bond		12-in. bond (aged)	
	Stress (psi)	**Capacity (lbf)**	**Stress (psi)**	**Capacity (lbf)**	**Stress (psi)**	**Capacity (lbf)**
	190	37685	178	68940	202	78778
	215	41853	187	70511	209	82577
	255	50953	187	74749	224	85785
	261	51161	203	75718	241	94262
	273	53233	212	80246	283	104750
	364	69067	231	84405	293	105580
	384	74305	236	89272		
	386	79130	247	97572		
	420	81343	255	98333		
Average	**306**	**59859**	**215**	**82194**	**242**	**91955**

This trend in bond strength reduction as a function of increase in bond length is expected for timber piles rehabilitated with FRP wraps. Herein, the forces are transferred into the timber through the outermost growth ring. The strength is then dependent on the interlaminar strength between the growth rings timber (peel strength) within the pile. As this was a weak plane in wood, it is typically avoided through sawing techniques (i.e., quarter sawn wood), but this was not possible for piles given the dimensional requirements.

The strength was further limited by the fact that the outside surface of the timber piles was uneven (not perfectly smooth) trunks with the bark removed. This resulted in a lower strength due to local bending induced stresses compared to other FRP-timber bonding applications wherein the FRP was bonded to flat boards spanning multiple growth rings.

Finally, epoxy was chosen for this work as it has been used extensively for repair of concrete structures and is promoted for use with timber as well. Epoxies exhibit good bond strength between different materials. Thus, they are well suited for bonding glass fibers to wood. However, they do not possess the strength of other adhesives used to bond wood to wood. These limitations (peel strength, uneven bonding area, and epoxy strength) reduce the bond strength to a lower value compared to other testing, but it is representative of the field conditions when repairing timber piles in the field.

To predict the bond strength for other lengths while accounting for the decreasing bond strength with bond length, a natural log function was used as a trend line, shown as the dashed line in Figure 103. This best fit equation was then rounded and a strength reduction factor was applied to generate the design equation shown below. This equation predicts a bond strength that reduces with bond length while following the trend of the experimental data. The minimum bond length is limited to 6 in. as the data spread at 6 in. was significant indicating that localized deficiencies in the timber or wrap application have a significant effect. The maximum bond length was limited to 24 in. due to the uncertainties in extrapolating the experimental data beyond 2 times the max tested length. A reduction factor of 0.6 was chosen for the design equation as this resulted in bond strengths that were less than one standard deviation below the average experimental values. This reduction factor was chosen as the remaining in-situ strength (in the repair area and the filler materials) will provide axial capacity due to FRP wrap confinement. The in-service timber and filler capacity cannot be accurately calculated given uncertainty surrounding the amount of rot, and was not included in the design calculations. However, they provide redundancy to the system which permits a higher reduction or knock-down factor.

Figure 103. Bond strength prediction: experimental vs. prediction

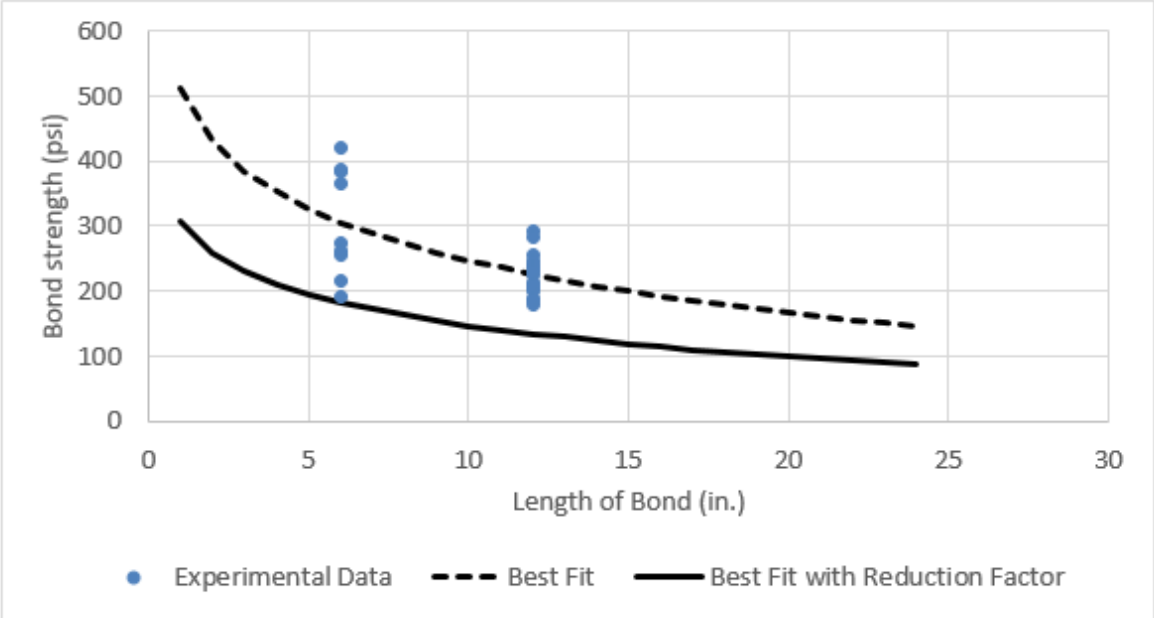

The bond strength design equation as per the curve fit data is:

$$\sigma = \varphi(-115 * \ln x + 510) \quad (4)$$

Where,

σ = the bond stress (psi),

φ = reduction factor (0.6), and

x = bond length, min of 6 inches, max of 24 inches (in.).

The bond strength design equation (4) calculates a lower stress compared to every experimental bond strength result reported herein. At 6 in. of bond length, the equation gives a bond stress of 182 psi, which is 60% of the average test value and 1.5 standard deviations from the average. Similarly, for 12 in. of bond, equation 4 predicts a bond stress of 135 psi, which is 60% of the average and 2.7 standard deviations from the average. Therefore, the bond strength design equation (4) becomes more conservative as the bond length increases.

Using the bond strength design equation (4), the maximum capacity was calculated using the diameter of a pile, which in this case is taken as 10.23 in. to match the average experimental value. Based on the maximum length of 24 in., the max bond capacity is 66,911 lbf. As shown in Figure 104, the predicted capacity at 6 in. of bond is 35,180 lbf and at 12 in. it is 51,908 lbf.

Figure 104. Bond capacity vs. bond length

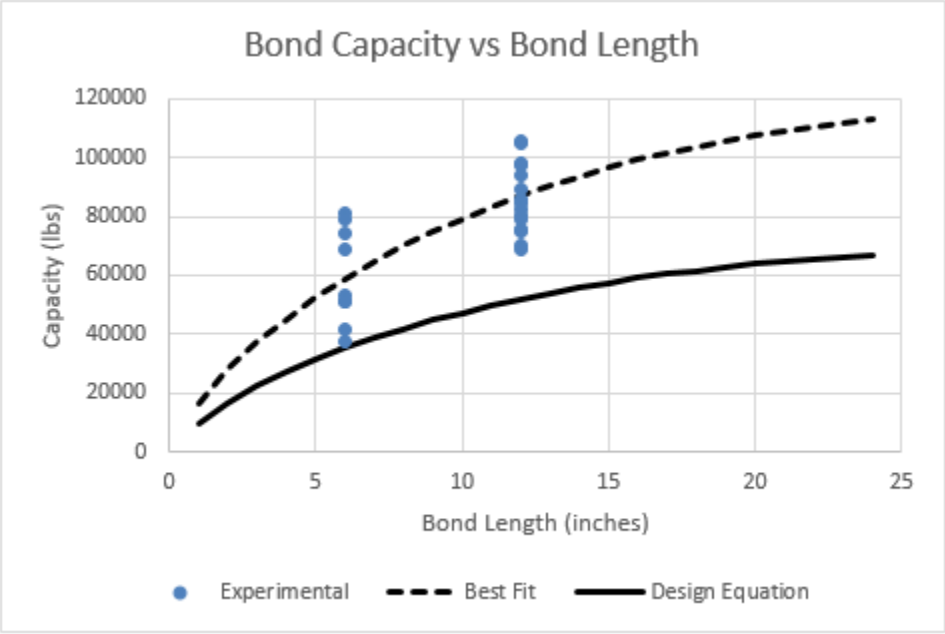

Table 3-2 of the *Timber Pile Manual* lists an allowable axial compression pile capacity for 10 in. southern pine piles as 94,000 lbf. However, the maximum bond capacity using the design equation proposed herein results in a total capacity of 66,911 lbf. LTRC would need to determine if this capacity is sufficient to meet their needs, or if changes to the design methodology would need to be made, possibly including:

- Adjusting the reduction factors to have lower conservativeness then the ones suggested in earlier sections of this report
- Accounting for a portion of the remaining capacity in the in-service timber pile
- Removing the rotten timber section and replacing with new timber section, then using FRP wraps to join the sections together and seal the repair (i.e., posting /splicing)
- Using mechanical or other means to create additional bond strength between the FRP and wood

Material Properties

The best performing systems were epoxy based unidirectional glass FRP. Material properties were provided from manufacturer's data sheets. Tested material properties are listed in Table 57. As previously discussed, the tensile strengths were not expected to be achieved in the configurations tested herein. However, these minimum material properties are recommended as tensile testing of composite wraps can be completed easily following ASTM D7565. Materials other than the ones tested by WVU are acceptable, as long as they meet minimum requirements. Minimum requirements are based off the tested products and are marked in Table 57.

Table 57. Manufacturer's material properties of tested products

Manufacturer	Tensile Strength (psi)	Modulus (psi)	Thickness per ply (in.)	Tensile Elongation (%)	Minimum fabric weight (oz./yd^2)
Fyfe	66,720	3,030,000*	0.05	1.76%	27
Sika	78,400	3,970,000	0.04*	1.82%	27
Simpson Strong-Tie	56,000*	3,300,000	0.05	1.70%	27

* minimum requirement

Test Results and Analysis for Traditional Splicing

This section provides data gathered through testing of timber piles after splice repair under shear, bending, and axial loading. Evaluation of the data was discussed and highlighted in this section.

Data Analysis under Shear Testing

Data were analyzed for maximum shear stress and deflection after plotting shear stress versus deflection diagrams. Maximum shear stress of each test specimen, induced at depth d/2, is determined using equations (1) and (2).

$$A = \frac{\pi d^2}{4} \tag{5}$$

$$\tau = \frac{4F}{3A} \tag{6}$$

d – Diameter of the pile cross section
A – Area of the pile cross section
τ – Shear Stress
F – Force applied to the pile

For simplicity, shear stress was computed using the cross-sectional area of each timber pile, neglecting the shear resistance offered by the splicing mechanism. A shear stress-displacement plot was made for each specimen, as shown in Figures 105, 106, and 107.

The shear tests were performed on three, 8-ft. long piles of each of the three repair methods, resulting in a total of nine tests (Table 18). Table 58 shows the maximum shear stress and the corresponding deflection for each of the nine tests, including their averages.

Table 58. Maximum shear stress and corresponding deflection*

Flat Steel Plate Splicing				
Test	**1**	**2**	**3**	**AVG**
Maximum Shear Stress (psi)	614	701	452	589
Deflection at Maximum Stress (in)	2.4	3.1	2.5	2.7
Steel C-Channel Splicing				
Test	**1**	**2**	**3**	**AVG**
Maximum Shear Stress (psi)	715	761	873	783
Deflection at Maximum Stress (in)	2.3	2.3	2.0	2.2
Wooden Plate Splicing				
Test	**1**	**2**	**3**	**AVG**
Maximum Shear Stress (psi)	484	528	610	541
Deflection at Maximum Stress (in)	1.7	2.1	1.5	1.8

*Note: Deflections shown here are recorded at the point of maximum shear stress.

Shear stress versus transverse deflection for timber piles spliced with flat steel plates is shown in Figure 105. The test data revealed a 40% variation in shear stress (500 psi vs 700 psi) which was attributed to the quality of pile specimens. Pre-existing flaws such as cracks and other natural variations of timber may have contributed to the shear stress (magnitude) variation. The random cracking was observed visually and can be attributed to internal flaws in large size timbers. It was observed that the first test exceeded the deflection that the LVDT was able to record due to improper zeroing technique.

Figure 105. Shear stress vs. deflection for steel plate splice

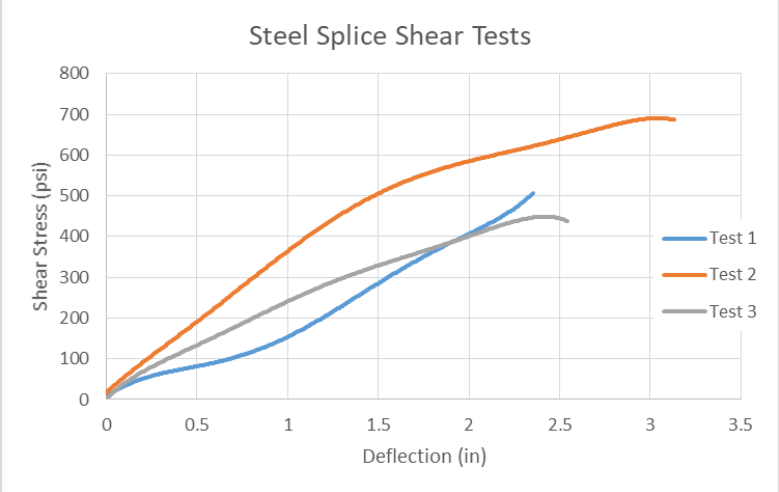

A graphical representation of shear stress versus deflection relationship for timber piles spliced with steel C-channel splicing is provided in Figure 106. From the data it is observed that shear failure mode is nearly identical in all piles. It is also noted that the C-channel

method of splicing is stronger than the steel plate splicing method. This is to be expected as the C-channel method provides higher shear resistance than the steel plate splice. Similar to the deflection response with steel plate shear testing, deflection peaked above the constraints of the test device (string pot) for test one of this method. The initial slope change in tests one and two could be attributed to initial internal adjustment of the test specimen and the test frame at the early stages of loading. The C-channel splicing digs into the wooden pile upon initial loading. These changes in slope may also be a result of yielding of steel at the load location, which is observed in multiple specimens of this repair type.

Figure 106. Shear stress vs deflection for C-channel splice

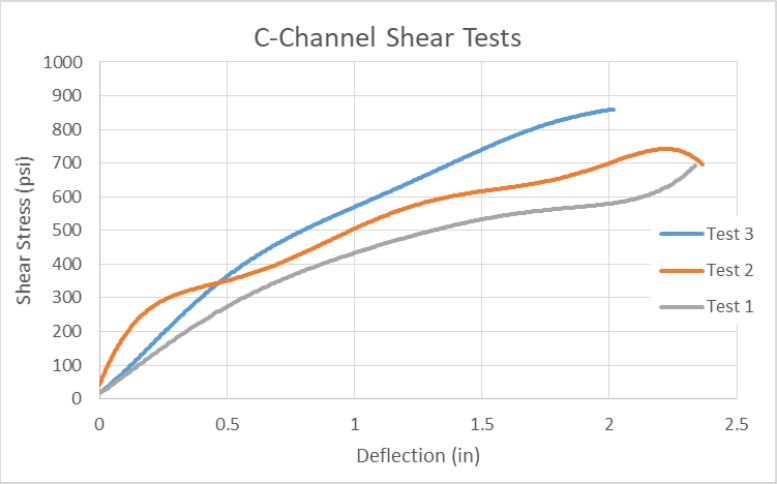

Figure 107 provides the shear stress versus deflection plots for tested specimens with the wooden plate splicing test group. The applied load induced an indentation in the splicing at the point of contact. The wooden plate splice, however, does not have the same yielding effect as the other two splicing methods. This method of splicing with wood was slightly weaker than the other two in terms of shear stress at failure.

Figure 107. Shear stress vs. deflection for wood splice

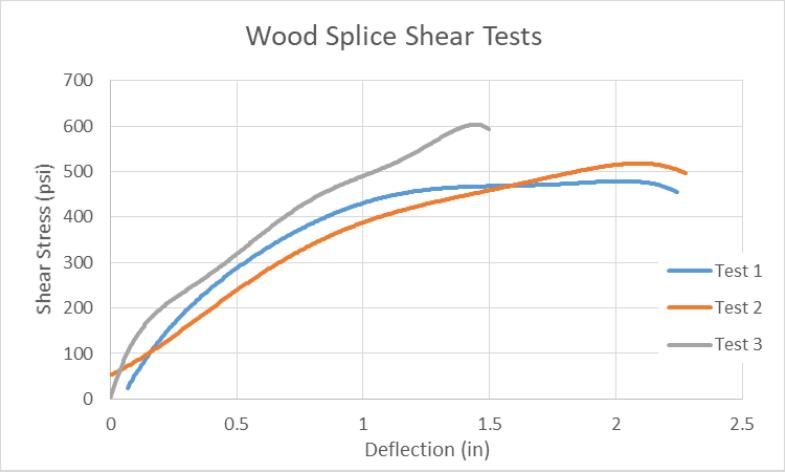

Shear Analysis - Summary and Failure Modes

In terms of shear strength of the piles based on the three methods of splicing, the C-channel method was the strongest and the wood plate method was the weakest, with a 30% variation. This observation was based on the maximum shear stress resisted by each of the splicing mechanisms. The C-channel splice method provides a higher shear stress resistance than the other two methods due to its large material volume and shape compared to the lesser volume of the flat steel plate splice. Its connection to the pile through its channel shape provides additional shear resistance to the specimen. Test 2 data (Table 58) revealed that the wooden plate method provided the least deflection at failure in comparison with the other two methods, indicative of a higher material stiffness over the other two methods. Under loading, the wooden splice plates interacted more cohesively than the steel plates or C-channel counterparts. This was largely attributed to the similarity in modulus of the splicing mechanism and the timber pile. In the steel and C-channel splicing the steel yielded prior to ultimate failure, allowing the piles to continue to deflect.

While this test data was helpful in terms of understanding the strengths of different splicing methods, it was important to keep multiple variables in mind. For example, what is to be considered a “failure?” Ultimate stress as found in this testing can be misleading at times. Visual signs of failure are observed before a pile reached its ultimate strength. Multiple signs of visual failure were observed during testing. For the steel plate and C-channel splicing methods, it was observed that the steel plate at the surface yielded significantly. The plates on the side of the pile would not yield but it was observed that the bolts would bend and yield internally. When a specimen cannot carry any more load while deflection is increasing under load application, it is determined failure took place and testing is terminated. These two forms of visual failure can be seen in the images provided in Figure 108 and Figure 109. In the case of the wood splicing method, indentation from the applied load as well as cracking

on the top and bottom plates were observed. This visual failure mode can be seen in Figure 110.

Figure 108. Yielding of top and bottom plates in steel splicing

Figure 109. Yielding of bolts in C-channel splicing

Figure 110. Cracking of top and bottom plates in wood splicing

Data Analysis under Bending Testing

The pile test data under bending were analyzed to establish maximum bending stress and deflection after plotting bending stress versus deflection curves. Cross sectional diameter of timber piles was measured and recorded. Modulus of rupture was determined using Equation 7.

$$\mathrm{MOR} = \frac{4\mathrm{Pa}}{\pi r^3} \tag{7}$$

MOR – Modulus of Rupture
P – Total applied load
a – Distance between applied loads
r – Radius of cross section

The bending tests were performed on three 16-ft. long piles using each of the three repair methods, giving a total of nine tests. Table 59 shows the maximum bending stress (MOR) and the corresponding deflection for each of the nine tests, including their averages.

Table 59. Maximum bending stress and corresponding deflection

Flat Steel Plate Splicing				
Test	**1**	**2**	**3**	**AVG**
Maximum Modulus of Rupture (psi)	6674	3647	3417	4579
Deflection at Maximum stress (in.)	3.6*	9.5	10.6	7.9
Steel C- Channel Splicing				
Test	**1**	**2**	**AVG**	
Maximum Modulus of Rupture (psi)	2826	4731	3778	
Deflection at Maximum stress (in.)	10.2	9.9	10.1	
Wooden Plate Splicing				
Test	**1**	**2**	**3**	**AVG**
Maximum Modulus of Rupture (psi)	4609	4860	2415	3961
Deflection at Maximum stress (in.)	6.3	7.6	5.4	6.4

*Note: Deflections shown here are recorded at the point of maximum bending stress.

Figure 111 shows the graphical relationship of bending stress versus deflection. Deflections were measured using a LVDT instead of a string pot in one of the bending tests with steel plate splice mechanism, which has exceeded the maximum deflection measurement capacity of the string pot. Hence, the data could not be included in Figure 111. However, the maximum stress was recorded and was included in the average. The maximum deflection recorded in this test was seen in Table 59.

Figure 111. Bending stress vs. deflection for steel splice

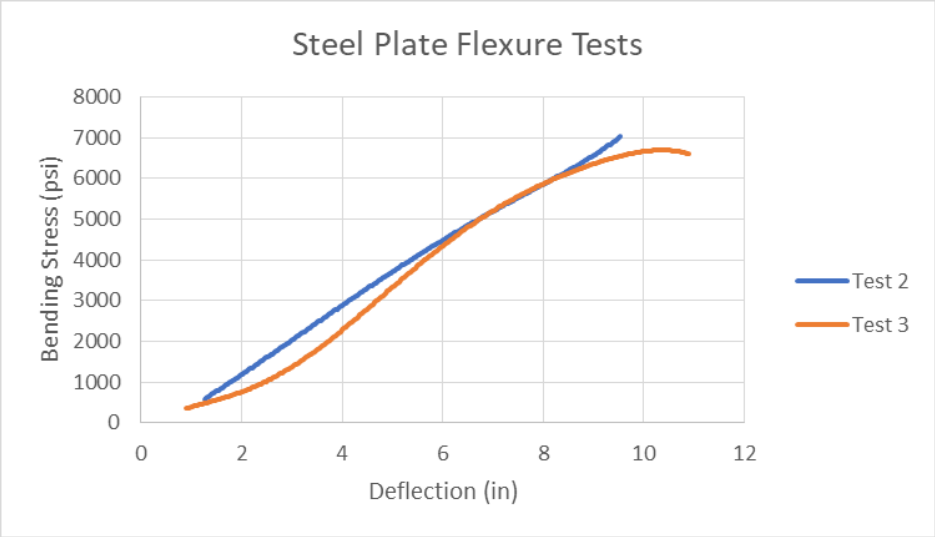

For the timber piles spliced with the C-channel three specimens were tested. The data for the third test specimen was not retrieved and was not included in Table 59 and Figure 112. Figure 112 provides the bending stress versus deflection relationship for timber piles with C-channel splicing. The data from the two tests have a large deviation in bending stress to failure. This was attributed to the strength of the timber pile itself. The failure behavior of the pile specimens was similar, but not identical. Both specimens deflected greatly before reaching maximum load, as C-channel splicing yields greatly under bending loading.

Figure 112. Bending stress vs. deflection for C-channel splice

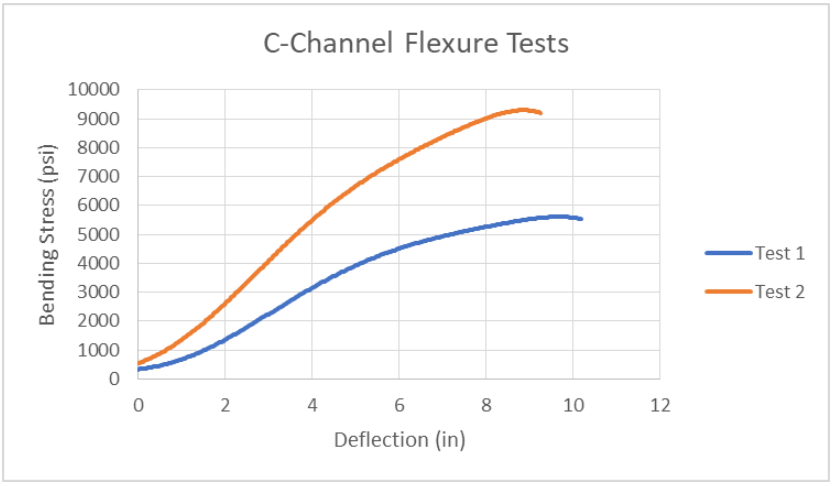

Figure 113 provides the graphical relationship of the bending stress versus deflection of specimens of wood splicing. Deflection is relatively low at failure. Also, there is no drastic change in slope leading to failure in the stress versus deflection curve. This signifies that the

splicing system causes the pile to split rather than yielding of splice, as compared to the other methods. Any change in slope leading to rupture signifies splitting or excess movement within the splicing mechanism itself.

Figure 113. Bending stress vs. deflection for wood splicing

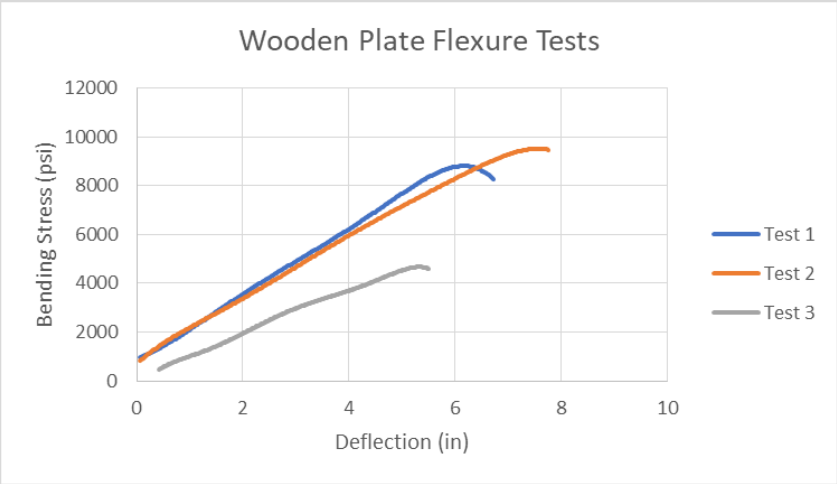

Bending Analysis - Summary and Failure Modes

The three different splicing methods exhibited similar strength to failure and large deformation to failure. The steel and C-channel methods exhibited higher deflection to failure compared to the wood plate splicing method. The disparity in results is attributed to the maximum load resistance of steel, which exceeds that of wood. The wooden plate method exhibited higher flexural rigidity than the steel splicing methods, due to higher bending moment of inertia of wood splice. Unlike the gradual yielding exhibited by steel splicing methods, the wooden plates exhibited splitting or cracking. The bending deformation pattern with increasing applied load is similar to the ones observed during shear testing.

The steel plate and C-channel splicing bowed a significant amount before yielding of the top and bottom plates. An image of the steel plate splice yielding is provided in Figure 114. When using the steel plate splicing method, a pile cracked along its entire span during one of the tests. This signifies that the pile split from the localized force exerted by bolts onto the timber pile at small locations. An image of this failure is shown in Figure 115. As identified in Figure 116, failure in the wooden plate splicing method left cracks along the top and bottom plates, similar to those in the shear test method.

Figure 114. Steel splice yielding during bending test

Figure 115. Steel splice cracked pile

Figure 116. Wood splicing crack during flexure test

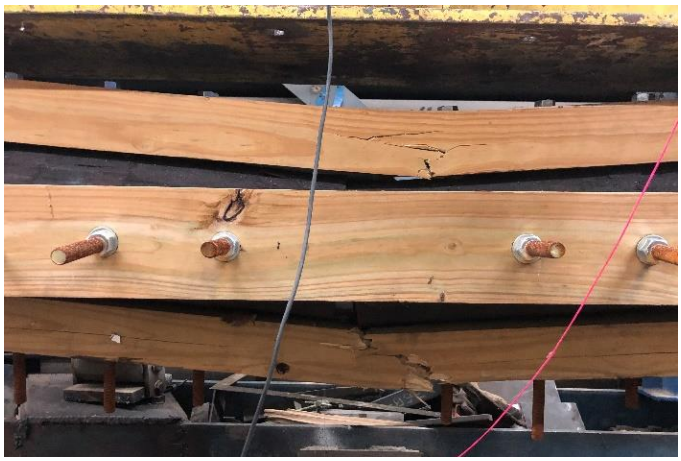

Data Analysis under Axial Testing

The test data developed under axial compression was analyzed to establish the maximum normal stress to failure and the corresponding deflection. Axial stress versus deflection plots were analyzed, hereunder. The cross-sectional area of each pile was taken into account using equation 5. Equation 8 was then used to determine the normal stress at each data point.

$$\sigma = \frac{F}{A} \tag{8}$$

σ – Axial Stress

F – Applied Load

A – Area of cross section

Axial stress in a pile is very important as it is the controlling force that carries the load from the superstructure to the foundation. The axial tests were performed on three 5 ft. long piles of each of the three repair methods, giving a total of nine tests. Table 60 shows the maximum axial stress and the corresponding deflection for each of the nine tests, including their averages.

Table 60. Maximum axial stress and corresponding deflection

Flat Steel Plate Splicing				
Test	**1**	**2**	**3**	**AVG**
Maximum Axial Stress (psi)	1038	856	831	908
Deflection at Maximum stress (in.)	0.4*	0.7	0.5	0.5
Steel C- Channel Splicing				
Test	**1**	**2**	**3**	**AVG**
Maximum Axial Stress (psi)	2214	1423	1412	1683
Deflection at Maximum stress (in.)	0.5	0.6	0.6	0.6
Wooden Plate Splicing				
Test	**1**	**2**	**3**	**AVG**
Maximum Axial Stress (psi)	1492	1494	1709	1565
Deflection at Maximum stress (in.)	0.6	1.1	0.3	0.7

Note: Deflections shown here are recorded at the point of maximum axial stress.

Figure 117 shows the axial stress versus deflection relationship for the test specimens with flat steel plate splicing. Piles did not have perfectly flush cuts at the ends where they were in contact with the steel plates at each end of the pile. Hence, there was an initial loading period

of each test when the pile settles into the stiff steel plates. Due to this settling period, actual axial deflection was skewed by a small amount and was evident in Figure 117, where the initial slope of the normal stress vs deflection curve was not linear. The ultimate axial stress was resisted by the specimen itself without much resistance in the axial direction offered by the splicing.

Figure 117. Axial stress vs. deflection for flat steel plate splice

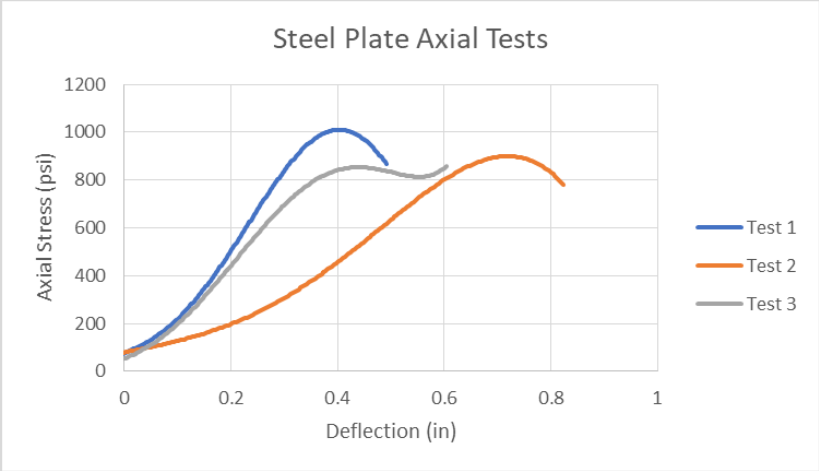

Figure 118 provides the axial stress versus deflection relationship for piles spliced with the steel C-channel splice. From Table 60 it is apparent that the C-channel splice was stronger than that of the flat steel plate splice method in resisting axial compressive loading. This variation was attributed to the secure connection that the C-channel provides to the pile through its material shape and area.

Figure 118. Axial stress vs. deflection for C-channel splice

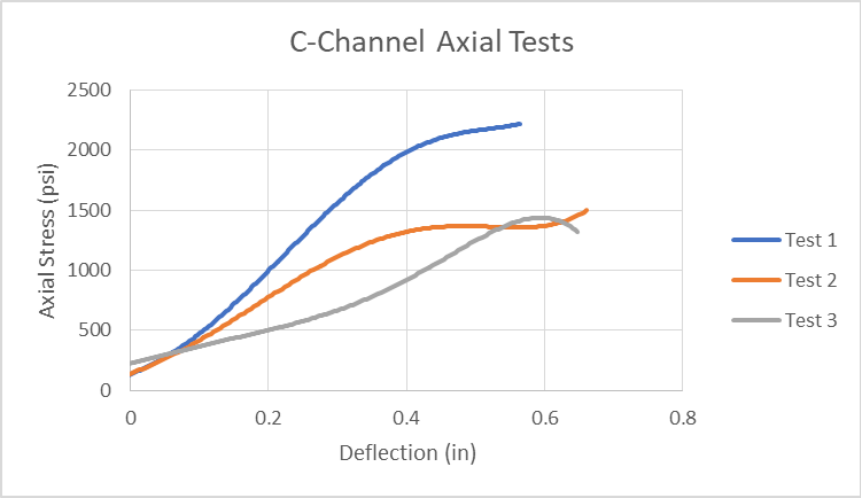

Figure 119 provides the axial stress versus deflection relationship for piles spliced with wood plate splicing. As seen in the axial stress versus deflection plot, test two provided a large amount of deformation due to axial loading. This was attributed to the possible "looseness" of the splice's connection with the pile, along with the gap separating the cut portions of the pile at the cut location. Each pile splice varies in this aspect and can be attributed to the pile assembly method. Results from the wood plate splice are comparable to those of the C-channel splice in terms of axial stress to failure.

Figure 119. Axial stress vs. deflection for wood splice

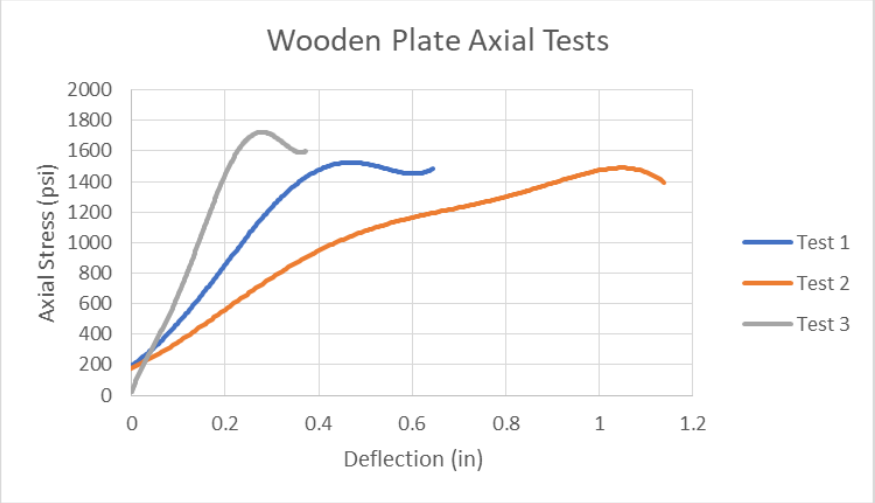

Axial Force Resistance Analysis - Summary and Failure Modes

It was apparent that the steel plate splicing method was the weakest to transfer axial forces because of lower flexural modulus than the other two methods. The C-channel method was the strongest of the three methods of splicing, with similar failure strength as the wooden plate method. All methods provide similar deformation due to axial loading. Results from all three splice methods revealed similar deformation values.

A common visual failure observed in majority of the tests was the cracking of the pile cross section at both ends where the pile was in contact with the steel plates. This is indicative of the influence of Poisson's effect in which failure occurs at higher axial loads due to the weak tensile resistance of wood along the cross section of the pile. A photograph of this failure mode is shown in Figure 120. Another observed failure was localized buckling along the pile near the contact surfaces. A photograph of this failure mode is shown in Figure 121.

Figure 120. Cracking of steel splice pile at contact surface

Figure 121. Buckling near contact surface of steel splice pile

Summary of Traditional Splicing Methods

The C-channel splicing method provides the maximum strength to failure. The high strength capacity was attributed to the C-channel's ability to resist bending stress induced by uneven end cuts. Also, this method provides maximum axial resistance as well as shear resistance, which was attributed to the additional resistance offered by the C-channel in terms of geometry and splice material volume as compared to the flat steel plate and wooden plate

methods. Deflections of test specimens obtained from the steel C-channel splice method were higher than the deflections from the wooden plate splice method under shear and bending conditions. Wooden plate spliced specimens provide adequate strength values under axial and bending conditions but lack in shear resistance. Additionally, the wooden plate splicing method was that the material exhibits stronger axial and bending stiffness, providing less deflection under loading. The higher stiffness from wood splicing led to cracking in timber and does not yield as much as steel channel under loading. Flat steel plate spliced specimens provide low axial loading resistance compared to the other two methods. Axial load resistance was the controlling factor for piles supporting superstructures. Therefore, the flat steel plate splicing method was the least viable option of the three in terms of strength. Table 61 gives the average stress at failure and corresponding deflection for each of the splicing methods.

Table 61. Average maximum stress and deflection for traditional splice methods

Method of Splicing	Steel Plate	C-Channel	Wooden Plate
Shear Stress (psi)	589	783	541
Deflection in Shear (in.)	2.7	2.2	1.8
Modulus of Rupture (psi)	4579	3778	3961
Deflection in bending (in.)	7.9	10.1	6.4
Axial Stress (psi)	908	1683	1565
Deflection in Axial (in.)	0.5	0.6	0.7

FRP Splicing Test Results and Data Analysis

Data Analysis of FRP Splicing under Shear Testing

Shear testing was conducted to determine the maximum shear stress and the corresponding deflection for each of the three FRP specimens tested herein. Table 62 shows that the maximum shear stress and the corresponding deflection for each of the three FRP spliced specimens. It also shows that the average maximum shear stress and average deflection at failure for FRP splicing. Figure 122 provides a graphical representation of the shear stress versus deflection.

Table 62 reveals that low deflection values at maximum stress are apparent with this splicing method, compared to the other splicing methods. FRP wrap completely confines pile specimens, covering the entire circumference of the spliced area. It also bonds to the timber creating a tight full shear transfer without slip between the splice mechanism and the pile. Because of these two reasons deflections are much smaller than traditional methods. As shown in Table 62, the maximum shear stress that the FRP spliced piles can withstand is comparable in magnitude to that of the steel plate splicing method.

Table 62. FRP splice maximum shear and corresponding deflection

Test	1	2	3	AVG
Maximum Shear Stress (psi)	657	643	539	613
Deflection at maximum Stress (in.)	0.9	0.9	0.9	0.9

Figure 122. Shear stress vs. deflection for FRP splice

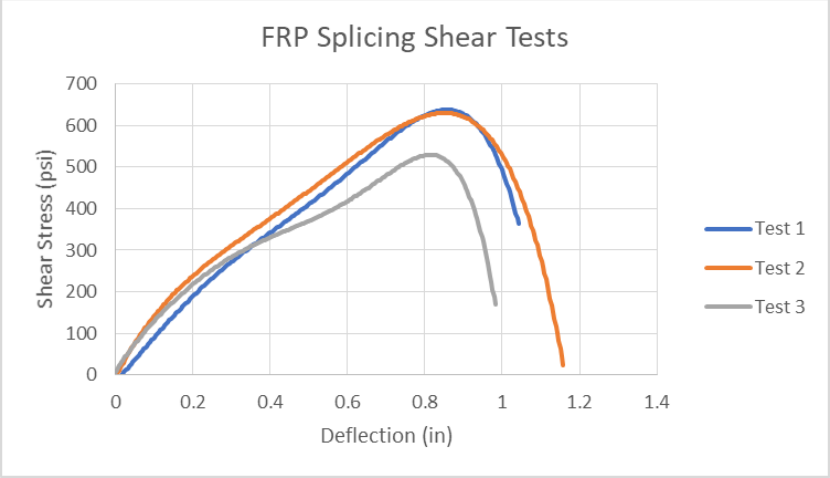

Discussion of Failure Modes in Shear for FRP Splicing

FRP splicing ruptures longitudinally near the neutral axis of the pile FRP wrap splitting between fibers running longitudinally along the pile are noted from the center of the tested specimens, because of maximum shear stress induced at the mid-depth of the test specimens. Furthermore, the failure mode revealed that the failure occurred in the hoop direction of fibers. This was to be expected as there are few fibers resisting forces in the hoop direction. Upon initial loading of each pile, it was observed that there was cracking at the contact surface of the applied load. This implied local buckling occurred from the compressive force induced under applied load. During testing and also during load retrieval, buckling related cracking was observed in the center of the splice (Figure 124).

Figure 123. Hoop failure in shear test

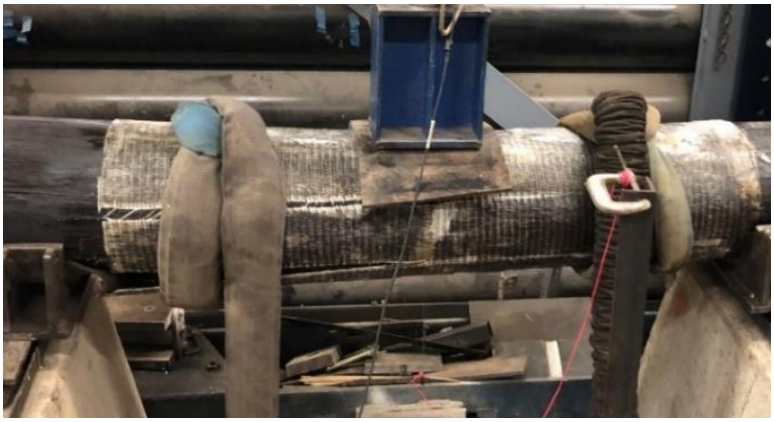

Figure 124. FRP splice cracking under applied load

Data Analysis of FRP Splicing under Bending Testing

The flexure test data was analyzed in terms of maximum bending stress versus the corresponding deflection (Table 63) Also provided in Table 63 were the average maximum bending stress and average deflection at failure for the thin FRP splicing. Figure 125 provides the bending stress versus deflection plot for piles spliced with FRP wraps. The test data revealed that FRP spliced test specimen provides lower deflection values as well as lower maximum stress values, than the traditional methods of splicing. This indicates that not enough reinforcement was provided through the FRP wrap to provide adequate resistance to bending stress. The "dips" in tests 2 and 3 in the bending stress versus deflection plots (Figure 125) are an indication of local buckling occurring under low induced stresses, which is discussed further in the following paragraph.

Table 63. FRP splice maximum modulus of rupture and corresponding deflection

Test	1	2	3	AVG
Maximum Modulus of Rupture (psi)	4064	4805	4258	4376
Deflection at Maximum Stress (in)	2.3	3.5	5.1	3.6

Figure 125. Bending stress vs. deflection for FRP splice

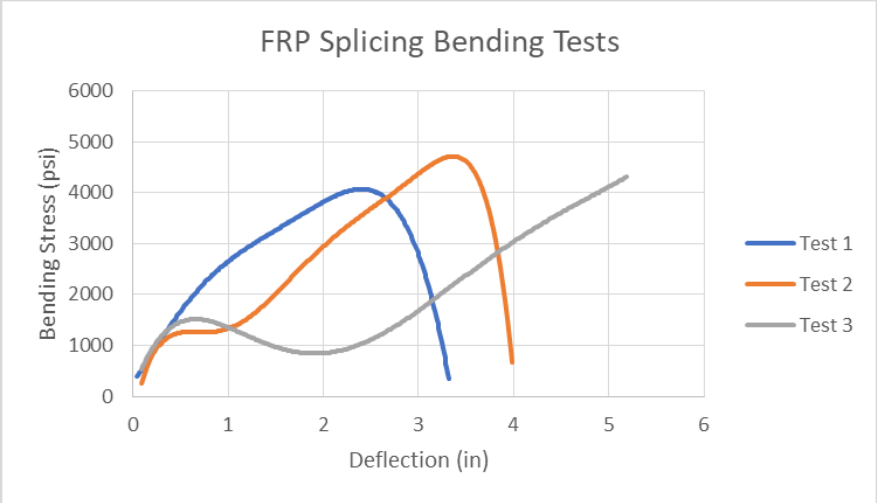

Discussion of Failure Modes in Bending for FRP Splicing

The lack of adequate quantity of fibers in the hoop direction caused the FRP to "unzip" along its length with increasing deformation. This deficiency could be remedied easily by adding a layer of fibers in the hoop direction on top of the longitudinal glass fabric layers. As in shear testing, ultimate failure happened rapidly and occurred between fibers in the longitudinal direction indicating failure in hoop fibers. Under bending, large portions of the FRP fabric

de-bonded from the pile (Figure 126). In one of the specimens, a different form of failure was observed, as shown in Figure 127. The splice failed at the center, splitting in the vertical direction of fibers. During testing, it was also noted that two of the specimens (tests number 2 and 3), cracked at the center of the splice under compression. This could be due to the fact that between the two halves of the pile there is a small gap, initiating local buckling (f_r) in high stress concentration on the compression surface at the center of the splice.

Figure 126. Debonding of splice at failure

Figure 127. FRP splice failure at center

Data Analysis of FRP Splicing under Axial Testing

The purpose of the axial test was to determine the maximum normal stress and its corresponding deflection for each of the three FRP specimens tested herein. Table 64 shows the maximum axial stress versus deflection for each of the three FRP spliced specimens tested in this program. It also shows the average maximum normal stress and average deflection at failure for FRP splicing. Figure 128 provides the normal stress versus

deflection relationship for piles spliced using FRP wrap. There is some variance in the data obtained from these three tests. However, taking the averages into account, it is clear that FRP splicing provides a significant amount of strength in axial compression, higher than the conventional splicing methods. The FRP splicing was the strongest out of all the splicing methods employed in this study. The strongest of the traditional methods is the C-channel splice, which failed slightly under 1700 psi. The FRP splicing resulted in axial compression failure at around 1750 psi.

Table 64. FRP splice maximum axial stress and corresponding deflection

Test	1	2	3	AVG
Maximum Axial Stress (psi)	1339	1776	2143	1753
Deflection at Maximum Stress (in)	0.5	0.6	0.7	0.6

Figure 128. Axial stress vs. deflection for FRP splice

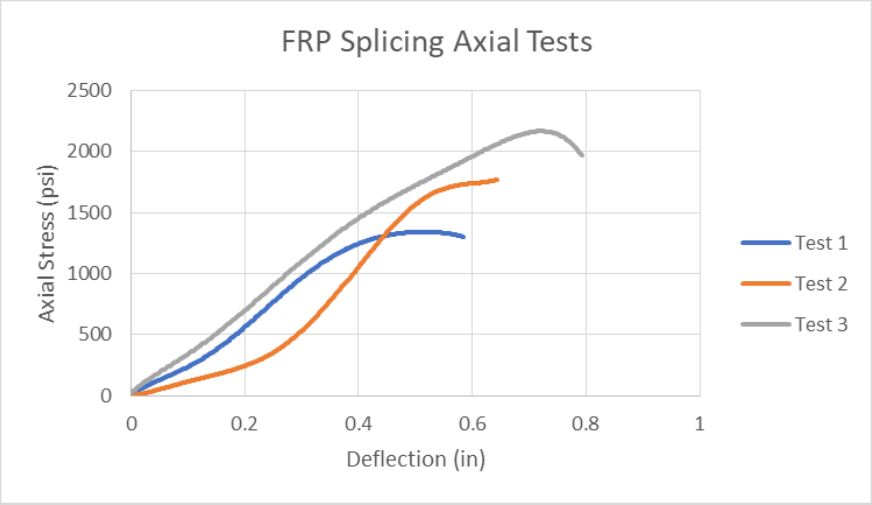

Discussion of Failure Modes in Axial for FRP Splicing

Due to the gap between the two halves of the pile specimen, bulging of fiber in the FRP wrap at the center is noticed. This occurred in each of the three specimens tested. Adding a layer of high strength caulking in the gap between pile's halves can help prevent bulging. In this test, bulging fibers were split in the hoop direction but remained intact in the longitudinal direction along the pile (Figure 129). Adding an additional layer of fibers, reinforcing the hoop direction can prevent splitting. As opposed to traditional methods, buckling effects were negligible at the end of these tested piles. Bolts were not used in this method, i.e., no internal forces are acting on the pile causing it to crack, and no high stress concentration is induced from bolting at the connector locations as in legacy connections. Each of the piles failed similarly as shown in (Figure 130).

Figure 129. Bulging in FRP splice during compression testing

Figure 130. FRP splice axial compression specimen

Summary of FRP Splicing Method Results

Splicing of timber piles with FRP wraps provides structural performance results that were comparable to legacy splicing methods. The shear stresses to failure of this method was comparable to that of traditional methods of splicing. Bending stresses, however, were not as high as anticipated, which could be improved easily by adding extra layers of fabric in the hoop direction of fibers. Placing more sheets with fiber orientation perpendicular to the existing wrap will greatly increase the amount of stress to failure in the hoop direction. The bending stress was not very critical for piles since 90% of the load tends to be axial load. This method was very effective to resist axial compressive stress. The absence of bolts in this splicing method prevented internal cracking due to reduced stress concentration. While using two wraps of FRP was effective, adding an extra layer of glass fabric along the hoop direction would decrease the amount of bulging (local debonding of wrap) in the center of the splice. In terms of deflection, FRP splicing performed well, and made the pile stiff. Table 65 incorporates the results of the FRP wrap repair method and other splicing methods.

Table 65. Average maximum stress and deflection for all splice methods

Method of Splicing	Steel Plate	C-Channel	Wooden Plate	FRP Wrap
Shear Stress (psi)	589	783	541	613
Deflection in Shear (in.)	2.7	2.2	1.8	0.9
Modulus of Rupture (psi)	4579	3778	3961	4376
Deflection in bending (in.)	7.9	10.1	6.4	3.6
Axial Stress (psi)	908	1683	1565	1753
Deflection in Axial (in.)	0.5	0.6	0.7	0.6

Guide Documents

Construction Guide

Fiber Reinforced Polymer (FRP) For Structural Repairs - This work shall consist of the repair of timber piles with an FRP-wrap system in accordance with these specifications and in reasonably close conformity with the lines, grades, dimensions and locations as shown on the plans or as established by the Engineer.

Testings

FRP Approvals: Material specifications, installation-construction procedures, and quality control plan must be submitted to the engineer and approved by DOTD prior to securing materials and beginning of installation.

FRP Quality Control: Quality assurance during installation of the FRP system components shall be described in a quality control plan. The quality control plan will include, but not limited to, the following:

- Certification that the contractor has been trained to apply the specific FRP wrap material
- Storage requirements
- Procedures to inspect wrap to ensure that it meets the manufacturer's instructions and those in these provisions

Test sections shall be made as per ASTM D7565 and tested according to ASTM D3039. If tested samples do not meet the minimum specifications, additional layers of FRP wrap must be applied to bring the total laminate up to the minimum specifications at no additional cost to the Department. Pull-off testing at non-critical areas should be conducted after installation of the FRP wrap as per ASTM D7522. All tested areas should be patched with the FRP system with one-foot square patches.

FRP Installation Requirements: Unless otherwise dictated by the FRP manufacturer's instructions, the following installation guidelines shall be followed for the entire FRP-wrap system (primer, resin, fabric, etc.):

- Area to be wrapped with FRP (as shown on the plans) shall be inspected for exterior cracks/voids and interior voids.

- Exterior cracks/voids shall be covered using approved crack filler and allowed to cure according to manufacture specifications.

- Interior voids shall be filled with approved bulk filler after repairing exterior cracks. Bulk filler can be mixed with sand to save resin. Allow filler to cure according to manufacture specifications.

- The ambient temperature and the temperature of the resin shall be between 55ºF and 95ºF at the time of mixing. The composite shall be applied when the relative humidity is less than 85% and the surface temperature is more than 5°F above the dew point. Contractor should provide verification of the temperature and humidity at the application location prior to use. The timber surface should be dry prior to wrapping.

- The moisture content in the timber prior to bonding shall be less than 25% to 30%.

- A compatible primer as recommended shall be applied to the timber/filler surface using a brush or roller ensuring the primer is worked into the wood surface. In the absence of a specified primer, the resin should be used.

- The FRP-wrap system (fabric/resin) shall be applied to the timber/filler surface using methods that ensure that the fabric is in intimate contact with the underlying timber. Follow the engineer's design for the number of layers of glass FRP fabric.

- Start and finish layers with the fabric being stapled onto the pile.

- Seams should be staggered and overlap by a minimum of 4 in. or as specified on the plans

- The wrap should be installed so that seams do not allow for water intrusion.

- Successive layers of wet composite materials shall be placed before curing begins (polymerization) on the previous layer.

- Shrink-wrap or other clamping systems that wrap around the pile should be avoided or used with care to prevent wrinkle formation.

- Adequate ventilation of the project area shall be maintained at all times.

- Containment shall be provided by the Contractor to prevent the spread of fibers and/or resin residue during construction. All contained or waste material shall be properly disposed of by the Contractor.

- Contractor shall read and apply all safety precautions for all components of a composite wrap system.

- Any voids over 2 in^2 between the wrap and timber must be filled with an injectable epoxy before protective coatings are applied. Filling of voids is required for completion of the work.

Coating System Application Notes: After the final wrap layer is completely polymerized, an acrylic paint or equivalent should be applied to the entire FRP-wrap area (color to be chosen by DOTD.)

Structural Load Rating

Structural load rating is used to determine the safe load capacity of a bridge based upon the relationship between capacity, dead loads, and live loads as per the requirements of the *AASHTO Manual for Bridge Evaluation* (MBE). DOTD using an in-house software program (TIMBER) to determine the inventory, operating and posting load of a timber bridge, based on allowable stresses. This section describes a methodology to use the same program by converting the FRP strength into a comparable timber strength.

Since the load exerted on a pile is constant regardless of the material, the load in the FRP (P_f) must equal the load in the unrepaired timber (P_t) because the decayed timber resistance is assumed to be zero. To compute an equivalent area of wood, P_f is first calculated by determining the current bond and axial capacities, with P_f taken as the minimum of those two values. By setting P_f equal to the timber capacity, the circumference of an equivalent area of wood can be back calculated based on a known allowable strength of wood. If the calculated circumference is less than the actual circumference, then the calculated circumference should be used in TIMBER as the FRP is weaker than the unrepaired pile. If the calculated circumference is greater than the actual circumference, the FRP is stronger than the unrepaired pile and the actual circumference should be used in TIMBER. Step-by-step calculations and two examples follow.

Assumptions:

The reduction factors were determined using the epoxy-based systems (as discussed in the design methodology) and are assumed to be the same for the phenolic and polyurethane systems.

The axial calibration factors were adjusted for the phenolic and polyurethane systems to ensure that a 0.5 in. thick wrap would have a stress equal to the Timber Piling Council formula for the stress based on clear samples.

Bending effects are not included herein, and piles should be braced to prevent bending.

Step 1: Determine the capacity of the repaired pile

The bond capacity is determined as follows, with calibration factors given in Table 66.

$$P_b = \varphi_b(C_{b1}\ln(x) + C_{b2})d * \pi * x \quad (9)$$

Where,
P_b = bond capacity (lbf),
φ_b = bond reduction factor (0.6),
x = bond length, max of 24 inches (in.),
C_{b1} = Bond calibration factor 1,
C_{b2} = Bond calibration factor 2, and
d = Diameter of timber pile (in.).

Table 66. Bond calibration factors

Resin System	C_{b1}	C_{b2}
Epoxy	-115	510
Phenolic	-60	225
Polyurethane	-30	135

The axial capacity is determined as follows, with calibration factors given in Table 67

$$P_a = \varphi_a(C_{a1}\ln(t) + C_{a2}) * \pi * (d + t) * t \quad (10)$$

Where,
P_a = axial capacity (lbf),
φ_a = reduction factor (0.35),
C_{a1} = Axial calibration factor 1,
C_{a2} = Axial calibration factor 2,
d = Diameter of timber pile (in.), and
t = FRP wrap thickness, max of 0.75 inch (in.).

Table 67. Axial calibration factors

Resin System	C_{a1}	C_{a2}
Epoxy	2650	18000
Phenolic	2000	6200
Polyurethane	-400	2250

The minimum capacity of the repaired pile is calculated by

$$P_f = \text{minimum}\ (P_b, P_a) \tag{11}$$

Where,
P_f = Controlling FRP capacity (lbf).

Step 2: Compute the TIMBER circumference

The equivalent TIMBER circumference of the pile is computed with

$$c = \sqrt{\frac{4\pi P_f}{\sigma_t}} \tag{12}$$

Where,
c = Equivalent circumference of timber pile under same load (in.), and
σ_t = Allowable stress of timber pile (psi) (1200 psi for southern pine).

If c > the actual circumference, use the actual circumference in TIMBER.

If c < the actual circumference, use c in TIMBER.

Three examples using this rating method follow on subsequent pages.

Example 1

A 7-in. diameter timber pile has been repaired with an epoxy-based FRP wrap for a total thickness of 0.35 in. (7 layers at 0.05 in. per layer). The FRP extends for 24 in. beyond the damaged area. Calculate the equivalent TIMBER circumference based on an allowable timber stress of 1100 psi (red oak).

Table 68. Example 1 properties

Diameter	d	7 in.
Thickness	t	0.35 in.
Bond length	x	24 in.
Allowable timber stress	σ_t	1100 psi
Bond reduction factor	φ_b	0.6
Bond calibration factor 1	C_{b1}	-115
Bond calibration factor 2	C_{b2}	510
Axial reduction factor	φ_a	0.35
Axial calibration factor 1	C_{a1}	2650
Axial calibration factor 2	C_{a2}	18000

Step 1: Determine the capacity of the repaired pile

- Bond capacity (Eqn. 9)

  $$P_b = \varphi_b * (C_{b1} * \ln(x) + C_{b2}) * d * \pi * x$$
  $$= 0.6 * (-115 * \ln(24) + 510) * 7 * \pi * 24 \ = 45{,}766 \text{ lbs}$$

- Axial capacity (Eqn. 10)

  $$P_a = \varphi_a * (C_{a1} * \ln(t) + C_{a2}) * \pi * (d + t) * t$$
  $$= \ 0.35 * (2650 * \ln(0.35) + 18000) * \pi * (7 + 0.35) * 0.35 = 43{,}045 \text{ lbs}$$

- Controlling capacity (Eqn. 11)

  $$P_f = \text{minimum } (P_b, P_a) = \ \text{minimum } (45{,}766 \ \& \ 43{,}045) = 43{,}045 \text{ lbs}$$

Step 2: Compute the TIMBER circumference (Eqn. 12)

$$c \ = \sqrt{\frac{4\pi P_f}{\sigma_t}} = \sqrt{\frac{4\pi 43045}{1100}} = 22.2 \ in.$$

Since 22.2 in. is greater than the actual circumference (21.9 in.), 21.9 in. should be used in TIMBER as the repair is stronger than the original pile.

Example 2

A 10-in. diameter timber pile has been repaired with an epoxy-based FRP wrap for a total thickness of 0.6 in. (12 layers at 0.05 in. per layer). The FRP extends for 15 in. beyond the damaged area. Calculate the equivalent TIMBER circumference based on an allowable timber stress of 1200 psi (southern pine).

Table 69. Example 2 properties

Diameter	d	10 in.
Thickness	t	0.6 in.
Bond length	x	15 in.
Allowable timber stress	σ_t	1200 psi
Bond reduction factor	φ_b	0.6
Bond calibration factor 1	C_{b1}	-115
Bond calibration factor 2	C_{b2}	510
Axial reduction factor	φ_a	0.35
Axial calibration factor 1	C_{a1}	2650
Axial calibration factor 2	C_{a2}	18000

Step 1: Determine the capacity of the repaired pile

- Bond capacity (Eqn. 9)

  $$P_b = \varphi_b * (C_{b1} * \ln(x) + C_{b2}) * d * \pi * x$$
  $$= 0.6 * (-115 \ln(15) + 510) * 10 * \pi * 15 \ = 56{,}145 \text{ lbs}$$

- Axial capacity (Eq. 10)

  $$P_a = \varphi_a * (C_{a1} * \ln(t) + C_{a2}) * \pi * (d + t) * t$$
  $$= 0.35 * (2650 * \ln(0.6) + 18000) * \pi * (10 + 0.6) * 0.6 = 116{,}410 \text{ lbs}$$

- Controlling capacity (Eqn. 11)

  $$P_f = \text{minimum}\,(P_b, P_a) = \ \text{minimum}\,(56{,}145 \ \& \ 116{,}410) = 56{,}145 \text{ lbs}$$

Step 2: Compute the TIMBER circumference (Eqn. 12)

$$c \ = \sqrt{\frac{4\pi P_f}{\sigma_t}} = \sqrt{\frac{4\pi 56145}{1200}} = 24.24 \ in.$$

Since the actual circumference is 31.4 in., 24.24 in. should be used in TIMBER to reflect the lower axial strength of the FRP. TIMBER will calculate the rating based on a 7.7-in. diameter timber member with 1200 psi allowable strength (i.e., a timber member with the same capacity as the FRP).

Example 3

A 12-in. diameter timber pile has been repaired with a phenolic-based FRP wrap for a total thickness of 0.25 in. The FRP extends for 10 in. beyond the damaged area. Calculate the equivalent TIMBER circumference based on an allowable timber stress of 1200 psi (southern pine).

Table 70. Example 3 properties

Diameter	d	12 in.
Thickness	t	0.25 in.
Bond length	x	10 in.
Allowable timber stress	σ_t	1200 psi
Bond reduction factor	φ_b	0.6
Bond calibration factor 1	C_{b1}	-60
Bond calibration factor 2	C_{b2}	225
Axial reduction factor	φ_a	0.35
Axial calibration factor 1	C_{a1}	2000
Axial calibration factor 2	C_{a2}	6200

Step 1: Determine the capacity of the repaired pile

- Bond capacity (Eqn. 9)

$$P_b = \varphi_b * (C_{b1} \ln(x) + C_{b2}) * d * \pi * x$$
$$= 0.6 * (-60 \ln(10) + 225) * 12 * \pi * 10 \ = 19{,}643 \text{ lbs}$$

- Axial capacity (Eqn. 10)

$$P_a = \varphi_a * (C_{a1} \ln(t) + C_{a2}) * \pi * (d + t) * t$$
$$= \ 0.35 * (2000 \ln(0.25) + 6200) * \pi * (12 + 0.25) * 0.25 = 11{,}541 \text{ lbs}$$

- Controlling capacity (Eqn. 11)

$$P_f = \text{minimum } (P_b, P_a) = \ \text{minimum } (19{,}643 \ \& \ 11{,}541) = 11{,}541 \text{ lbs}$$

Step 2: Compute the TIMBER circumference (Eqn. 12)

$$c \ = \sqrt{\frac{4\pi P_f}{\sigma_t}} = \sqrt{\frac{4\pi 11541}{1200}} = 10.99 \ in.$$

Since the actual circumference is 37.7 in., 10.99 in. should be used in TIMBER to reflect the lower bond strength of the FRP. TIMBER will calculate the rating based on a 3.5 in. diameter timber member with 1200 psi allowable strength (i.e., a timber member with the same capacity as the FRP).

Inspection Guide

The inspection of FRP wrap systems can be done via visual or with nondestructive evaluation equipment. Section 6.6 of the *Federal Highway Administration* (FHWA) *Bridge Inspection Reference Manual* (2012) has detailed information regarding the inspection of FRP components with the material summarized herein for inspection of FRP wraps on timber piles [65].

Visual Inspection

Visual inspection involves examining the wrap for visual damage including voids, discoloration, wrinkling, scratches and cracking. Voids occur when air or water is trapped under the FRP surface during installation, and sometimes can form into blisters during FRP installation if moisture is trapped under the surface. Blisters are easily seen (Figure 131), but voids may not be visually apparent. To detect voids, tap testing can be conducted using a small hammer to tap the surface. A clear, sharp sound indicates areas of good bond while dull thuds indicate voids. More advanced techniques will be discussed in the next section.

Figure 131. Blisters under FRP wrap

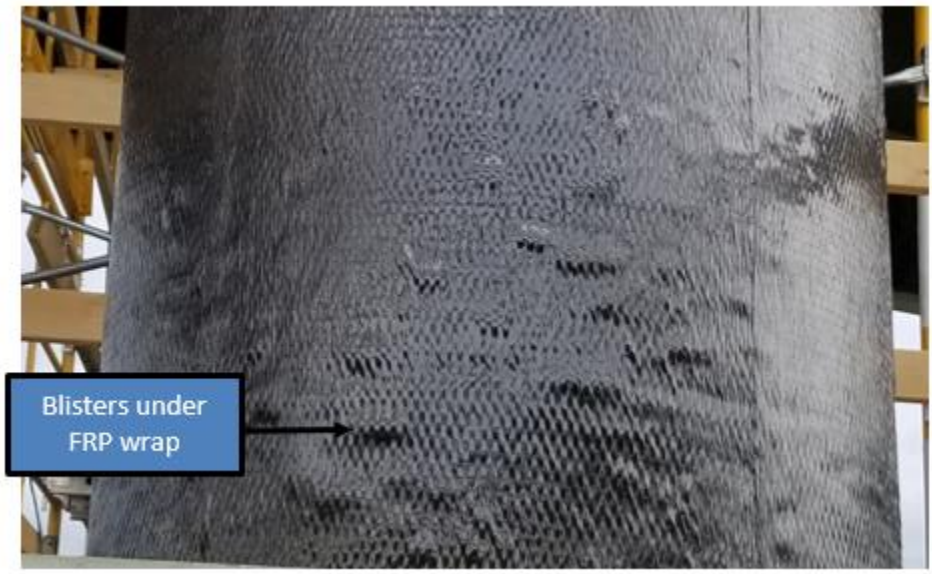

Discoloration can be a sign of UV degradation, fire exposure, excessive strain, voids or moisture infiltration. The original color of the FRP wrap should be noted in the inventory reports so that color changes over time can be noted as FRP wraps vary in color from off-white (Aquawrap) to dark brown (phenolic). Typically, damage resulting in discoloration results in the composite turning white as the glass fibers are exposed, as shown in Figure 132.

Figure 132. UV degradation of FRP wrap

Wrinkles (Figure 133) are often caused due to poor lay-up of the fibers, however it is typically not a structural problem as this testing program did not see any detrimental results due to wrinkling. Wrinkles should be noted in the initial inspection and monitored to ensure no cracks or delamination develop around a wrinkle.

Figure 133. Wrinkle in FRP fabric

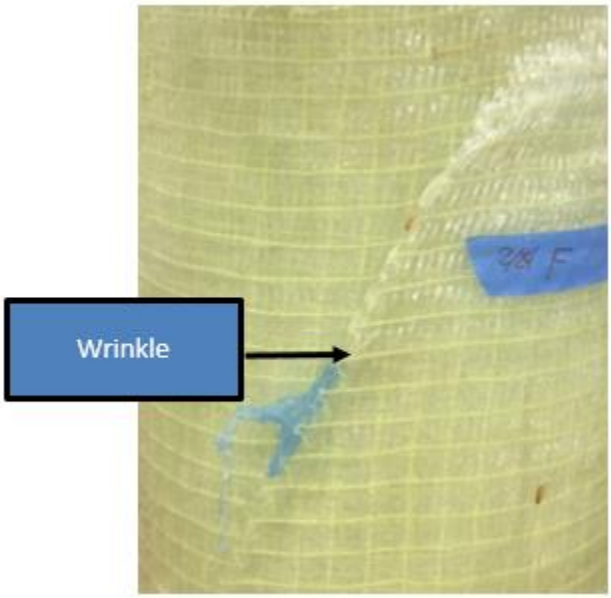

Cracks are the most critical inspection item as this testing program illustrated, i.e., a cracked FRP wrap has significantly reduced strength. Cracks often have discoloration around the crack, and broken fibers are typically visible. Cracked wraps should be assumed to have zero remaining strength.

Figure 134. Cracks in FRP wrap

Advanced Inspection Techniques

In lieu of tap testing, a digital tap hammer (Figure 135) can be used to provide a more objective measure of voids. Digital tap hammers measure the time response of ultrasonic waves, displaying the response time in microseconds. Solid areas have lower response times than voided areas, with a difference of 10% indicating debonding. Typically, good bonds have a reading of around 1140, but this should be verified in the field to calibrate to the in-situ conditions. Digital tap hammers work best for FRP composites under 1/2 in. thick.

Figure 135. Digital tap hammer

Infrared thermography (IRT) is another advanced inspection technique that works well for FRP wraps. IRT works by heating the surface of the composite with a portable heater for about 60 seconds, making sure not to exceed 140°F to avoid damaging the composite. A portable infrared camera is used to acquire an infrared image, which shows the surface temperature profile of the test area using different colors. In the infrared image, brighter colors represent higher temperatures. Defect-free areas conduct heat through the thickness efficiently while debonded areas act as thermal insulation, which impedes the heat flow (especially if they consist of air pockets). Therefore, debonded areas have higher surface temperatures compared to surrounding defect-free areas. In the infrared image, these high temperature spots (corresponding to subsurface debonds or defects) are typically seen as areas with brighter colors compared to the surrounding areas. It should be noted that infrared thermography is a near-surface defect detection technique, which will identify a defect depth limited to approximately 1 in. Also, it should be noted that there is a small temperature variation due to natural inhomogeneity in most FRP-wrapped components, so the temperature difference between a “hot spot” and the surrounding area should be at least 3 to 4°C for classifying the hot spot as a debond.

Figure 136 shows both a digital image and an infrared image of a blister on an FRP surface. The blister is 12.6°C hotter than the surrounding area and clearly shows up as a defect. IRT can be used to detect the extents of blisters, voids, and cracks in an objective manner.

Figure 136. Digital image and infrared image of a blister

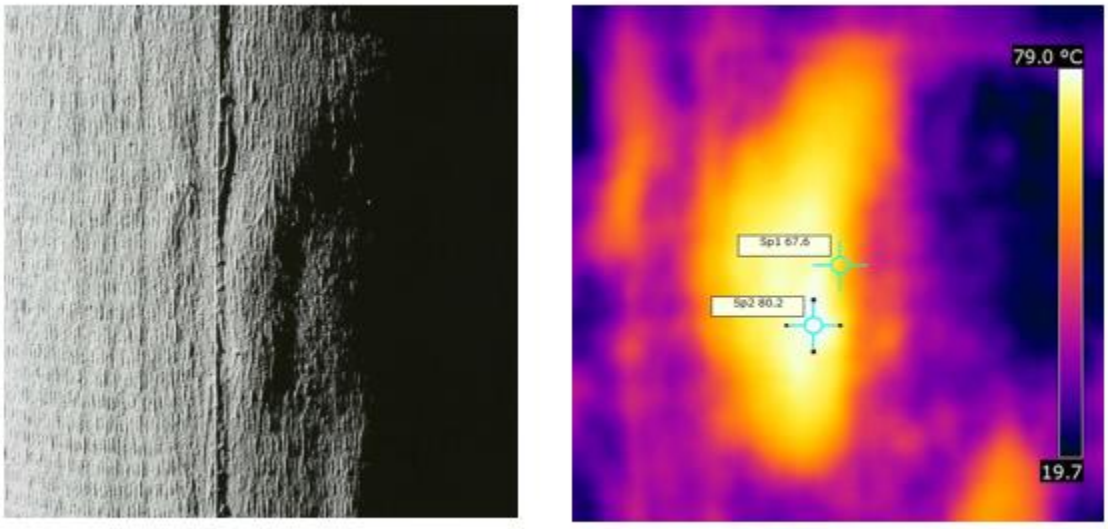

(a) Digital Picture b) Infrared Image

DOTD Demonstration Workshops

Two workshops are scheduled to begin June 2021 to train personnel on the design, installation, inspection and repair methods required for FRP wraps to rehab timber piles. Each workshop will include two hours of virtual instruction on the design, inspection, and repair of FRP-wrapped piles. Dates for training will be scheduled between DOTD and WVU-CFC.

Conclusions

- Design methodologies and rating equations are based on the testing program carried-out herein for epoxy-based FRP wraps. The controlling limitation is the bond capacity of the pile due to the timber strength.
- Epoxy-based FRP wrap systems had the highest pull-off, bond and axial compressive strengths while phenolic and polyurethane systems had lower strengths.
- Polyurethane systems exhibited the lowest bond and compressive strengths, compared with the bond and compressive strengths of specimens prepared with other resins such as epoxy.
- The bond strength of epoxy systems is controlled by the underlying timber strength as the FRP-timber bond strength exceeds the timber peel strength parallel to the grain. This limits the overall bond capacity.
- Pull-off testing resulted in similar bond results as the bond testing.
- Bond tests under wet/dry cyclic conditions showed higher bond strength than the FRP-wrapped samples without wet/dry cycles because of post curing of the resin. The test samples were prepared under dry conditions and no moisture ingress was found during wetting process.
- Increasing the number of wraps increased the capacity of the pile, although an increase in compressive strength in terms of load resistance per unit area did not increase proportionately.
- Full-scale test specimens with total cross sectional cut after rehabilitating with FRP wrap, failed at stresses similar to those without cuts for bond and axial compression, i.e., indicating tests replicate field conditions.
- Combined axial and bending testing was not conclusive due to localized failures.
- Paste-like crack fillers were shown to seal external cracks well, while sand was shown to be an effective means to increase the yield of bulk fillers.
- Bulk fillers that foam are best at filling voids. However, their strength is lower than the non-foaming fillers.

- Visual inspection can be conducted on FRP-wrapped timber piles, with infrared thermography (IRT) or digital tap hammer offering more objective inspection data.
- Based on the laboratory and field experiences, traditional (legacy) splicing methods are more cumbersome to rehabilitate than FRP-wrapping techniques.
- Of the traditional methods of timber pile repair analyzed, the steel C-channel splicing provides the maximum resistance under shear, bending and axial forces because of its high stiffness and material strength.
- Traditional (legacy) splicing methods cause larger movement in the pile system due to loose connections caused by the bolted splice mechanism; however, FRP-wrap splicing has no movement under loading due to 100% bond between the wrap and the substrate (timber pile).
- Traditional splicing methods are more expensive than the FRP-wrap rehab techniques in terms of material, transportation, and labor costs.
- FRP-wrapped timber piles provide a strong, cost efficient, and long-lasting solution as compared to traditional (legacy) splicing methods; additional improvements in strength and stiffness can be made by changing the fiber type, orientation and number of wraps.

Recommendations

- Additional testing should be completed using longer bond lengths for bond testing and additional layers for compression testing to verify the design equations.
- Methods should be researched to increase the bond capacity, i.e., new resin systems or better interface systems providing high friction between FRP and timber substrate.
- The remaining timber strength or the strength of the fillers should be determined to reflect the additional capacity these materials offer.
- Longer samples should be made to conduct combined axial and bending with greater flexural moments.
- Traditional splicing methods should be tested under combined loading to further evaluate strength capacities and deflection limits.
- Field evaluations of traditional splicing techniques must be carried out to establish service life of spliced pile systems.
- Field evaluations of FRP-wrapped systems should be conducted to establish the durability of the proposed methods and to nondestructively evaluate for any potential voids behind the FRP wraps.
- Additional testing should be completed for piles repaired with a FRP-wrap splice mechanism, adding addition layers of fabric to reinforce the hoop fiber direction to improve shear and bending capacity.
- Develop design and field-splicing specifications using FRP wraps to rehabilitate deteriorated timber piles.
- Develop a training program for construction workers on installation of FRP-wrap systems for timber piles.

Acronyms, Abbreviations, and Symbols

Term	Description
AASHTO	American Association of State Highway and Transportation Officials
ACI	American Concrete Institute
AQ	Aquawrap
C	Centigrade
CCA	Chromated Copper Arsenate
COV	Coefficient of Variation
DOT	Department of Transportation
EPI	Emulsified polymer isocyanate
F	Fahrenheit
FHWA	Federal Highway Administration
ft.	Foot (feet)
FRP	Fiber Reinforced Polymer
FY	Fyfe
HMR	Hydroxymethylated resorcinol
in	Inch(es)
in^2	Square inches
IRT	Infrared thermography
DOTD	Louisiana Department of Transportation and Development
LTRC	Louisiana Transportation Research Center
lbf.	Pound force
min	Minute
mm	Millimeter
mph	Miles per hour

Term	Description
MUF	Melamine urea formaldehyde
NDS	National Design Specification
oz.	Ounce(s)
PF	Phenol formaldehyde
PH	Phenolic
PRF	Phenol resorcinol formaldehyde
psi	Pound force per square inch
PVC	Polyvinyl Chloride
PU	Polyurethane
RF	Resorcinol formaldehyde
SBVR	South Branch Valley Railroad
SST	Simpson Strong-Tie

References

[1] AASHTO, Maintenance Manual for Roadways and Bridges, Washington DC: American Association of State Highway and Transportation Officials, 2007.

[2] D. E. Breyer, K. E. Cobeen, K. J. Fridley and D. G. Pollock, "Chapter 4: Properties of Wood and Lumber Grades," in *Design of Wood Structures - ASD/LRFD*, New York, McGraw-Hill, 2015, pp. 186-187.

[3] C. Carll and A. C. Wiedenhoeft, "Moisture- Related Properties of Wood and the Effects of Moisture on Wood and Wood Products," in *MNL18, Moisture Control in Buildings: The Key Factor in Mold Prevention*, 2nd ed., 2009, pp. 54-78.

[4] R. M. Rowell, "Moisture Properties," in *Handbook of Wood Chemistry and Wood Composites*, R. Rowell, Ed., CRC Press, Taylor & Francis Group, 2005, pp. 77-98.

[5] M. A. Ritter, Timber Bridges: Design, Construction, Inspection, and Maintenance, Washington, DC.: U. S. Department of Agriculture, 1990.

[6] R. N. Emerson, "In Situ Repair Technique for Decayed Timber Piles," in *Structures 2004: Building on the Past, Securing the Future*, 2004.

[7] Army and Air Force, "Bridge Inspection, Maintenance, and Repair (TM 5-600/AFJPAM 32-1088)," Joint Departments of the Army and Air, Washington, DC, 1994.

[8] A. Mohammadi, J. H. Gull, R. Taghinezhad and A. Azizinamini, "Assessment and Evaluation of Timber Piles Used in Nebraska for Retrofit and Rating," Miami, FL, 2014.

[9] F. W. Klaiber, D. J. White, T. J. Wipf, M. Mekkawy and J. Koskie, "Investigation of Steel-Stringer Bridges: Superstructures and Substructures, Volume II: Final Report," Bridge Engineering Center, 2007.

[10] T. J. Wipf, F. S. Fanous, F. W. Klaiber and A. S. Eapen, "Evaluation of Appropriate Maintenance, Repair and Rehabilitation Methods for Iowa Bridges," Iowa Department of Transportation, 2003.

[11] S. W. Ainge, "Repair and Strengthening of Bridge Substructures," Milwaukee, WI, 2009.

[12] P. Caiza, M. Shin and B. Andrawas, "Load Rating and Retrofit Testing of Bridge Timber Piles Subjected to Eccentric Loading: FHWA-ICT-12-014," Illinois Center for Transportation, November 2012.

[13] J. Dahlberg, B. Phares, J. Bigelow and F. W. Klaiber, "Timber Abutment Piling and Back

Wall Rehabilitation and Repair," Bridge Engineering Center, 2012.

[14] M. W. Hagos, "Repair of Heavily Decayed Timber Piles Using Glass Fiber Reinforced Polymers (GFRP) and Cementitious Grout," Winnipeg, Canda, 2001.

[15] T. Jimenez, D. Kost and J. Percival, "A Case Study on the use of Advanced Fiber Wrap Composites for Timber Piles Repair and Protection of a Pier Structure," *Coastal Engineering Practice*, pp. 10-14, 2011.

[16] R. Liang and H. V. S. GangaRao, "Fiber-Reinforced Polymer (FRP) Composites in Environmental Engineering Applications," in *Developments in Fiber-reinforced polymer (FRP) Composites for Civil Engineering*, N. Uddin, Ed., Woodhead Publishing, 2013, pp. 410-468.

[17] B. King and H. GangaRao, "Rehabilitation of Timber Railroad Bridges using Glass Composite Fabrics," in *Repairing and Rehabilitating the Buildings and Bridges of the Americas-Hemispheric Workshop on Future Direction*, Mayguëz, Puerto Rico, 2001.

[18] S. M. Petro, H. V. S. GangaRao, U. B. Halabe, S. Aluri, A. W. Smith, B. King, W. E. Steele and A. Vasudevan, "WVDOH RP# 173: Carbon Fiber Reinforced Polymer Composites Used to Repair and Rehabilitate Wood Railroad Bridges," WVU-CFC, June 2007.

[19] P. Vijay, G. Hota, R. Liang and M. Skidmore, "Rapid Restoration of Rail Road Timber Bridges Using Polymer Composites," in *ANTEC*, 2011.

[20] P. K. Mallick, Fiber-Reinforced Composites: Materials, Manufacturing and Design, Boca Raton: CRC Press, Taylor and Francis Group, 2007.

[21] E. J. Barbero, "Chapter 4: Manufacturing Processes," in *Introduction to Composite Materials Design*, CRC Press, Taylor & Francis Group, 2011, pp. 72-75.

[22] M. Saafi and E. Asa, "Extending the Service Life of Electric Distribution and Transmission Wooden Poles Using a Wet Layup FRP Composite Strengthening System," *Journal of Performance of Constructed Facilities,* vol. 24, no. 4, pp. 409-416, August 2010.

[23] ASTM International, ASTM Standard C881: Standard Specification for Epoxy-Resin-Base Bonding Systems for Concrete, West Conshohocken, PA: ASTM, 2015.

[24] AASHTO, AASHTO LRFD Bridge Design Specifications, U.S Customary Units with 2015 Interim Revisions, 7th ed., 2015.

[25] ASTM International, ASTM Standard D25: Standard Specification for Round Timber Piles, West Conshohocken, PA: ASTM, 2017.

[26] ASTM International, ASTM Standard D2899: Standard Practice for Establishing

Allowable Stresses for Round Timber Piles, West Conshohocken, PA: ASTM, 2017.

[27] J. G. Collin, Timber Pile Design and Construction Manual, Birmingham: Timber Pile Counsel, 2002.

[28] ACI Committee 440, "ACI 440.2R-08 Guide for the Design and Construction of Externally Bonded FRP Systems for Strengthening Concrete Structures," American Concrete Institute, July 2008.

[29] AASHTO, "Guide Specifications for Design of Bonded FRP Systems for Repair and Strengthening of Concrete Bridge Elements," 2012.

[30] X. Song, H. Tang, W. Zhang and X. Gu, "Compressive Stress Strain Relationship of Wood confined with Fiber Composite Sheets," *Advanced Materials Research,* Vols. 133-134, pp. 1207-1211, 2010.

[31] H. Najm, J. Secaras and P. Balagru, "Compression Tests of Circular Timber Column Confined with Carbon Fibers Using Inorganic Matrix," *Journal of Materials in Civil Engineering,* vol. 19, no. 2, pp. 198-204, 1 Feb 2007.

[32] W. Zhang, X. Song, X. Gu and H. Tang, "Compressive Behavior of Longitudinally Cracked Timber Columns Retrofitted Using FRP Sheets," *Journal of Structural Engineering,* vol. 138, pp. 90-98, 2012.

[33] R. S. Abihari, "Rehabilitation of Timber Railroad Bridges Using Glass Fiber Reinforced Polymer Composites," Morgantown, WV, 2007.

[34] G. Davis, "The Performance of Adhesive Systems for Structural Timbers," *International Journal of Adhesion and Adhesives,* vol. 17, no. 3, pp. 247-255, 1997.

[35] C. B. Vick, "Adhesive Bonding of Wood Material," in *Wood handbook – Wood as an engineering material. Gen. Tech. Rep. FPL-GRT-113.*, Madison, US Department of Agriculture, Forest Service, Forest Products Laboratory, 2009.

[36] J. S. Lyons and M. R. Ahmed, "Factors Affecting the Bond between Polymer Composites and Wood," *Journal of Reinforced Plastics and Composites,* vol. 24, no. 4, pp. 405-412, 4 November 2005.

[37] D. Talakanti, "Testing and Evaluation of Wood-GFRC Adhesive Interface Integrity under Accelerated Aging and Mechanical Fatigue," 1997.

[38] C. B. Vick, "Coupling agent improves durability of PRF bonds to CCA-Treated Southern Pine," *Forest Products Journal,* vol. 45, no. 3, pp. 78-84, 1995.

[39] C. B. Vick, "Hydroxymethylated Resorcinol Coupling Agent for Enhanced Adhesion of Epoxy and Other Thermosetting Adhesives to Wood," in *Wood Adhesive*, Madison, WI,

Forest Products Society, 1996, pp. 47-55.

[40] ASTM International, ASTM D905: Standard Test Method for Strength Properties of Adhesive Bonds in Shear by Compression Loading, West Conshohocken, PA: ASTM, 2013.

[41] American Institute of Timber Construction, Timber Construction Manual, New York: John Wiley & Sons, 1985.

[42] ASTM International, ASTM Standard D2559: Standard Specification for Adhesives for Bonded Structural Wood Products for Use under Exterior Exposure Conditions, West Conshohocken, PA: ASTM, 2012.

[43] ASTM International, ASTM Standard D7522: Standard Test Method for Pull-Off Strength for FRP Bonded to Concrete Substrate, West Conshohocken, PA: ASTM, 2015.

[44] D. J. Gardner, J. F. Davalos and U. A. Munipalle, "Adhesive Bonding of Pultruded Fiber-Reinforced Plastic to Wood," *Forest Products Journal,* vol. 44, no. 5, pp. 62-66, May 1994.

[45] G. M. Raftery, A. M. Harte and P. D. Rodd, "Bond Quality at the FRP–Wood Interface using Wood-Laminating Adhesives," *International Journal of Adhesion and Adhesives,* pp. 101-110, 2009.

[46] S. Ghasemzadeh, S. Kajorncheappunngam, R. K. Gupta and H. V. S. GangaRao, "Durability of Glass-Epoxy-Wood Hybrid Composites for Rehabilitation of Railroad Crossties," in *The Durability of Fiber-Reinforced Polymer (FRP) Composites for Construction: Proceedings of the First International Conference (CDCC_98)*, Sheerbrooke, 1998.

[47] P. Chow, S. L. Lewis, A. J. Reinsehmidt and E. J. Barenberg, "Effects of Natural and Accelerated Aging on Oak Crossties," in *Proceedings of the American Wood Preservers Association*, Toronto, 1987.

[48] J. F. Davalos, P. Qiao and B. S. Trimble, "Fiber-Reinforced Composite and Wood Bonded Interfaces: Part 1. Durability and Shear Strength," *Journal of Composites Technology & Research*, pp. 224-231, 2000.

[49] J. F. Davalos, P. Qiao and B. S. Trimble, "Fiber-Reinforced Composite and Wood Bonded Interfaces: Part 2. Facture," *Journal of Composites Technology & Research,* pp. 232-240, 2000.

[50] R. Lopez-Anido, D. G. Gardner and J. L. Hensley, "Adhesive Bonding of Eastern Hemlock Glulam Panels with E-Glass/Vinyl Ester Reinforcement," *Forest Products Journal*, pp. 43-47, 2000.

[51] G. M. Raftery, A. M. Harte and P. D. Rodd, "Bonding of FRP Materials to Wood using Thin Epoxy Glue Lines," *International Journal of Adhesion & Adhesives*, pp. 580-588, 2009.

[52] J. P. Alexander, "Evaluating the Durability of Wood/FRP Bonds through Chemical Kinetics Using a Range of Mechanical Test Methods," Thesis: University of Maine, Orono, 2000.

[53] C. Tascioglu, B. Goodell and R. Lopez-Andio, "Bond Durability Characterization of Preservative Treated Wood and E-Glass/Phenolic Composite Interfaces," *Composites Science and Technology*, pp. 979-991, 2003.

[54] B. Herzog, B. Goodell, R. Lopez-Anido, L. Muszynski, D. Gardner, W. Halteman and Y. Qian, "The Effect of Creosote and Copper Naphthenate Preservative Systems on the Adhesive Bond Lines of FRP/Glulam Composite Beams," *Forest Products Journal*, pp. 82-90, 2004.

[55] K. Laosiriphong, "Development and Evaluation of Glass Fiber Reinforced Composite/Wood Railroad Crossties," Thesis: West Virginia University, Morgantown, 2000.

[56] A. H. Houshmandyar, "Rehabiliation and Field Evaluation of Discared Timber Railroad Ties Using Thermoset GFRP Composites," Thesis: West Virginia University, Morgantown, 2004.

[57] S. Talukdar and N. Banthia, "Performance of Sprayed Fiber Reinforced Polymer Strengthened Timber Beams," *Advances in Materials Science and Engineering*, pp. 1-6, 2010.

[58] H. A. Toutanji, "Durability Characteristics of Concrete Columns Confined with Advanced Composite Materials," *Composite Structures*, pp. 155-161, 1999.

[59] A. Smith, "Rehabilitation of Timber Railroad Bridges Using Glass Fiber Reinforced Polymer Composite Wraps," Morgantown, WV, 2004.

[60] ASTM International, ASTM D7565: Standard Test Method for Determining Tensile Properties of Fiber Reinforced Polymer Matrix Composites Used for Strengthening of Civil Structures, West Conshohocken, PA: ASTM, 2017.

[61] ASTM International, ASTM D3039: Standard Test Method for Tensile Properties of Polymer Matrix Composite Materials, West Conshohocken, PA: ASTM, 2017.

[62] H. V. S. GangaRao, R. K. Gupta, P. Vijay, R. Liang, U. Halabe, M. Skidmore, R. Creese and M. Pavlick, "RP270: Phase One: Determine Structures Where FRP Wraps Would Be Beneficial," West Virginia University Constructed Facilities Center, Morgantown, 2013.

[63] R. R. Rajappa, "Behavior of FRP Wrapped Concrete Cylinders," MSCE Thesis: West Virginia University, Morgantown, 2004.

[64] J. Wan, S. Smith and P. Qiao, "FRP-to-Softwood Joitns: Experimental Investigation," in *Proceedings of the fifth international conference on FRP composites in civil engineering*, Beijing, 2010.

[65] FHWA, Bridge Inspector's Reference Manual, Arlington: Federal Highway Administration - National Highway Institute, 2012.

Appendix

Appendix A

Improvement for FRP Splice

A.1 Improved Design

Timber piles wrapped with three lateral unidirectional layers of wrap performed well compared to the three traditional splicing mechanisms under axial compressive loading. However, shear and bending capacities of FRP wrap splicing were lower than those of traditional splicing methods. To improve shear and bending capacities, failure modes and strength capacities of the FRP splice from the bending and shear tests were taken into consideration. Piles spliced with the FRP wrap that were tested under shear and four-point bending loading failed because of weakness (inadequate amount of fiber) in the hoop direction. To account for this failure mode, a modified design was developed, i.e., a six-layer, (three layers each in hoop and longitudinal directions) bidirectional FRP wrap design. This six-layer design was aimed at reinforcing the hoop direction to prevent unzipping mode of failure as seen in three-layer wrap configuration as per earlier testing. Three additional layers of FRP wrap were added to the original splice design. The same unidirectional Sika fabric was used (dry density of 0.092 lb/in^3) with six total layers, with fiber orientation of three layers each in the hoop and longitudinal directions of the pile [$90_3/0_3$]. For clarity, the (0) direction runs along the pile length and the (90) direction refers to the “hoop” or circumference of the pile.

A.2 Testing Methods

Shear and bending tests were performed in the same manner as initial shear and bending testing (Sections 2.3.2 and 2.3.3 – Damich, 2021). For additional data evaluation based on extra wraps in the hoop direction, three specimens were tested. One with the six-layer splice design under shear dominant loading, the other two under bending dominant loading. The shear specimen and one of the bending specimens were repaired, using virgin FRP wrap. A pile with the three-layer unidirectional fabric design that was taken to failure earlier under four-point bending was repaired using three additional virgin layers of fabric, with the strength dominant fiber direction aligned with the hoop direction of the pile. This repaired specimen was tested again under four-point bending load condition. An additional pile was spliced with virgin FRP wrap using the six-layer bidirectional splice design and tested under four-point bending loading condition.

A.3 Shear Analysis for Improved FRP Wrap

The maximum shear stress and its corresponding deflection from the six-layer shear test specimen are provided in Table 3-1 (see Damich, 2021). The shear stress versus deflection plot or this test is shown in Figure A-1. This splice performed very well compared to the three traditional splicing methods and the three-layer FRP splice, having shear stress to failure of 987 psi. Deflection recorded at maximum stress is higher for this specimen than deflections recorded during the testing of the original three-layer design specimens, whose dominant fiber orientation was in the longitudinal direction only. Figure A-1 indicates that the initial failure occurred before the ultimate stress was reached. This can be seen from Figure A-1 as the stress-deflection curve reach a plateau after about 1 in. of deflection. This could be due to de-bond or perhaps localized failure at a concentrated point within the splice.

Table A-1 – New FRP splice maximum shear stress and corresponding deflection

Test	6-Layer	3-Layer (avg)
Maximum Shear Stress (psi)	987	613
Deflection at Maximum Stress (in)	2.0	0.9

Three layers of GFRP added in the hoop direction of the field specimen as described in section 2.5 (see Damich, 2021).

Figure A-1 – Six-layer FRP shear stress vs. deflection

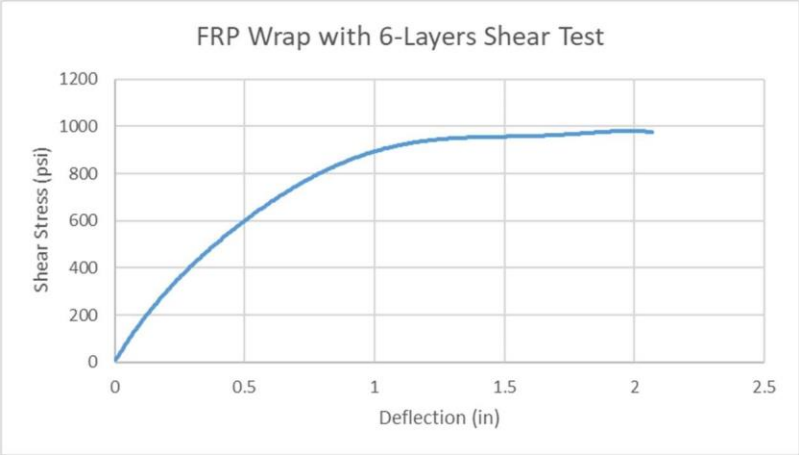

A.3.1 Summary and Failure Modes of Six-Layer FRP Wrap Under Shear

Higher deflection recorded in this test is attributed to additional movement after initial failure occurred. In Figure A-1 the slope levels were not matching, after about 0.8 in. of deflection

where the stress versus deflection plot was getting to be nonlinear. Deflection at failure of this six-layer FRP rehab specimen compared well with the three-layer FRP splice specimens, i.e., differences in deflection is about 10%. Failure mode was ductile as it failed in a more conventional manner than the three-layer FRP splice mechanism. In the pristine six-layer FRP composite wrap specimen, lateral compression of fiber was noted at the center of the splice (Figure A-3), unlike the unzipping in the original three-layer design. This failure is expected as the compressive strength of Sika Glass/Epoxy composite is slightly lower than its tensile strength. No unzipping of fabric occurred in the six-layer wrap test, indicating hoop direction reinforcement was sufficient to provide adequate confinement strength.

Figure A-2 – Six-layer FRP splice shear test

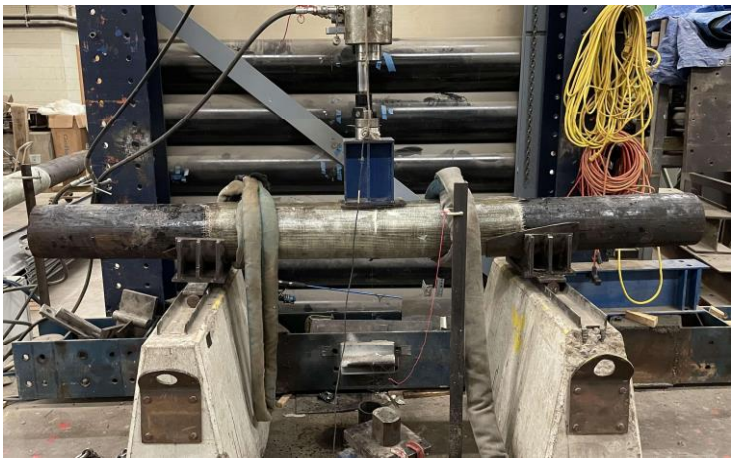

Figure A-3 – Compressive failure of fabric

A.4 Bending Analysis for Improved FRP Wrap

Bending testing was performed in the same manner as discussed in Section 2.3.3 with failure modes and calculations are consistent with those of Section 2.4.2 (Damich, 2021).

Data was analyzed for maximum bending stress and its corresponding deflection for both the aforementioned bending tests (Table 3-2 – Damich, 2021). The re-wrap specimen recorded a lower maximum bending stress and higher deflection at failure than the six-layer splice specimen. The maximum bending stress recorded in the re-wrap test is similar to the maximum bending stress recorded from the test data of the original three-layer FRP wrap spliced specimens. As expected, the deflection recorded at maximum bending stress for the re-wrap test is higher than the deflection recorded in the original three-layer splice design testing because of higher bending load to failure. The six-layer pristine specimen showed an increase in bending stress to failure with lower deflection than the deflections obtained from the original splice design testing with three layers, indicating higher stiffness of the six-layer wrapped beam.

Table A-2 – New FRP splice maximum MOR and corresponding deflection

Test	Original 3-layer GFRP spliced pile	Re-Wrap of failed pile with 3 layers	6-Layer AVG
Maximum Modulus of Rupture (psi)	2188	2321	2974
Deflection at Maximum Stress (in.)	3.6	5.0	2.7

A bending stress versus deflection plot for the repaired (or re-wrapped) test specimen is provided in Figure A-4. The slope of the curve is lower than that of other FRP spliced specimens due to inadequate bending transfer across the joint. Large deflections from this test are attributed to already failed original splice. With the three bottom layers having already failed, no significant de-bond between the splice mechanism and the pile is noted. The bending strength capacity of the re-wrapped pile is attributed to the three additional layers added to the splice, before re-testing that specimen.

Reference: D. Damich, “Timber Bridge Splicing with Fiber Reinforced Polymer Wraps” MSCE Thesis Submitted to West Virginia University, August 2021.

Figure A-4 – FRP re-wrap bending stress vs. deflection

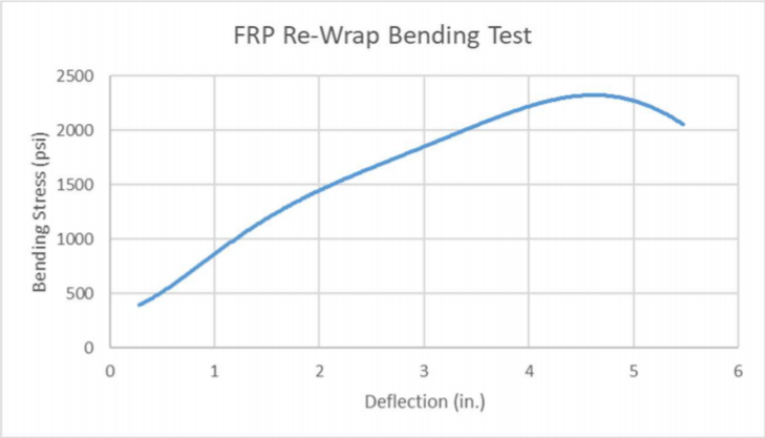

The bending stress versus deflection plot for the six-layer pristine FRP wrap splice design is provided in Figure A-5. The change in slope at 1800 psi in the stress versus deflection plot indicates that de-bond may have occurred during testing. This de-bond was likely the result of inconsistency in wrapping during the hand-layup assembly of the FRP splice. It was also noted that the resin mix for this splice was of higher viscosity than usual, which can result in inconsistent soaking of resin in the fabric causing higher void content and weaker bond. Although these inconsistencies may be present potentially, overall capacity and stiffness was still higher than that of the original FRP wrap test specimens.

Figure A-5 – Pristine six-layer FRP bending stress vs. deflection

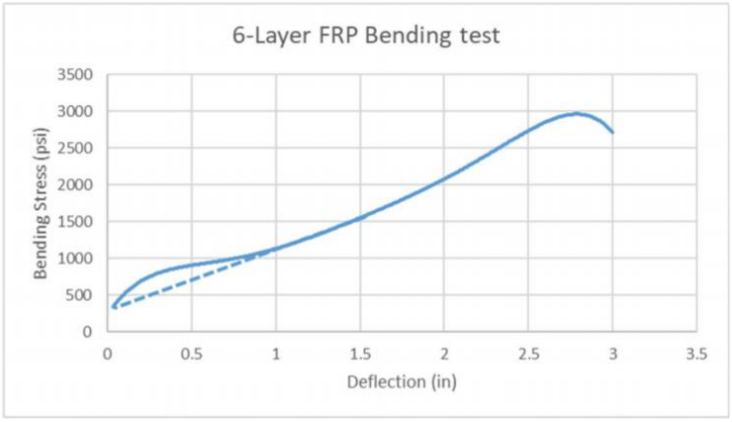

A.4.1 Summary and Failure Modes

Performance of the re-wrapped (already failed and repaired) specimen at failure provides slight increase (6%) in bending stress capacity from the original design and resulted in larger deflection than the deflection of three-layer specimen at ultimate stress. It was concluded that

the remaining and already failed original splice did not contribute any bending resistance to the system. This means that nominal increase in bending capacity has been attained due to confinement from hoop direction fibers. Visual failure modes observed during the testing of the re-wrapped specimen supports this conclusion. The visual failure mode observed was the splitting of fabric between fibers in the hoop direction, lacking adequate reinforcement in the longitudinal direction of the pile (Figure A-6), and the nominal strength increase is attributed to confinement of the pile through hoop direction fibers.

Figure A-6 – Splitting of fabric in re-wrap test

Results from the pristine six-layer FRP wrap splice test specimen reveal that additional layers of wrap do help in increasing the strength capacity of the system. Inconsistencies, such as the higher than usual viscosity of the resin, were noticed during wrapping of this specimen. Visual failure modes confirm these inconsistencies as they differ from other testing of FRP wrap splicing. The main failure mode was debonding of layers and buckling of the FRP splice (Figure A-7). Figure A-7 indicates areas of voids (and de-bond) within the FRP splice zone. Even with these inconsistencies, performance has improved still from the original three-layer FRP design by about 36%. To prevent these inconsistencies, hand-layup wrapping must be performed more carefully, making sure that the resin mixture is not overly viscous and complete soaking is achieved.

Figure A-7 – Crumbling of FRP during six-layer bending test

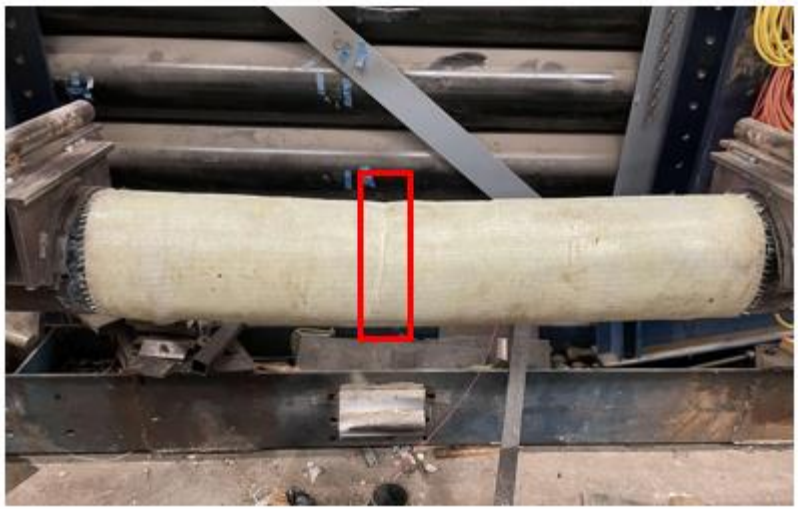

A.5 Conclusions from Improved FRP Splice

Adding extra layers of FRP wrap to the original three-layer splice design increased both the shear and bending strengths of the pile. Table A-3 provides a comparison of results from the shear tests of the new six-layer FRP splice design and the original three-layer FRP splice. The new six-layer FRP design showed a significant increase (61%) in shear capacity from the original three-layer design. Two inches deflection for the six-layer shear testing was higher than the recorded deflections during the shear testing of the original three-layer FRP splice specimens (0.9 in. average). The higher deflection is attributed to the additional movement in the splice after initial failure (at 1 in. deflection) due to fiber buckling or de-bond and to 36% higher stress to failure contributed by extra layers of wrap material. Table A-4 provides a comparison of results from bending testing of the new six-layer FRP splice design and the original three-layer FRP splice. The re-wrap bending specimen showed a slight increase in bending stress (6%) at the cost of a larger deflection. The six-layer design under bending provides a significant increase (36%) in bending capacity and a higher system stiffness.

When the FRP splice mechanism fails, it is better to completely replace the FRP splice with a new splice, noting that re-wrapping does not help increase bending capacity.

Table A-3 – FRP splice shear test comparisons

Test	6-Layer	3-Layer AVG
Maximum Shear Stress (psi)	987	613
Deflection at Maximum Stress (in.)	2.0	0.9
Percent Increase in Stress (%)	(987-613)/613 ~ 61	-

Table A-4 – FRP splice bending test comparisons

Test	Re-Wrap	6-Layer	3-Layer AVG
Maximum Modulus of Rupture (psi)	2321	2974	2188
Deflection at Maximum Stress (in)	5.0	2.7	3.6
Percent Increase in Stress (%)	[(2321-2188) / 2188] *100% ~ 6	[(2974-2188) / 2188] *100% ~ 36	-

Appendix B

Timber Pile Load Rating Method

Current load rating methods account for only concentric load action on timber piles and neglect the bending action from eccentric loading conditions. It should be noted under certain loading scenarios, bending effects could be as high as those from axial loads acting on timber piles.

The Allowable Stress Design (ASD) method is adopted herein for bridge timber pile rating. The load rating of timber piles under concentric axial loading by neglecting any pile bending is:

$$\text{Timber Pile Rating} = 20* \frac{\text{Axial Load Capacity} - \text{Dead Load on Pile}}{\text{Live Load on Pile}} \quad (13)$$

Axial load capacity of a pile bent can be performed using frame analysis. However, the analysis is simplified here by considering that the axial load of a truck is seated directly over a pile bent with a cross beam or otherwise known as pile cap. A typical pile bent has four timber piles (occasionally three piles) connected by a pile cap and diagonal braces. Hence bending effects are neglected, to simplify the computations of pile capacity under axial loads. The "as-driven" pile resistance is not considered in the proposed rating computation because our focus is only on retrofitting in-service timber pile. Most of the pile driving capacities are determined using Engineering News Formula, which is based on the driving hammer weight and drop height. The driving capacity varies approximately from 51 kips to 69 kips, which is based on the design and construction practices of different state department of transportation. Here, the focus is on inventory rating only and leads to determining loads can safely cross a bridge for a long time.

Based on the NDS (2018) formula given below, the allowable compression stress parallel to grain, F_c' after accounting for adjustment factors is:

$$Fc' = F_c (C_D * C_t * C_u * C_p * C_{cs} * C_{sp}) \quad (14)$$

Where,

F_c= Reference compressive stress for treated timber of circular section and it is taken as 1200 psi for the case-study herein,

C_D= Load duration factor=0.9 for allowable compressive stress under dead load and 1.5 for live load stresses. As per conservative design practice, this is taken as 1.0 for this design example

C_t= 1.0- for temperature below 90°F

C_u= 1.0- for treated piles (different for untreated timber)

C_{cs}= 1.0- critical section factor for timber piles

C_p= single pile column stability factor representing combined buckling and crushing mode as described below (Ylinen formula as given: "Design of wood structures-ASD/LRFD P.383 Breyer, et al, 7th Edition McGraw-Hill, 2015 & AFPA 2005)

C_{sp}=1.0- simple pile factor (depends on load sharing by different piles, but we are assuming all piles shape the same amount of load due to bracings, with no sway)

$$C_p = \left(\frac{1+F_{cE}/F_c^*}{2c}\right) - \left[\left(\frac{1+F_{cE}/F_c^*}{2c}\right)^2 - \left(\frac{F_{cE}/F_c^*}{c}\right)\right]^{1/2} \quad (15)$$

$$Fc^* = F_c\,(C_D)\;(C_t)\;(C_u)\,(C_{sp}) \quad (16)$$

$$F_{cE} = \frac{0.822 * E'_{min}}{\left(\frac{le}{d}\right)^2} \quad (17)$$

Where,

$E'_{min} = E_{min}$ (reference modulus of elasticity) (C_t)

l_e= exposed pile length above mud line + embedment length (~3 ft.) below mud line

c= 0.85 for round columns as per AFPA 2005

Note: Any bending interaction with axial loads is neglected and size factor (C_F) is taken as 1.0. In addition, impact factors for timber piles are not considered in bridge designs due to better damping of timber over steel or concrete.

Determination of axle capacity of a 10 in. diameter red oak timber pile of 8 ft. height above mud line:

F_c= 1200 psi,

$C_{F=}$ 1.0 (Size factor may vary depending on pile diameter & assumed as 1.0 herein) and it could be as high as 1.1 in compression

E_{min}= 0.85 * 10^6 psi

E'_{min}= E_{min} (C_M) (C_t) (C_T) (C_i)

Where,

C_M = wet service factor is typically taken as 0.75, but herein 1.0 is used because timber piles have been in service in a rehabilitation scenario (0.75 must be used for new timber)

C_i = incising factor = 1.0 for large red oak timber since it accepts treatment better than white oak

C_T= Buckling stiffness factor is 1.0 for large size members (p. 384, Breyer 2015)

C_t= C_i= 1.0

Therefore,

E'_{min}= E_{min} (for this case and other design scenarios may be different)

A= π (r=5)^2 ≅ 78.5 in^2

y = weak axis

Timber Pile Capacity using Ylinen equation:

Case-1: Full section (10 in. dia) capacity computations

$$\left(\frac{l_e}{d}\right)_{max} = \left(\frac{k_{el}}{d}\right)_{=\text{weak axis}} = \left(\frac{(K_e=1)*(8'+3')*12"}{(d=10")}\right)=13.2$$

Where,

K_e=1.0 because of hinge-hinge boundary condition assumption, and k_e can vary from 0.65 to 2.4 depending upon the end conditions

Note: It is impossible to attain full fixity for timber in the field due to loosening of connectors with time under dynamic load action and freeze-thaw cycling on bridge super structures.

$F_{cE}= \frac{0.822*E'_{min}}{\left(\frac{le}{d}\right)^2} = \frac{0.822\ (0.85*10^6)}{13.2^2}$ = 4000 psi

$F_c^* = F_C\ (C_D)\ C_M)\ (C_F)\ (C_i)$ = 1200 (1) (1) (1) (1) =1200 psi

C_D= Load distribution factor which is assumed as 1 since the pile bent is assumed to have no sway

$F_{cE} / F_c^* = \frac{4000}{1200}$ = 3.33 > 1.0

So,

C_p= 1.0, F_c' = F_c and P= 1200 $(\pi(\frac{10}{2})^2)$ = 94,200 lbs =94.2 kips

Case-2: Suppose the timber pile is left with only 4 in. diameter of quality wood at the mud line due to rotting, then the pile capacity is:

$F_{cE}= \frac{0.822*E'_{min}}{\left(\frac{le}{d}\right)^2} = \frac{0.822\ (0.85*10^6)}{(\frac{((8'+3')(12"))^2}{(4")^2})} = \frac{0.7*10^6}{33^2}$ = 642.8 psi

$F_{cE} / F_c * = \frac{642.8}{1200}$ = 0.536

$\frac{1+F_{cE}/ F_c*}{2c} = \frac{1+0.536}{2(0.85)}$ = 0.903 ≅ 0.9

C_p= 0.9 - $\sqrt{0.9^2 - \frac{0.536}{0.85}}$ = 0.9 - $\sqrt{0.81 - 0.63}$ = 0.9- 0.425 = 0.475

F_c' = F_C (C_D) (C_M) (C_t) (C_F) (C_p) (C_i) = 1200 (1.0) (0.75) (1.0) (0.475) (1.0) =428 psi

Allowable P = F'$_c$ A = 428 * (π* (r=2) ^{2}) ≅ 5370 lbs. = 5.4 kips

Case-3: Suppose the 8 ft. long pile is cut at the top and bottom of the rotten parts, then the contribution (allowable P) from the timber is "ZERO" and that cut part is wrapped with FRP wrap of say 0.25 in. thick glass FRP wrap after inserting treated solid timber in the cut portion of the pile. Computations for the pile capacity of FRP wrap (neglecting any contribution of newly inserted timber) based on FRP wrap delamination from timber pile substrate are given below:

ε_{frp} = strain in FRP wrap to buckle as thin rectangular strip = $\frac{0.822}{(\frac{le}{t})^2}$ (Euler buckling equation)

Where, t is the thickness of FRP composite wrap.

Based on our experimental data, we assume strain to local buckling for hand lay-up members is approximately 2000 με.

From the above Euler buckling equation, the compression load capacity of the wrapped timber pile is controlled by the GFRP composite wrap, which fails around 2000 με (micro strains). Therefore, from the limited laboratory-based test data, we assumed the failure strain of GFRP wrap after delamination from timber pile is 2000 με. It should be noted that the experimentally observed failure strain (~ 2000 με) is a function of manufacturing process (hand lay-up versus pultrusion or compression molding or vacuum infusion process), type of resin used to develop bond for the wrap around the timber substrate quality of timber substrate, quality of in-situ application by hand, and other parameters.

Thus,

l_e = 3 in. for t = 0.15 in.

l_e = 5 in. for t = 0.25 in.

E_{frp} = 2.5 * 10^6 psi (for hand lay-up only, and higher value is found from experimental data for pultruded composites)

$F_{u,frp}$ = (2000 * 10^{-6})*(2.5*10^6) = 5000 psi at buckling (allowable) << 30,000 psi @ failure, and 10,000 psi as the allowable limit with the factor of safety of 3.0

Using moisture reduction factor, C_M of 0.75 to the allowable stress of FRP wrap, and other aging factors (say 0.9) as well as 0.7 for flexural buckling (as per ACMA-ASCE-LRFD, 2021). It should be noted that moisture reduction factor (0.75) is used only for FRP wrap and not for in service pile because FRP wrap is new in service, resulting in potential loss of strength over its service life.

$F^*_{c,frp}$ = (5000 psi)(0.75)(0.7)(0.9) (2π (r = 5 in.) (t = 0.25 in.)) ≅18,500 lbs ≅ 18.5 kips

Since the design is based on case 3, proceed with the pile rating capacity using allowable P = 9.8 kips. Assume Dead Load= 2 kips/pile.

Timber Pile Rating= $\frac{20\ (\ 18.5-(D.L.=2)}{live\ load\ on\ pile} = \frac{20 * 16.5}{live\ load\ on\ pile}$

Determination of Live Load on Pile cap:

Live load on pile is based on one of the axles of HS 20-44 truck over the pile cap and assuming two truck axles of a two-lane bridge exert forces simultaneously over four piles of the pile bent, the live load per pile on a four-pile bent is:

Live Load/ pile = $\frac{32\ \text{kips/axle}+32\ \text{kips/axle}}{4}$ = 16 kips/pile (neglected impact and other axle effects on the bent)

Pile Rating:

Pile Rating= $\frac{20\ (16.5)}{16}$ ≅ 20 kips = HS 20-44

If the rating number is over 20 kips, limit this number to HS 20-44 loading)

Note: The PI did not account for axial load resistance offered by the remaining timber pile area (πr^2) because of post wrap instability beyond FRP wrapped buckling or bending effects from eccentric loading. The design is developed based on the debonding mode of failure between the GFRP wrap and the timber substrate; however, another potential failure mode within a timber pile is likely, but not considered in this design approach because the in-situ integrity of a pile has to be established non-destructively before adopting the approach proposed herein.

If the timber pile capacity of the 4 in. diameter portion is added to the resistance offered by the GFRP wrap, then the total axial load carrying capacity is ≅ 27.2 kips (= 7.18 + 20), which results in much higher pile rating than needed for HS 20-44 truck loading conditions.